

DFT techniques for interpretation and solution of practical problems



Prof. Jose A Alarco¹ and Prof. Ian D.R. Mackinnon²

¹School of Chemistry and Physics, ²School of Earth and Atmospheric Sciences
Science Faculty, Queensland University of Technology
Brisbane, Australia

Meeting of Physics
Webinar Lima – Perú
August 12-14, 2021

Acknowledgement of Traditional Owners

QUT acknowledges the Turrbal and Yugara, as the First Nations owners of the lands where QUT now stands. We pay respect to their Elders, lores, customs and creation spirits. We recognise that these lands have always been places of teaching, research and learning.

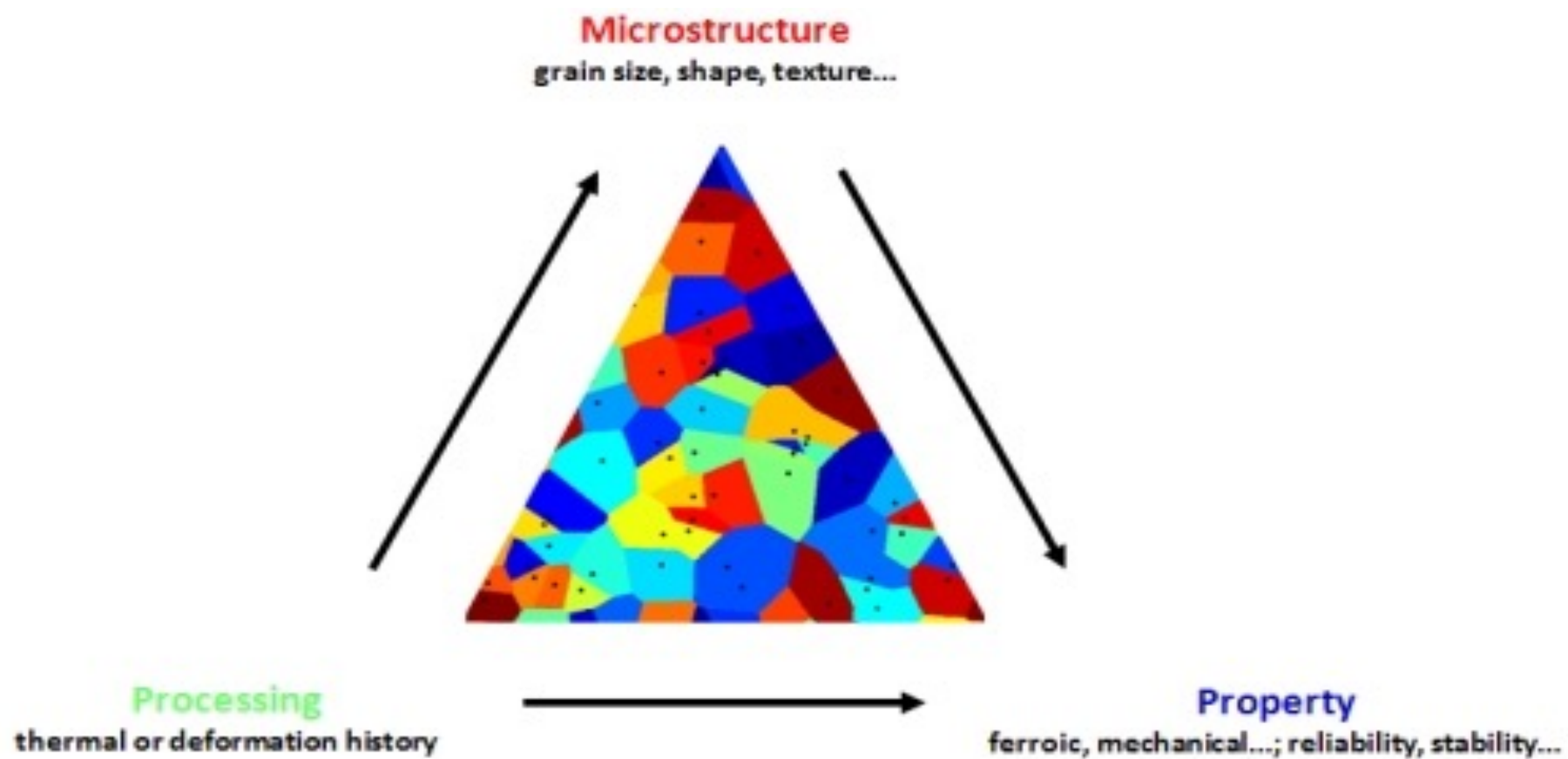
QUT acknowledges the important role Aboriginal and Torres Strait Islander people play within the QUT community.

Outline

- Motivation
- Brief explanation of Density Functional Theory (DFT)
- Example of DFT use for practical outcomes in battery science and technology
- Example of DFT use for improved understanding of superconductor materials symmetry and insight on mechanisms
- Collaboration opportunities
- Conclusions.

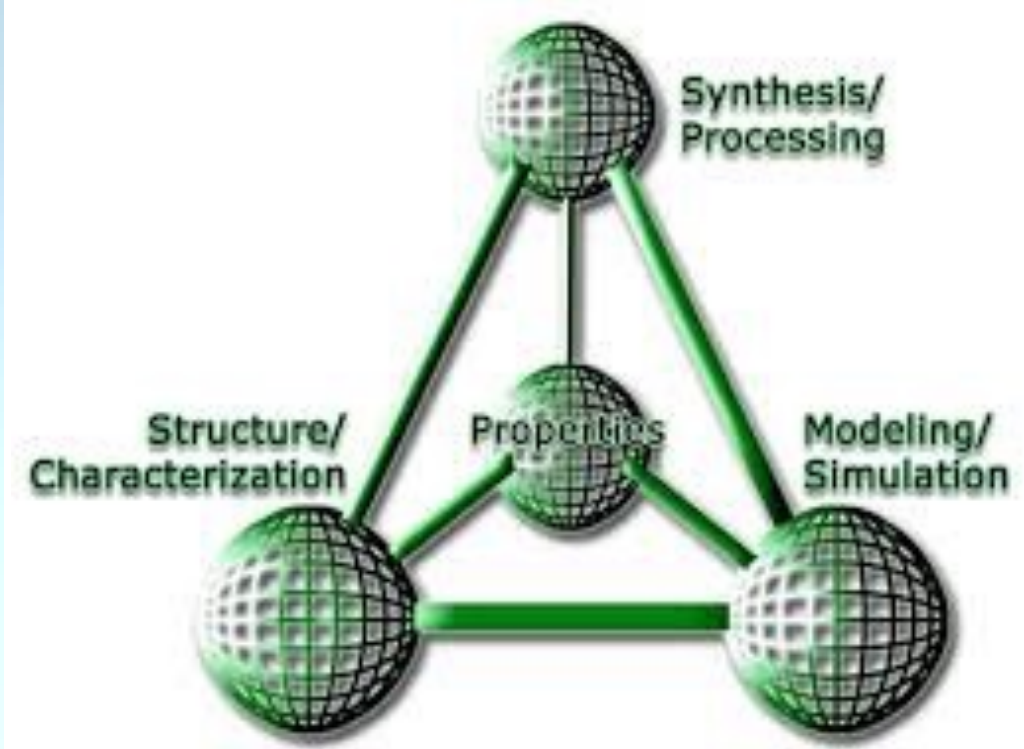
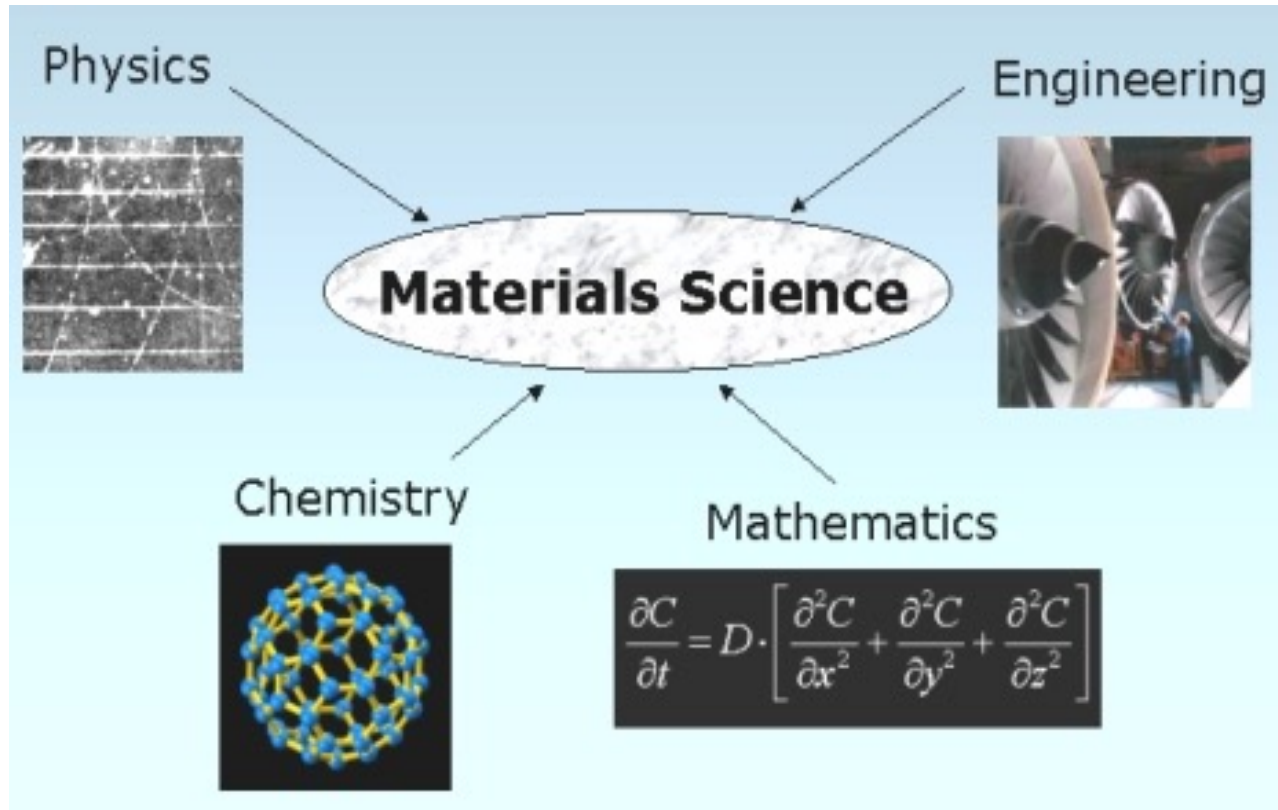
Motivation

Earlier Definition of Materials Science



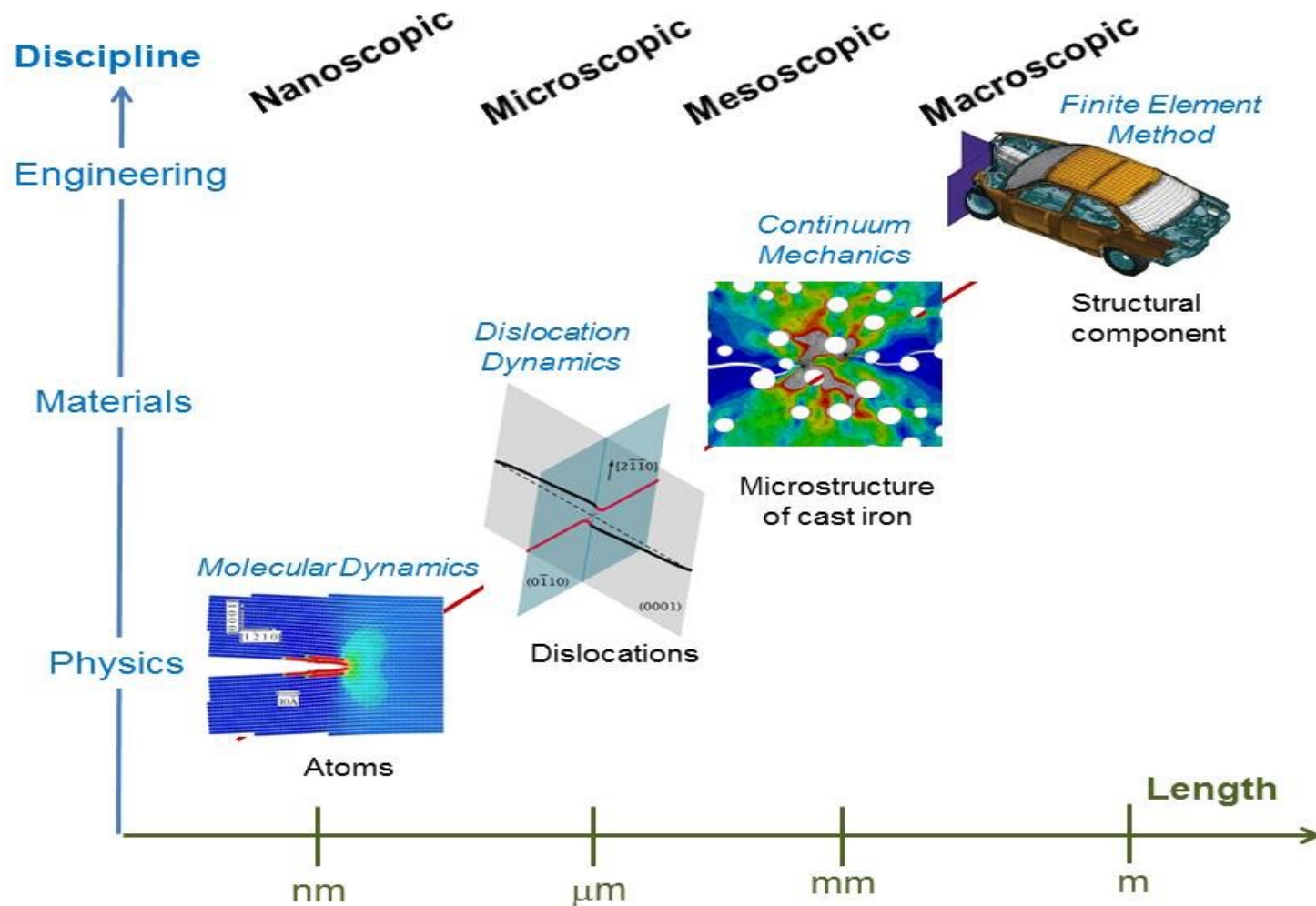
www.google.com

More Recent and Inclusive Definition of Materials Science



www.google.com

Computational Modeling



Simulation

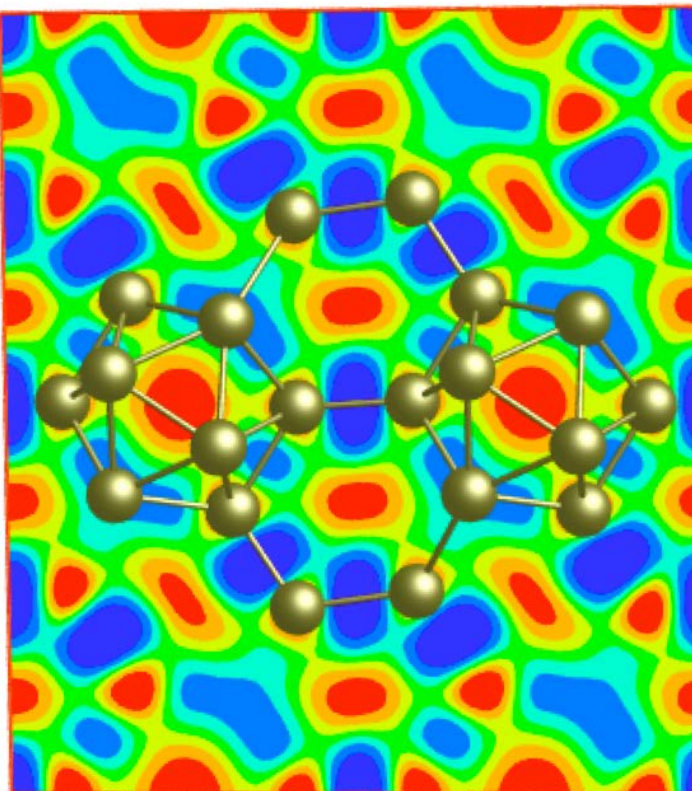
Visualization

Prediction!

www.google.com

Brief explanation of Density Functional Theory (DFT)

Computational Quantum Chemistry/Physics



Atomistic Modeling

Simulation

Visualization

Prediction!

Density Functional Theory

Many Body Schrodinger's equation

More than one electron

$$\hat{H} \Psi(\mathbf{r}_1, \mathbf{r}_2, \dots, \mathbf{r}_N) = E \Psi(\mathbf{r}_1, \mathbf{r}_2, \dots, \mathbf{r}_N)$$

$$\hat{H} = -\frac{1}{2} \sum_i^N \nabla_i^2 + \hat{V}_{ext} + \sum_{i < j}^N \frac{1}{|\mathbf{r}_i - \mathbf{r}_j|}$$

$$\hat{V}_{ext} = - \sum_{\alpha}^{N_{at}} \frac{Z_{\alpha}}{|\mathbf{r}_i - \mathbf{R}_{\alpha}|}$$

**Time independent, non-relativistic
Schrodinger equation
Born-Oppenheimer approximation**

**Kinetic energy, interaction
with external potential and
electron-electron interaction**

**Electron-atomic nuclei interaction
(of interest in materials simulation)**

An Introduction to Density Functional Theory, N.M. Harrison

CRICOS No.00213J

Many Body Schrodinger's equation

More than one electron

$$\Psi_{HF} = \frac{1}{\sqrt{N!}} \det [\phi_1 \phi_2 \phi_3 \dots \phi_N] \quad \text{Hartree-Fock ansatz}$$

Hartree-Fock energy

$$E_{HF} = \int \phi_i^*(\mathbf{r}) \left(-\frac{1}{2} \sum_i^N \nabla_i^2 + V_{ext} \right) \phi_i(\mathbf{r}) d\mathbf{r}$$
$$+ \frac{1}{2} \sum_{i,j}^N \int \frac{\phi_i^*(\mathbf{r}_1) \phi_i(\mathbf{r}_1) \phi_j^*(\mathbf{r}_2) \phi_j(\mathbf{r}_2)}{|\mathbf{r}_i - \mathbf{r}_j|} d\mathbf{r}_1 d\mathbf{r}_2$$
$$- \frac{1}{2} \sum_{i,j}^N \int \frac{\phi_i^*(\mathbf{r}_1) \phi_j(\mathbf{r}_1) \phi_i(\mathbf{r}_2) \phi_j^*(\mathbf{r}_2)}{|\mathbf{r}_i - \mathbf{r}_j|} d\mathbf{r}_1 d\mathbf{r}_2$$

Coulomb energy

**Exchange
energy**

Introduction to DFT

$$n(\mathbf{r}) \Rightarrow \Psi(\mathbf{r}_1, \dots, \mathbf{r}_N) \Rightarrow v(\mathbf{r}),$$

Function $y=f(x)$, from a number x we go to a number $y=f(x)$

Simple example of functional $N[n]$, from the function $n(\mathbf{r})$ we go to a number N

$$N = \int d^3 r n(\mathbf{r}) = N[n],$$

Another example where the functional depends on a parameter

$$v_H[n](\mathbf{r}) = q^2 \int d^3 r' \frac{n(\mathbf{r}')}{|\mathbf{r} - \mathbf{r}'|}, \quad \text{Hartree potential}$$

Introduction to DFT

- Hohenberg-Kohn Theorem

$$n(\mathbf{r}) = N \int d^3r_2 \int d^3r_3 \dots \int d^3r_N \Psi^*(\mathbf{r}, \mathbf{r}_2, \dots, \mathbf{r}_N) \Psi(\mathbf{r}, \mathbf{r}_2, \dots, \mathbf{r}_N).$$

Given the **ground state density $n_0(\mathbf{r})$** , it is possible to calculate $\Psi_0(\mathbf{r})$

$\Psi_0[n_0]$ is a functional

$$\boxed{\Psi_0(\mathbf{r}_1, \mathbf{r}_2, \dots, \mathbf{r}_N) = \Psi[n_0(\mathbf{r})].}$$

$$\boxed{O_0 = O[n_0] = \langle \Psi[n_0] | \hat{O} | \Psi[n_0] \rangle.}$$

$$E[\Psi] = \int \Psi^* \hat{H} \Psi d\mathbf{r} = \left\langle \Psi \left| \hat{H} \right| \Psi \right\rangle$$

$$E[\Psi] \geq E_0$$

Minimized by n_0

**Average total energy
for specified state
Energy is a functional**

**Variational theorem
Ground state**

Introduction to DFT

- Kohn-Sham equations:

$$\left(-\frac{1}{2} \nabla^2 + v^C(\mathbf{r}) \right) \psi_i(\mathbf{r}) + \int v^{xc}(\mathbf{r}, \mathbf{r}') \psi_i(\mathbf{r}') d\mathbf{r}' = \epsilon_i \psi_i(\mathbf{r})$$

$$v^C(\mathbf{r}) = - \sum_a \frac{Z_a}{|\mathbf{R}_a - \mathbf{r}|} + \int \frac{\rho(\mathbf{r}, \mathbf{r}')}{|\mathbf{r} - \mathbf{r}'|} d\mathbf{r}'$$

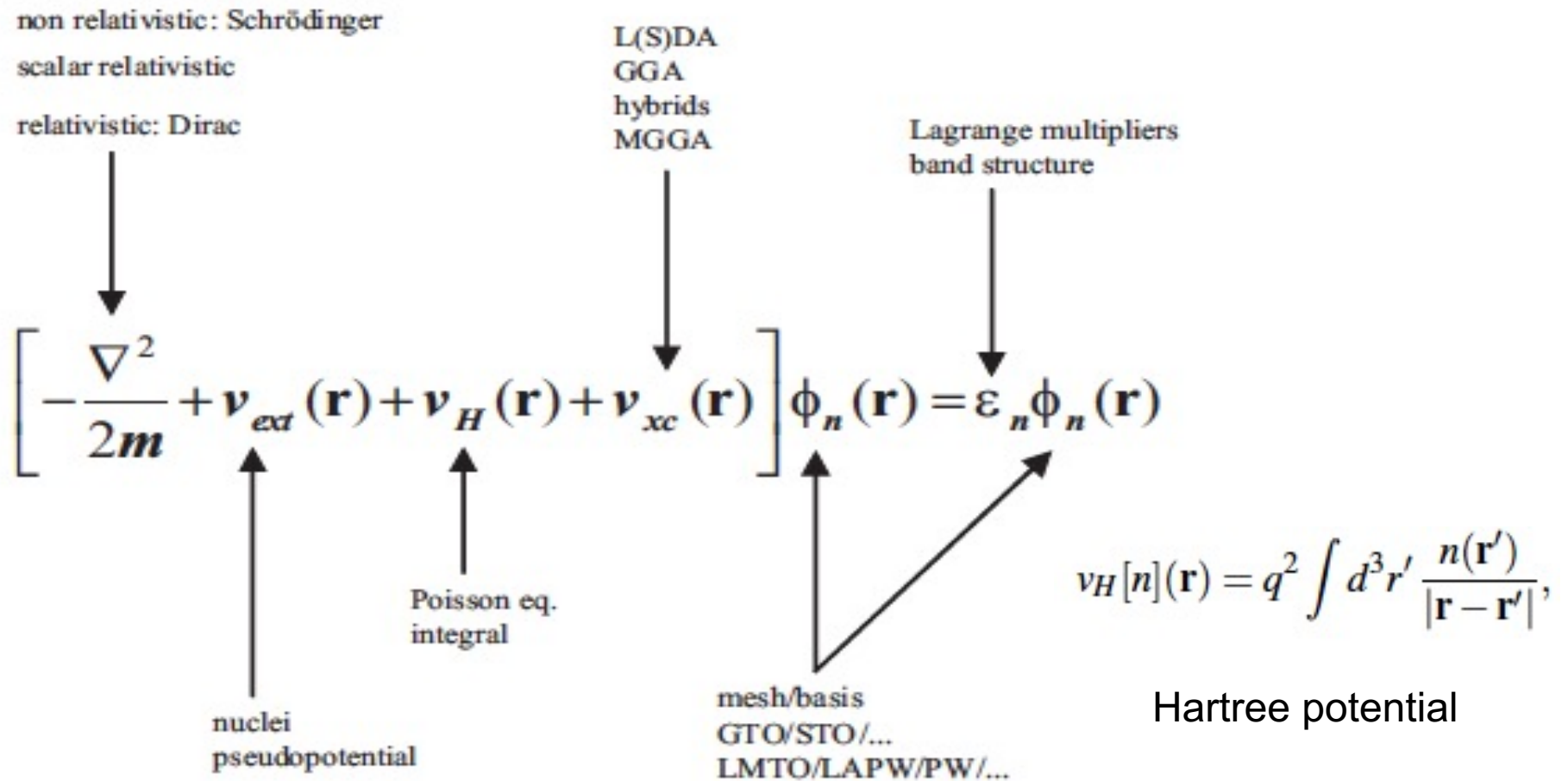
Coulomb potential

$$\rho(\mathbf{r}, \mathbf{r}') = \sum_{\alpha} \psi_{\alpha}^*(\mathbf{r}) \psi_{\alpha}(\mathbf{r}')$$

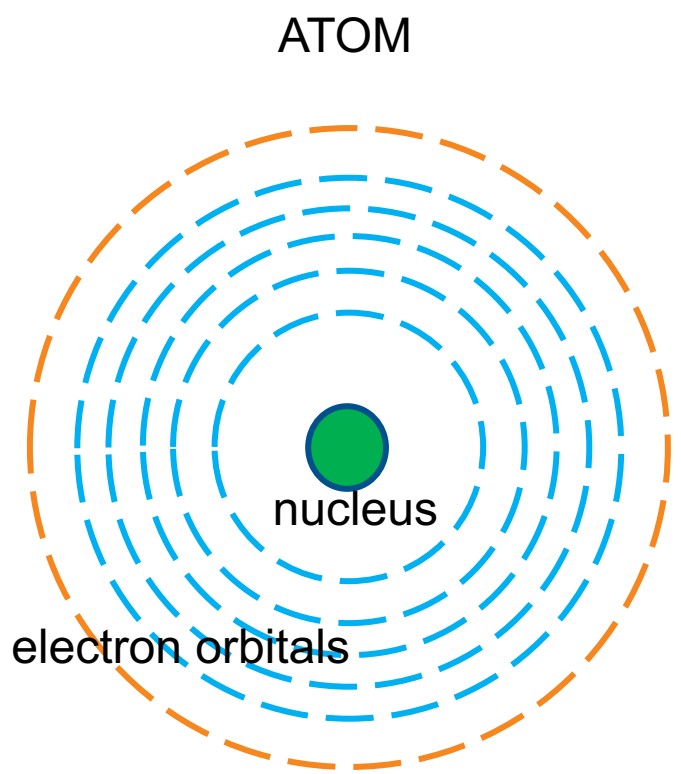
Electron density matrix

$v^{xc}(\mathbf{r}, \mathbf{r}')$ Exchange correlation potential -
Hides complexity of many body interaction

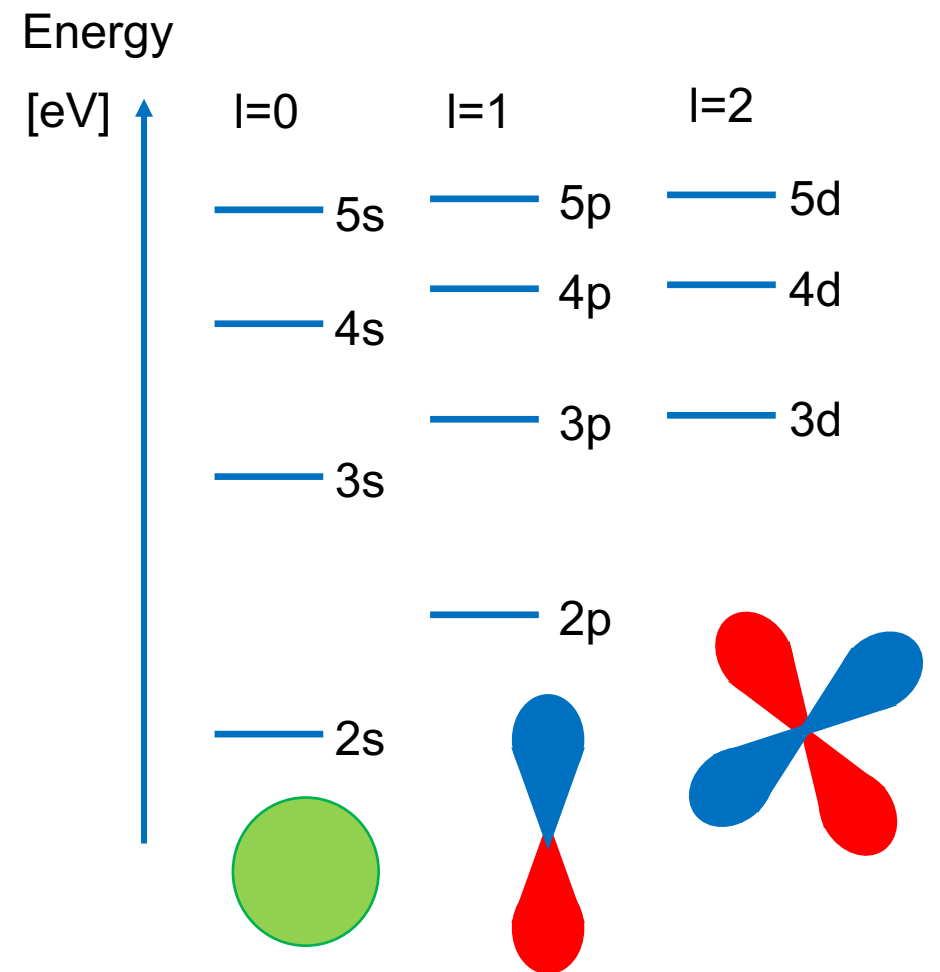
Introduction to DFT- Pseudopotentials



Origin of Electronic Bands



Valence electrons
Core electrons



Origin of Electronic Bands

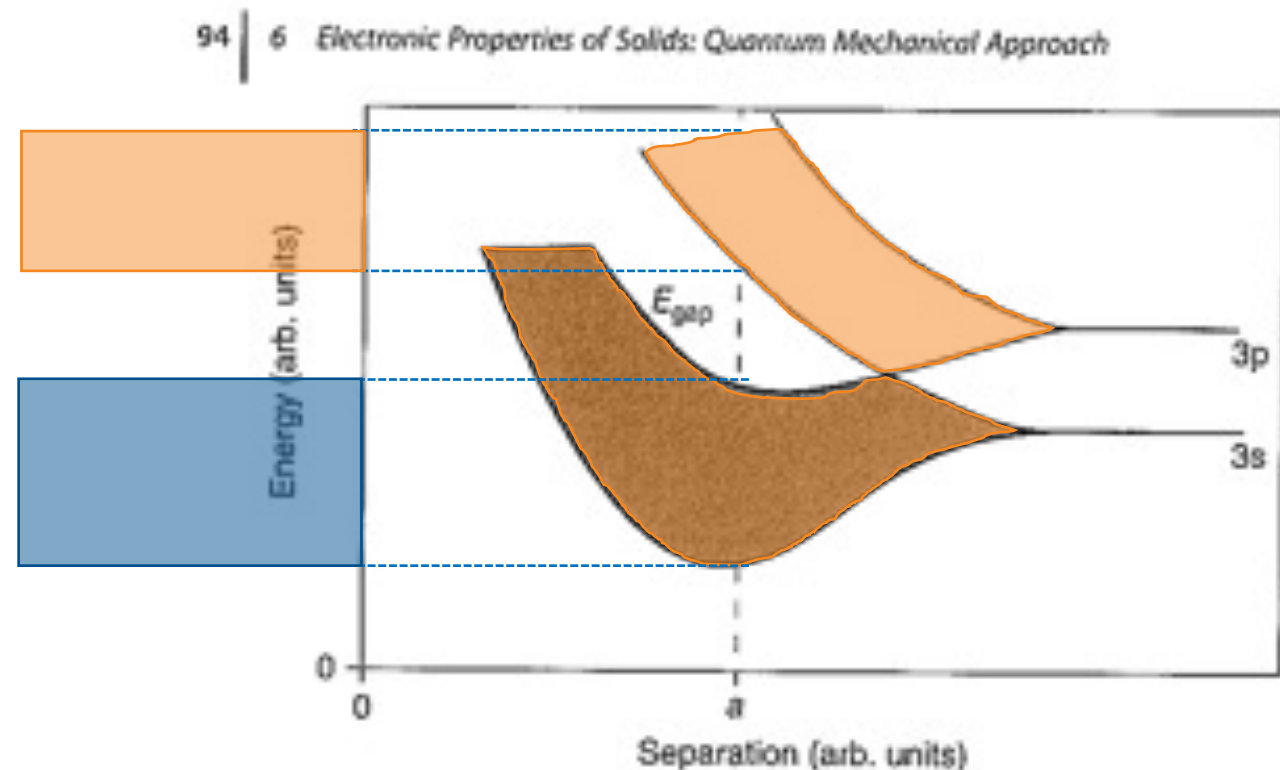
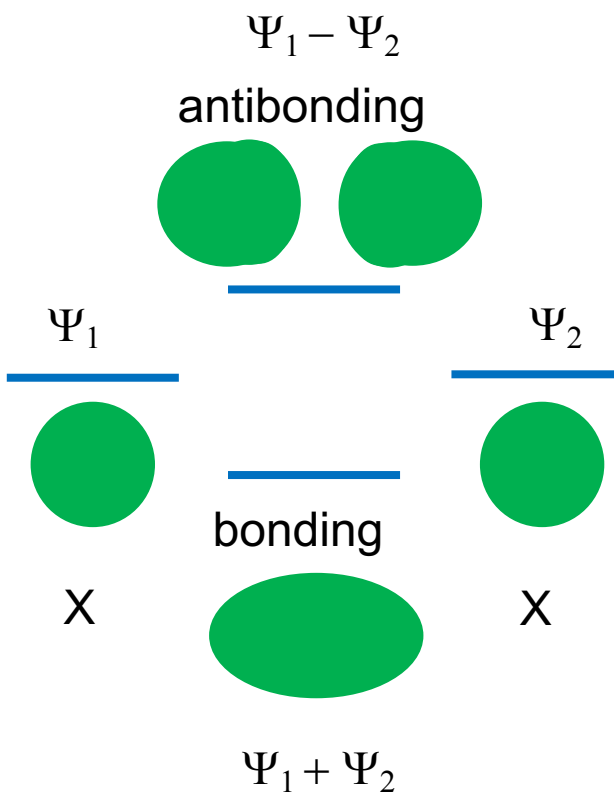


Figure 6.2 Band formation in Si. The lower band corresponds to the sp^3 states and is completely filled.

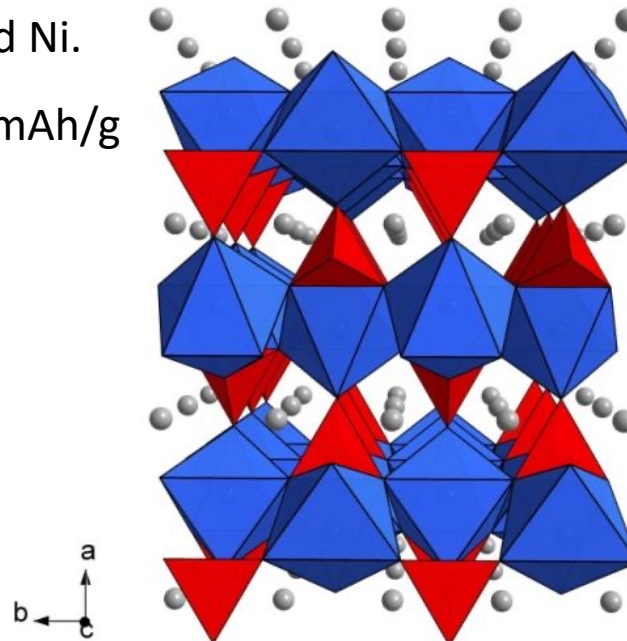
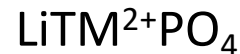
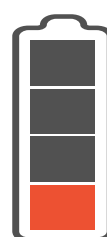
Adapted from Solid State Electronic Devices, Ben G. Streetman

Example of DFT use for practical outcomes in battery science and technology

Olivine phosphates



- LiMPO₄, M=Mn, Fe, Co and Ni.
- Theoretical capacity: 170 mAh/g
- Voltage plateau:
 - LiMnPO₄: 4.1 V
 - LiFePO₄: 3.45 V
 - LiCoPO₄: 4.8 V
 - LiNiPO₄: 5.1 V



Charging
Discharging



Main processes during charging/discharging

- Diffusion of Li ions
- Migration of electrons

Ionic diffusivity: $10^{-13} \sim 10^{-16} \text{ cm}^2/\text{s}$;
Electronic conductivity: $10^{-9} \sim 10^{-10} \text{ S/cm}$

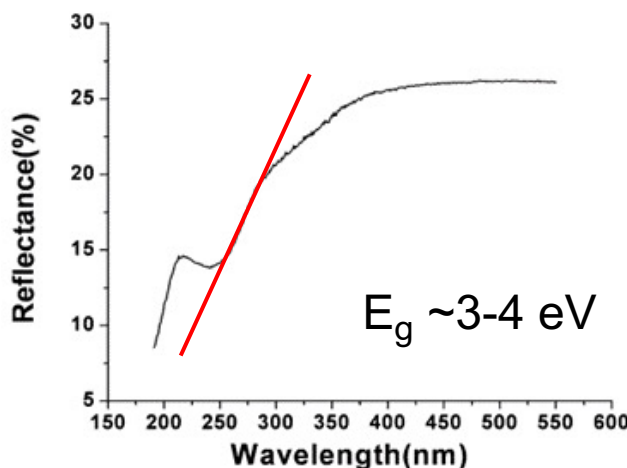
Legend:
● Li
● Fe
● P

Transport mechanism of LTMP

➤ Electronic structure

- Large band gap
- Localized valence band maximum

(Johannes et al., 2012)



UV-Vis diffusion reflectance for LiFePO₄
(Zhou et al. 2004).

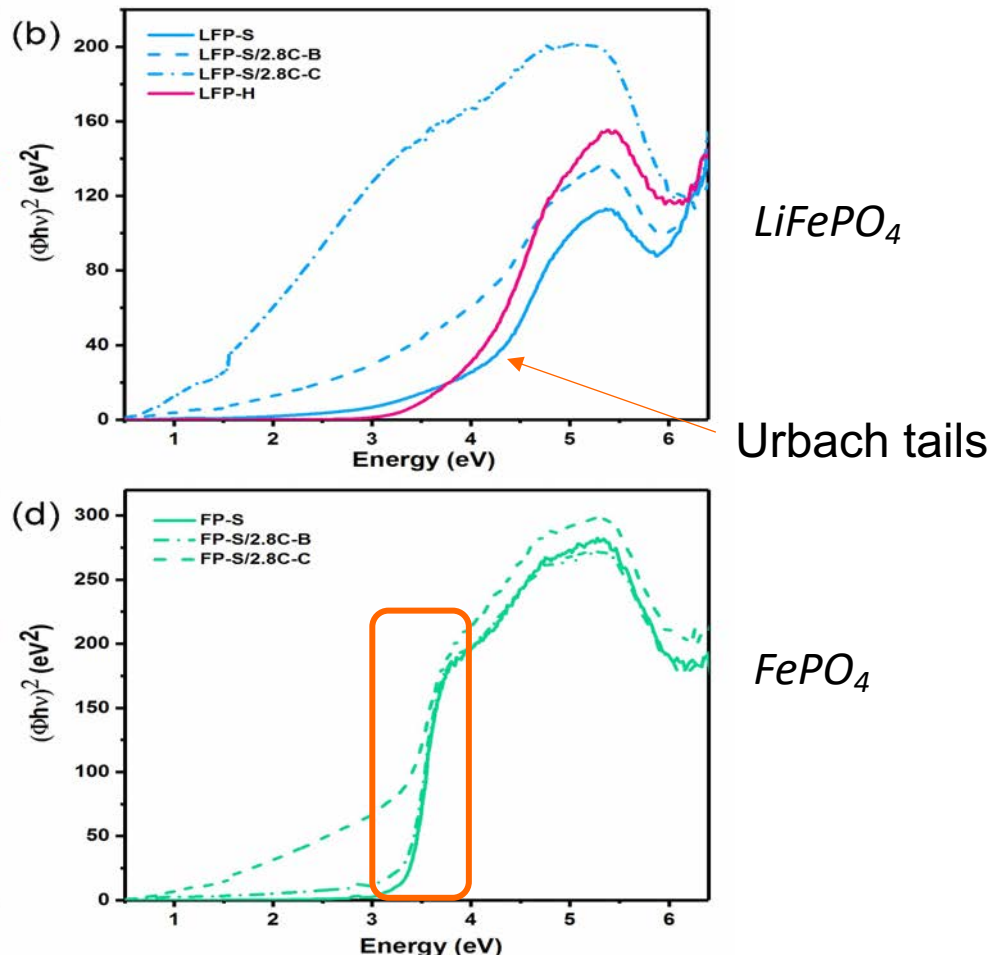
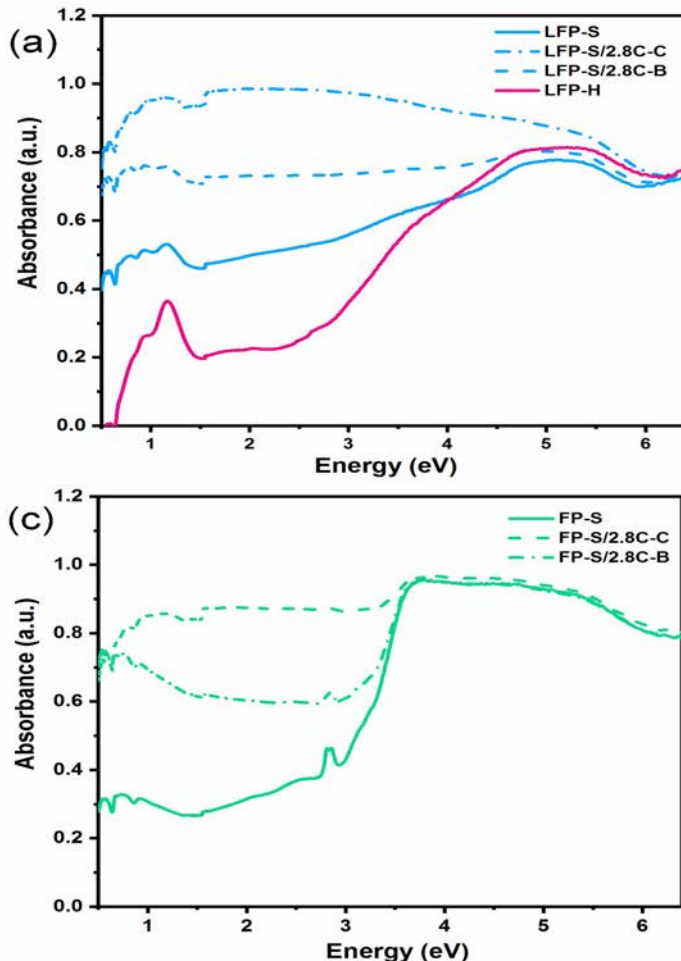
CRICOS No.00213J

➤ Small polaron hopping

- Thermally activated
- Activation energy (E_a) for LiFePO₄: 156 meV – 630 meV
- Hopping rate is related to the concentration of small polaron and Li vacancy (Hoang et al., 2011)
- $E_a = \frac{1}{4}$ optical electron transfer energy

(Furutsuki et al., 2012)

Optical absorbance and Tauc plots



UV-Vis-NIR absorbance spectra

Tauc plots (Kubelka Munk function)

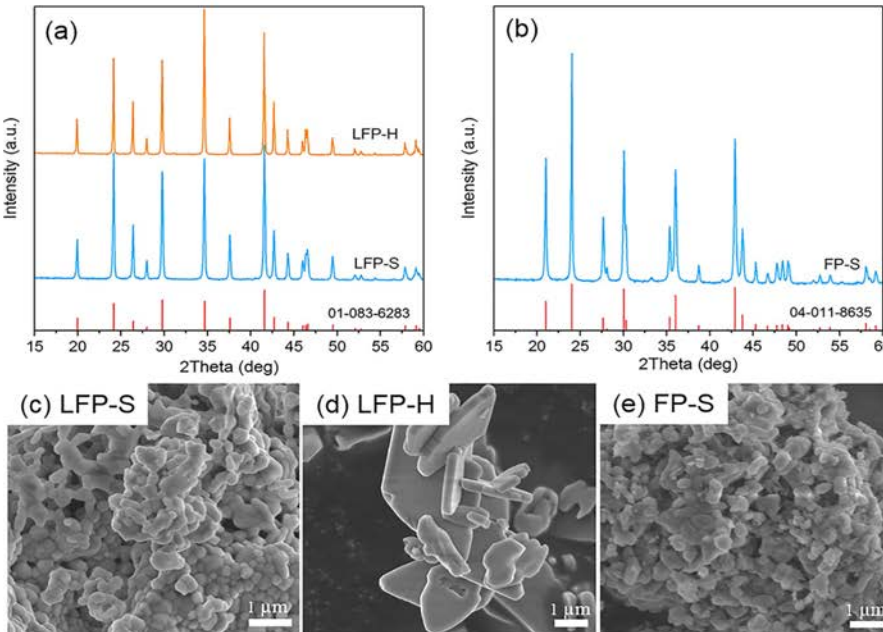
X-ray photoemission (XPS)

Samples:

LFP-H: Hydrothermal, Li:Fe:P=3:1:1

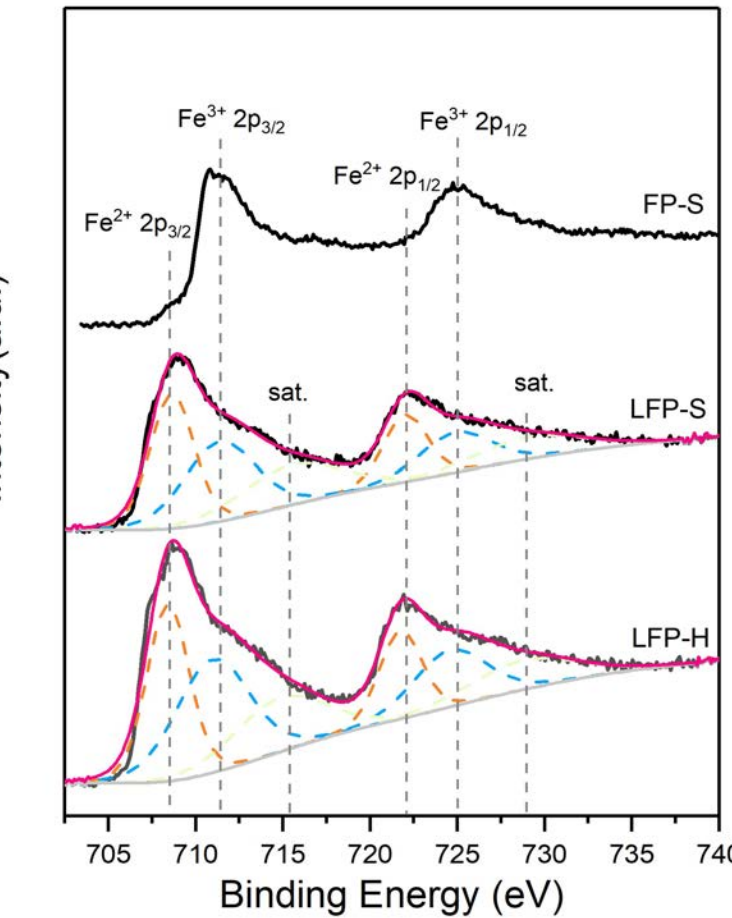
LFP-S: Solution based method, Li:Fe:P=1:1:1

FP-S: Chemically delithiated with H_2O_2



SEM micrographs and XRD patterns for the LFP samples.

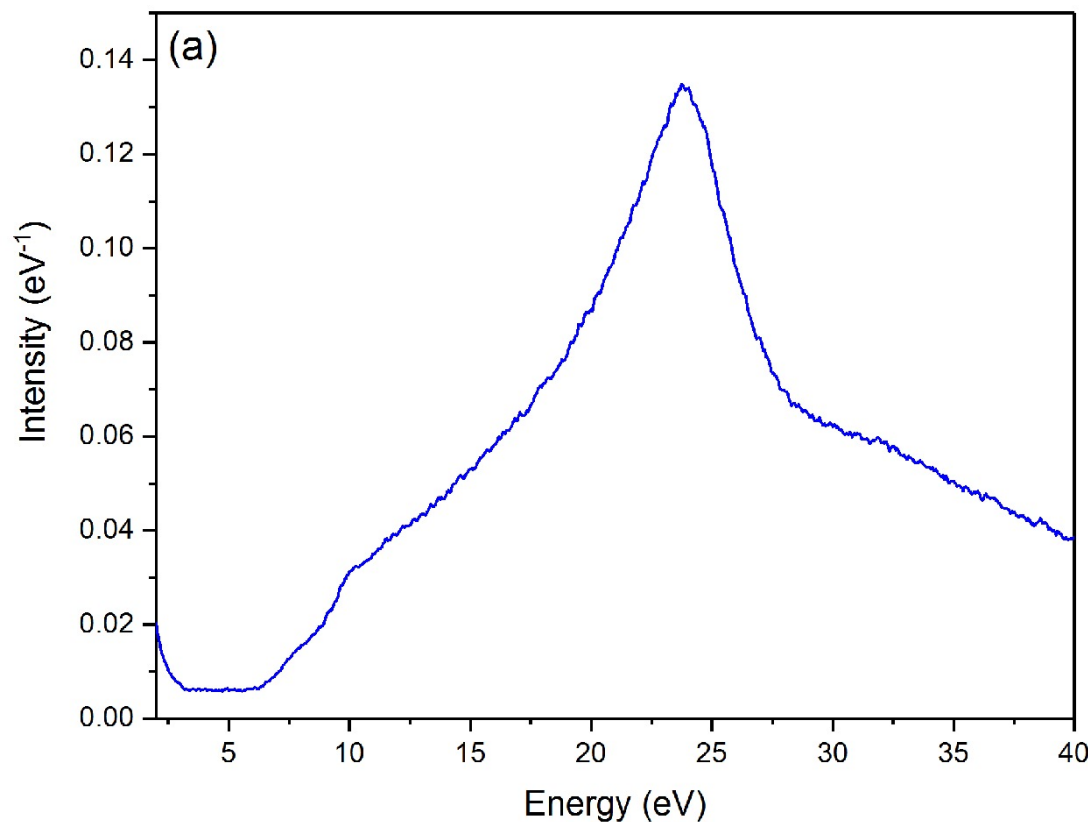
CRICOS No.00213J



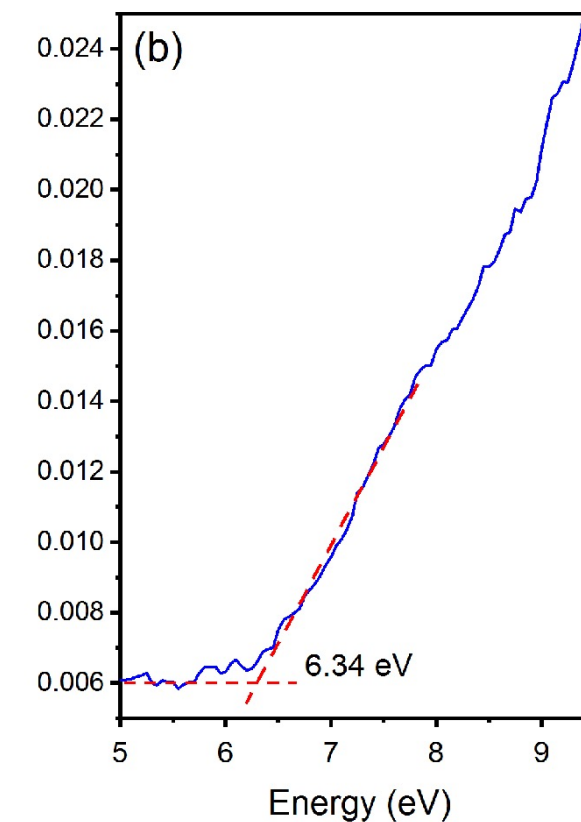
High resolution Fe-2p XPS spectra.

Y. Zhang et al., RSC Adv. 9 (2019) pp 1134-1146.

EELS in the TEM for LFeP



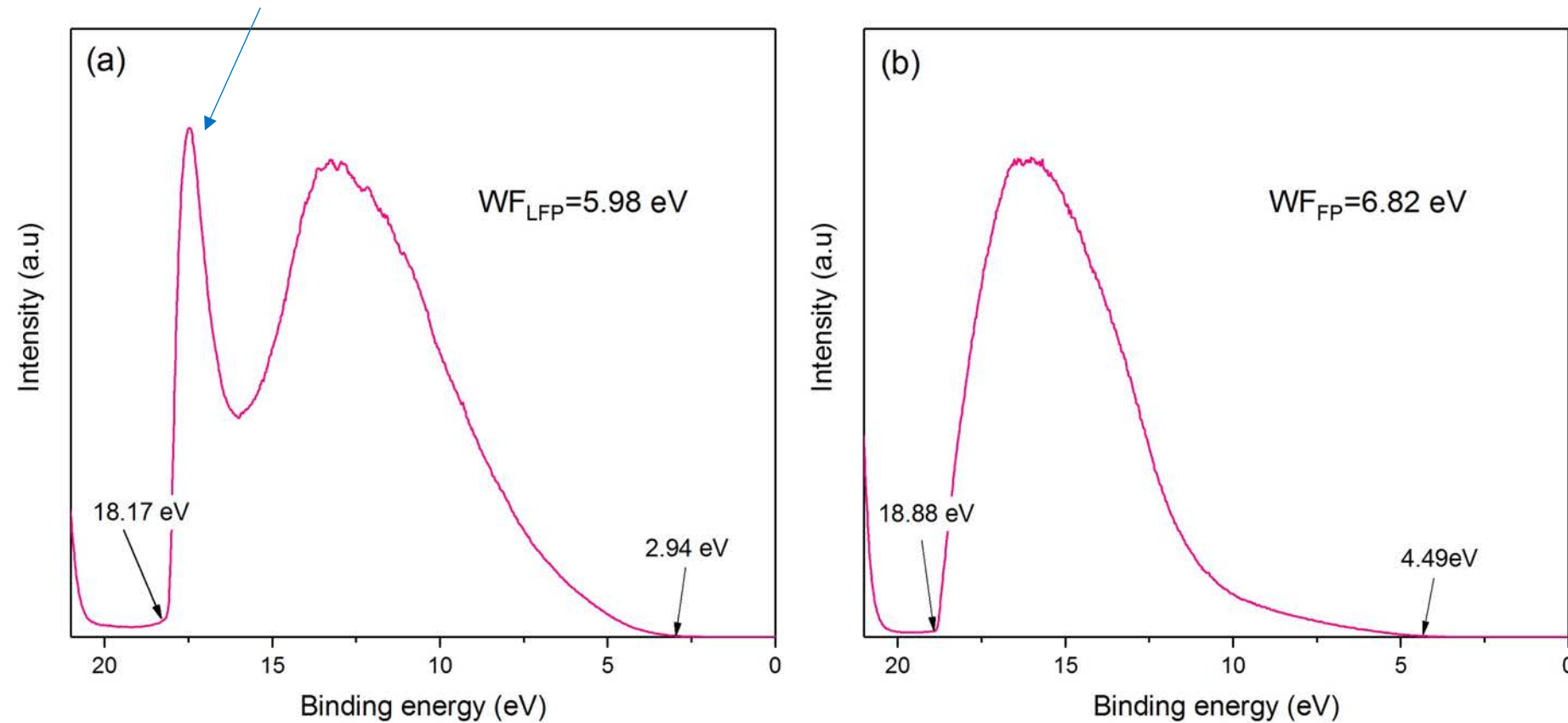
(a) Low electron energy loss spectrum (LEELS) for
 LiFePO_4 .



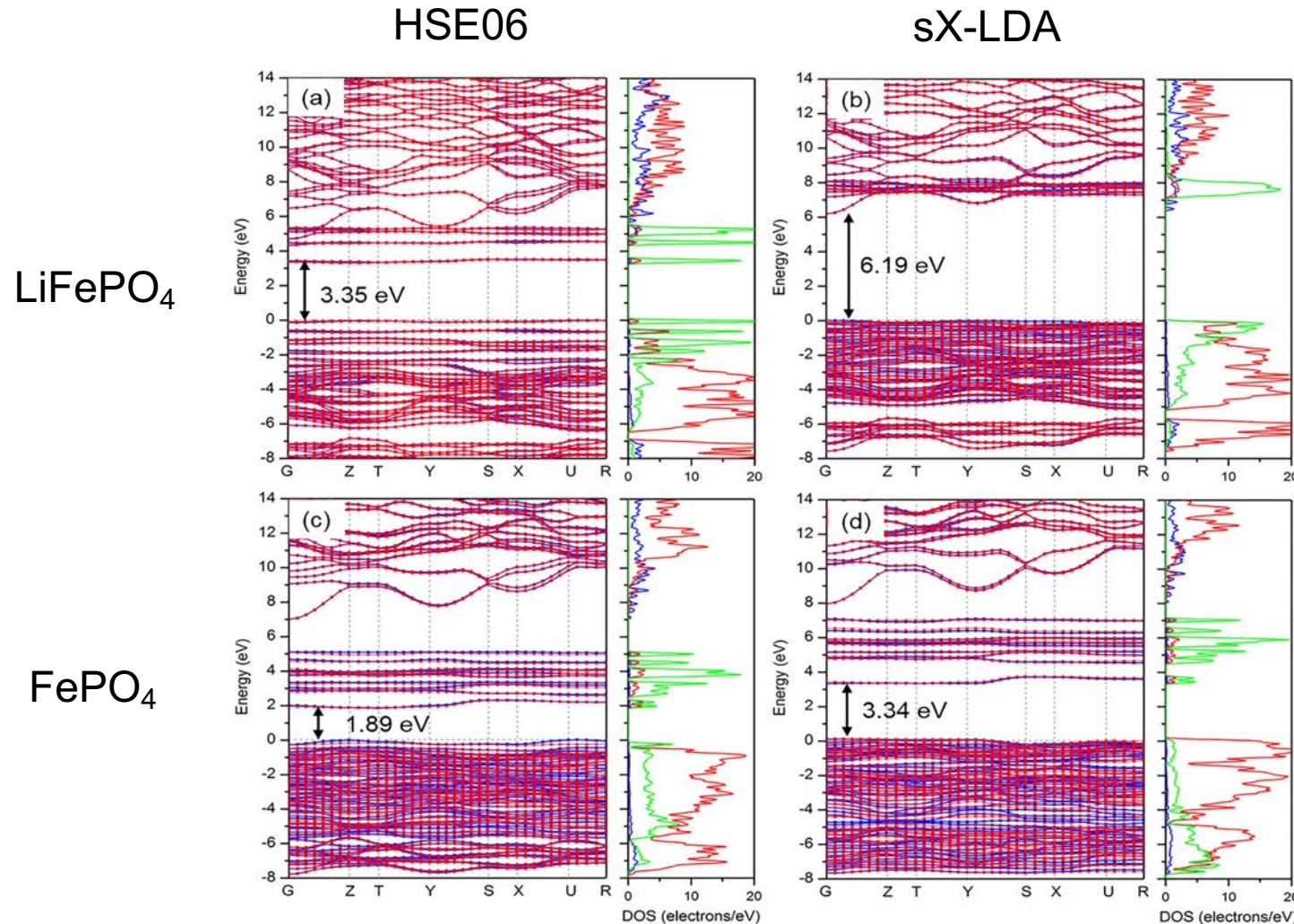
(b) Magnification of the onset of
energy loss in LEELS.

UV photoemission (UPS)

Sign of Negative electron affinity



Comparison of DFT functionals

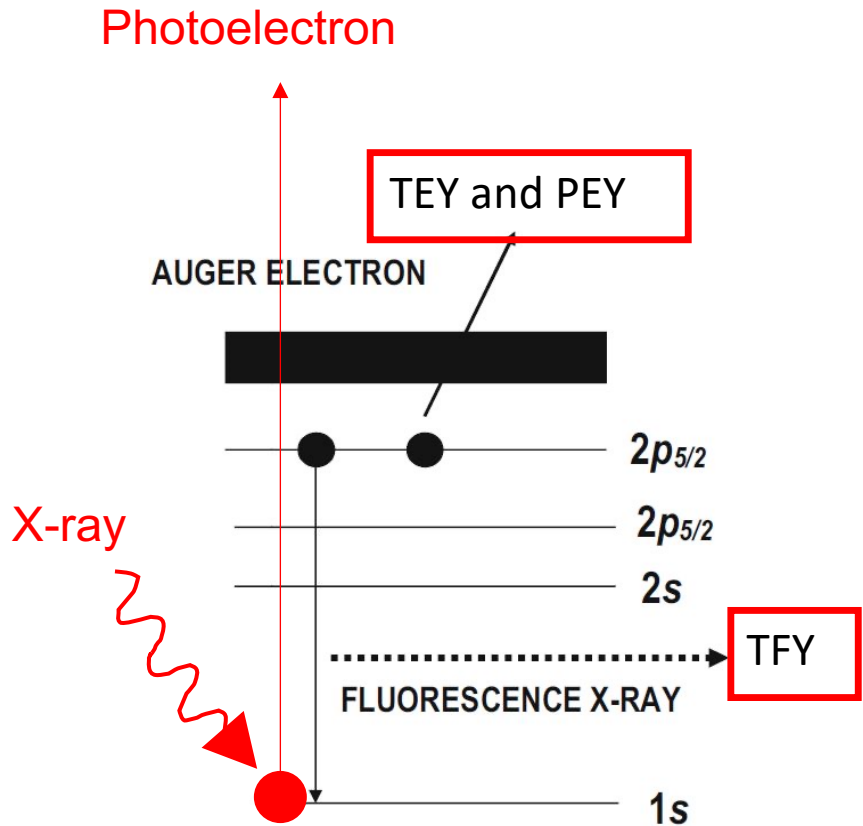


Soft X-ray Absorption Spectroscopy (Australian Synchrotron)



CRICOS No.00213J

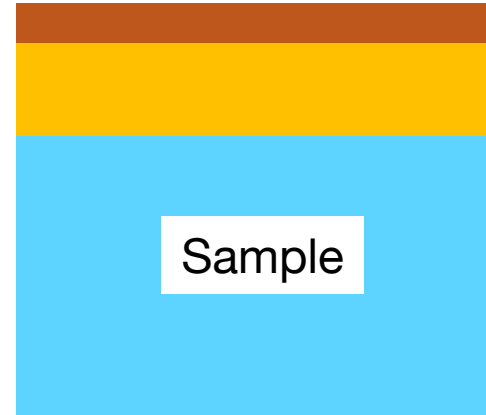
Soft X-ray Absorption Spectroscopy



PEY Surface Sensitive
 (~1nm)

TEY (~3-50nm depth)

TFY (~50-300nm depth)

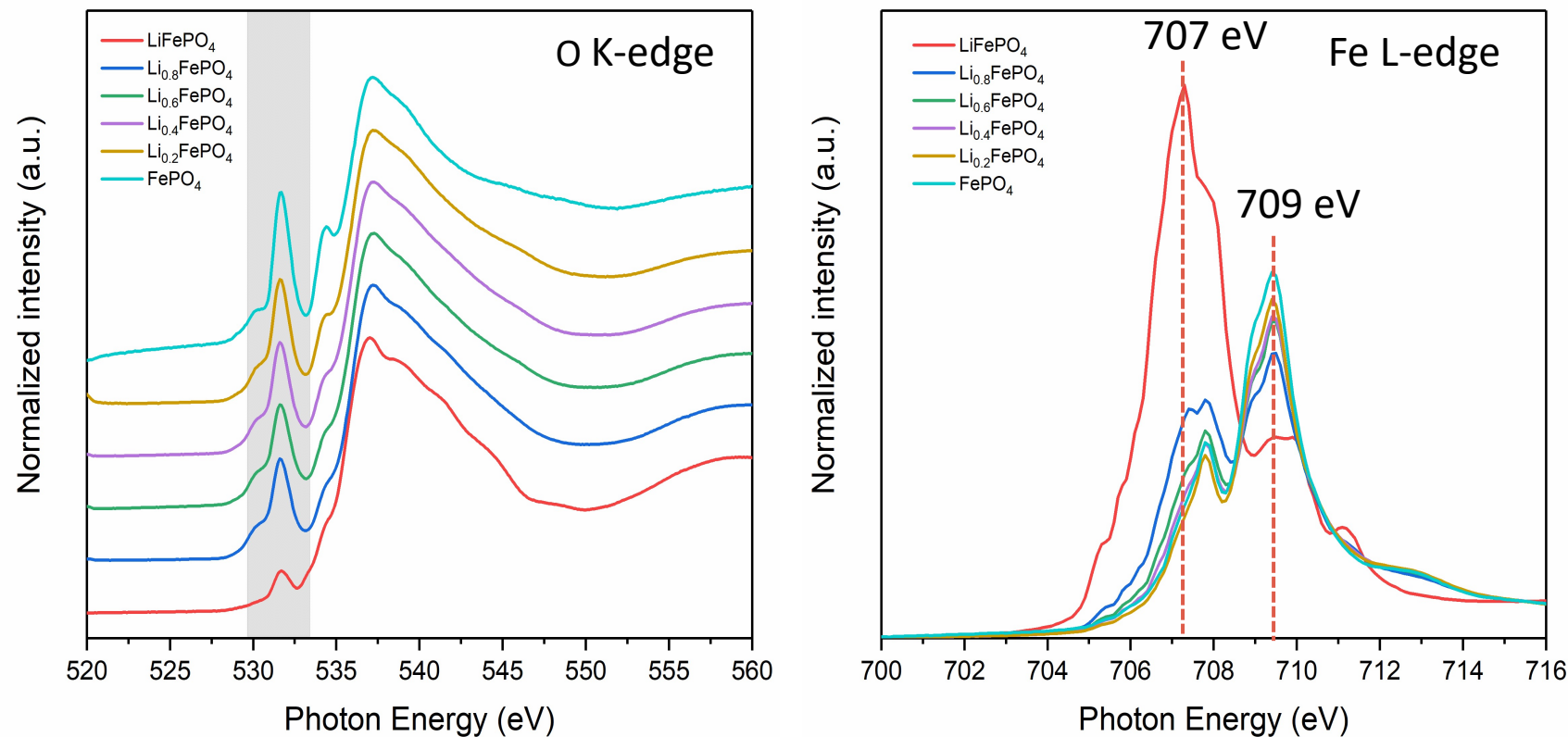


PEY – Partial Electron Yield

TEY – Total Electron Yield

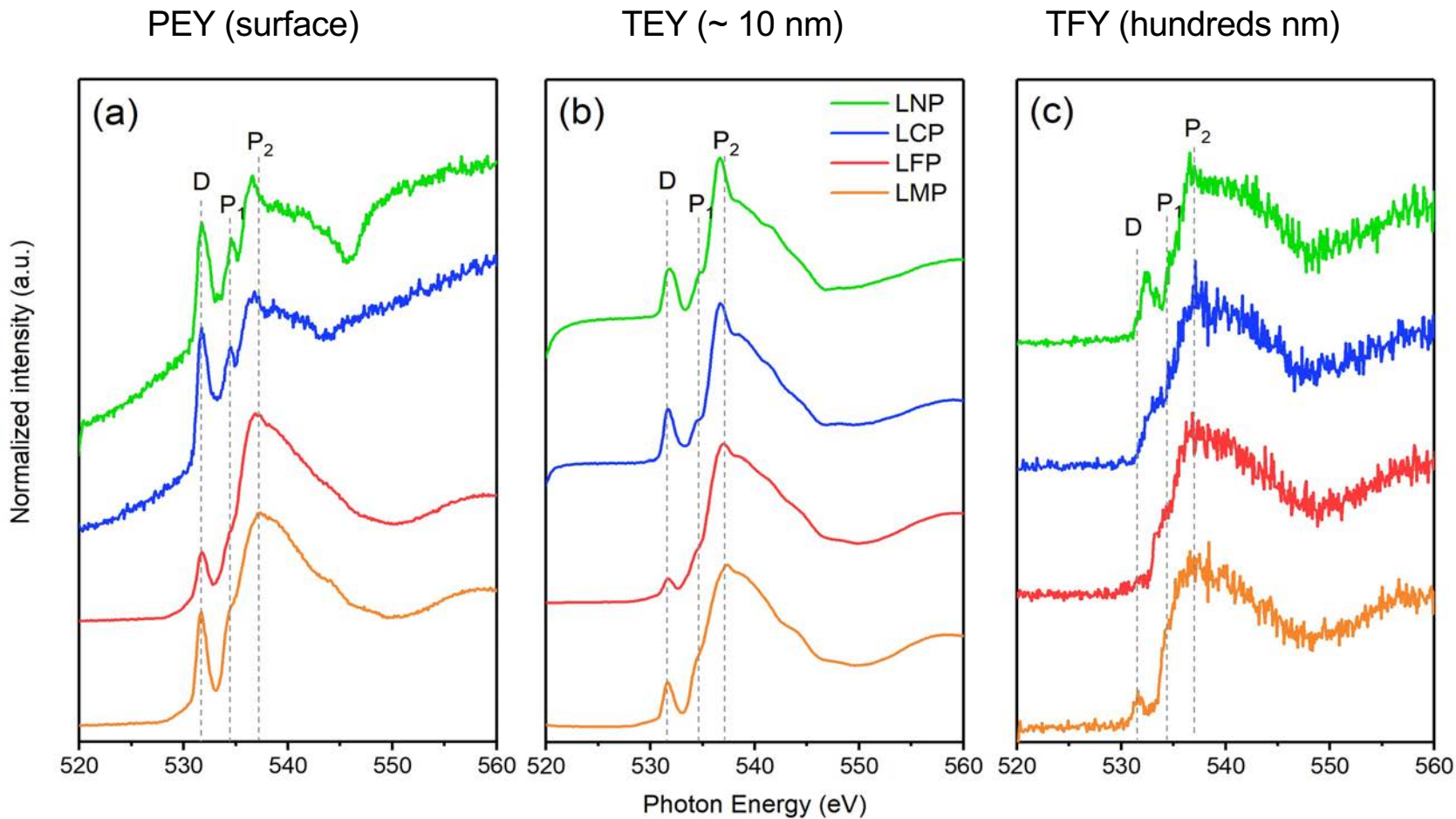
TFY – Total Fluorescence Yield

O K-edge and Fe L-edge of LFeP vs Li

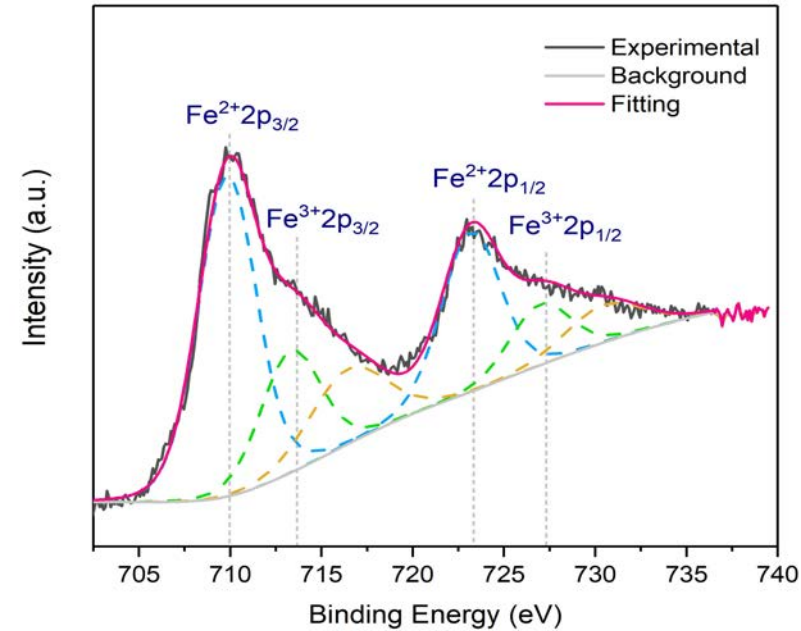
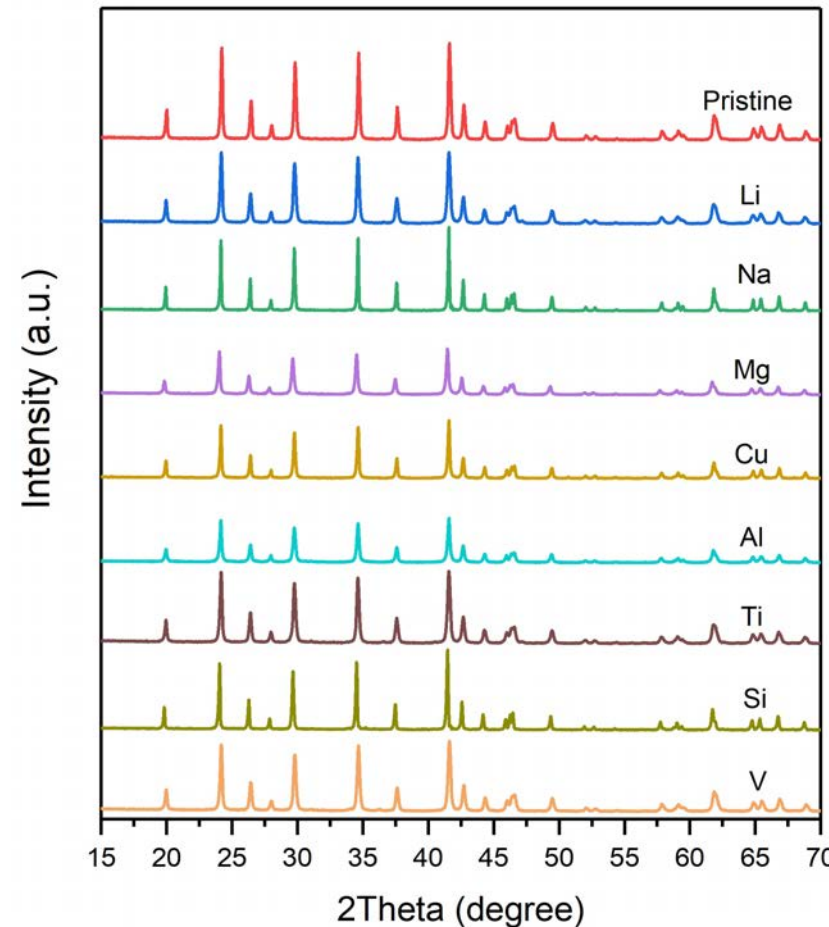


O K-edge and Fe L-edge spectra for chemically delithiated LiFePO₄ samples (TEY).

LiMPO₄ O-K edges



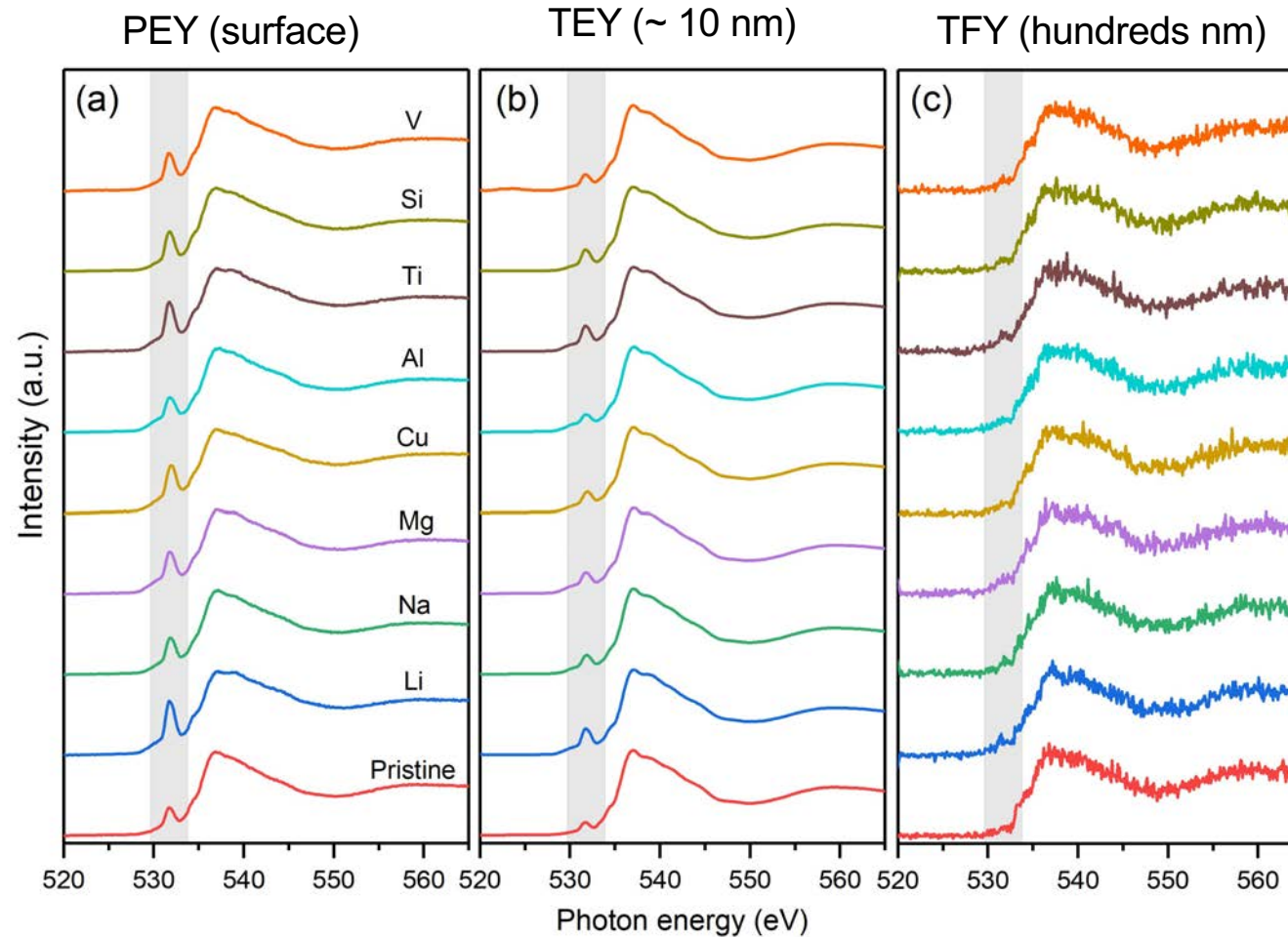
Preferential doping at the surface layer of LFeP



	Pristine	Li	Na	Mg	Cu	Al	Ti	Si	V
$\text{Fe}^{2+}\%$	0.72	0.47	0.52	0.48	0.50	0.47	0.46	0.59	0.52
$\text{Fe}^{3+}\%$	0.28	0.53	0.48	0.52	0.50	0.53	0.54	0.41	0.48

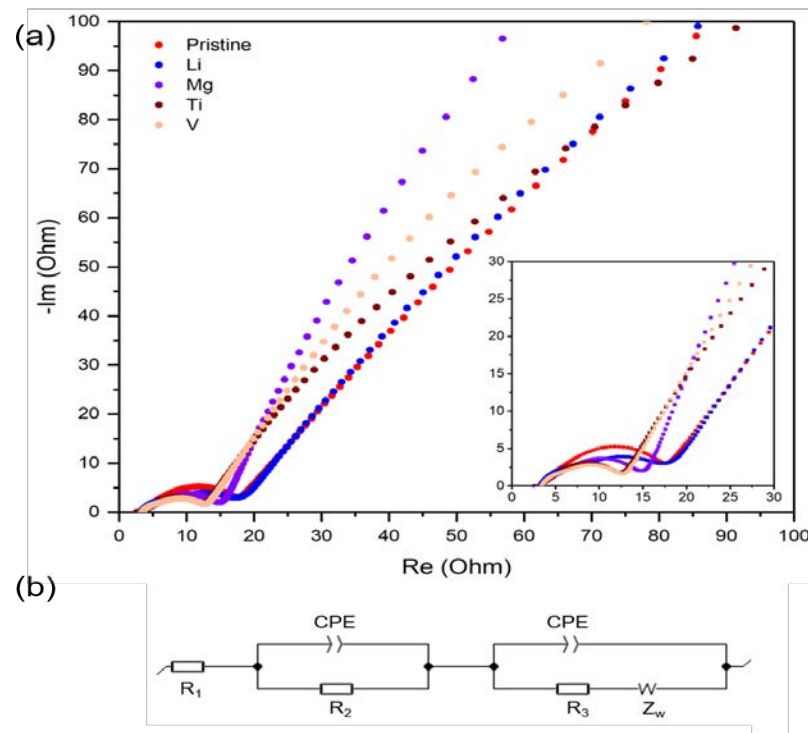
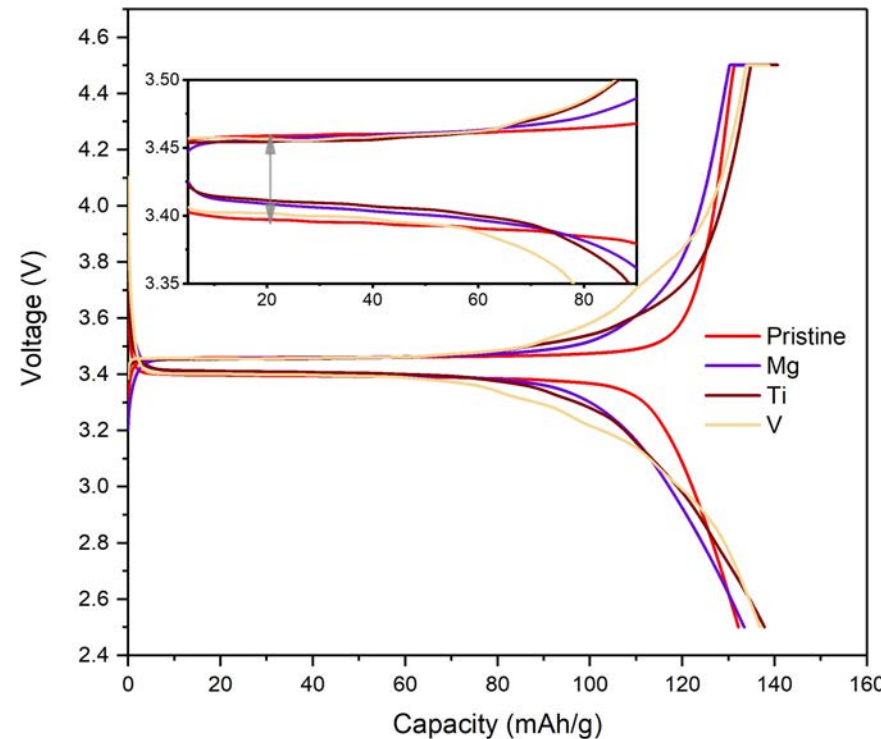
XRD patterns for the pristine and doped LiFePO_4 samples.

Preferential doping at the surface layer of LiFePO₄



O K-edge spectra for the pristine and doped LiFePO₄ samples with (a) PEY, (b) TEY and (c) TFY modes.

Preferential doping at the surface layer of LFeP



	Pristine	Li	Mg	Ti	V
R_1/Ω	3.22	3.20	3.51	3.72	3.62
R_2/Ω	16.34	4.91	2.93	1.25	4.03
R_3/Ω	12.8	7.12	8.09	7.37	4.04
Polarization/mV	61.8	-	48.1	43.3	54.5

Transmission Electron Microscopy

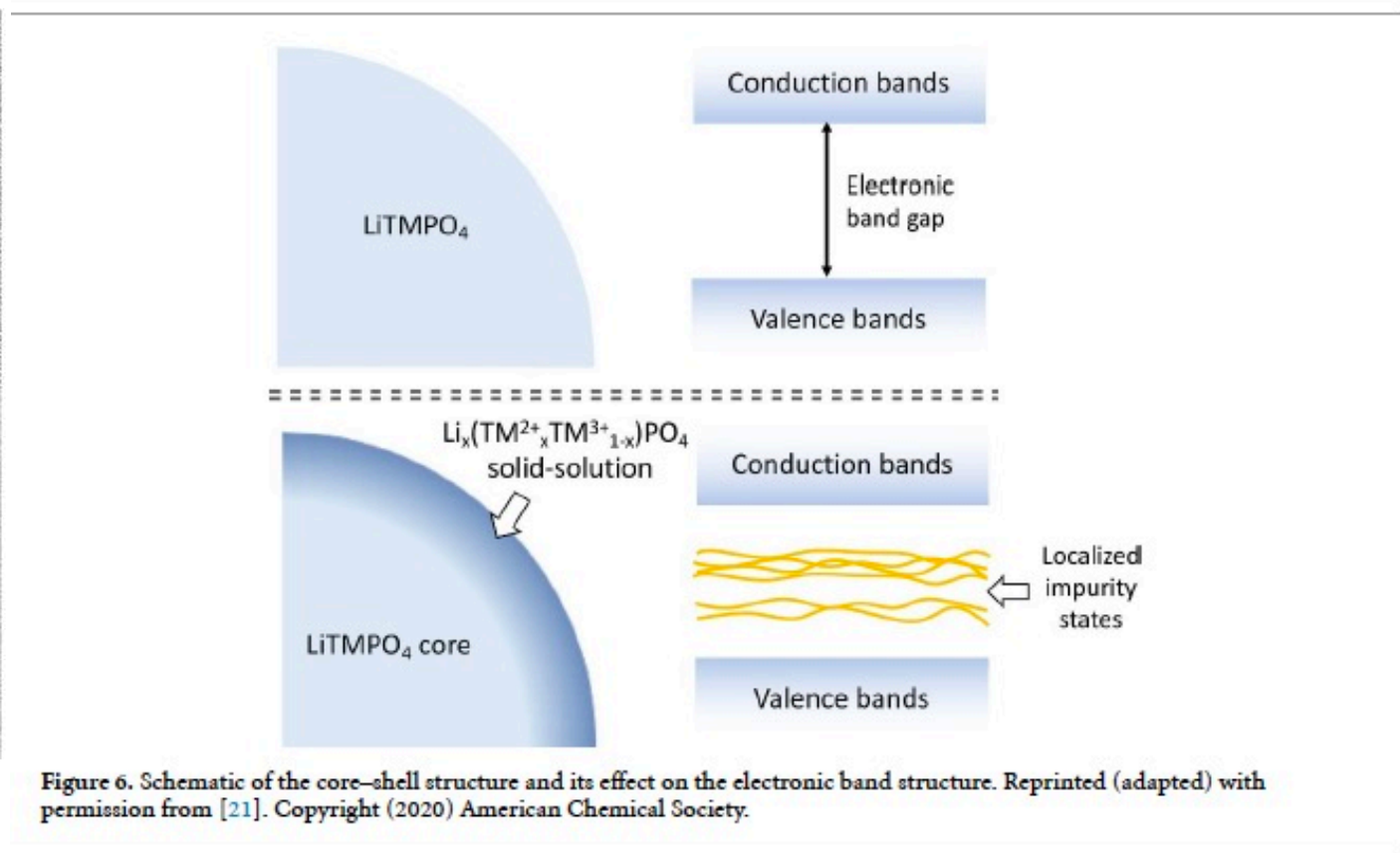
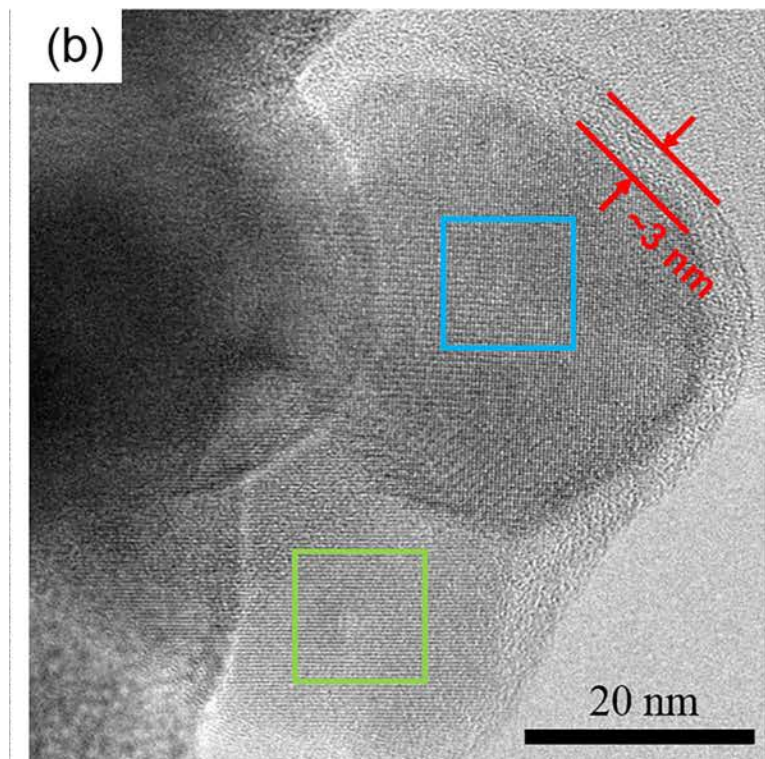
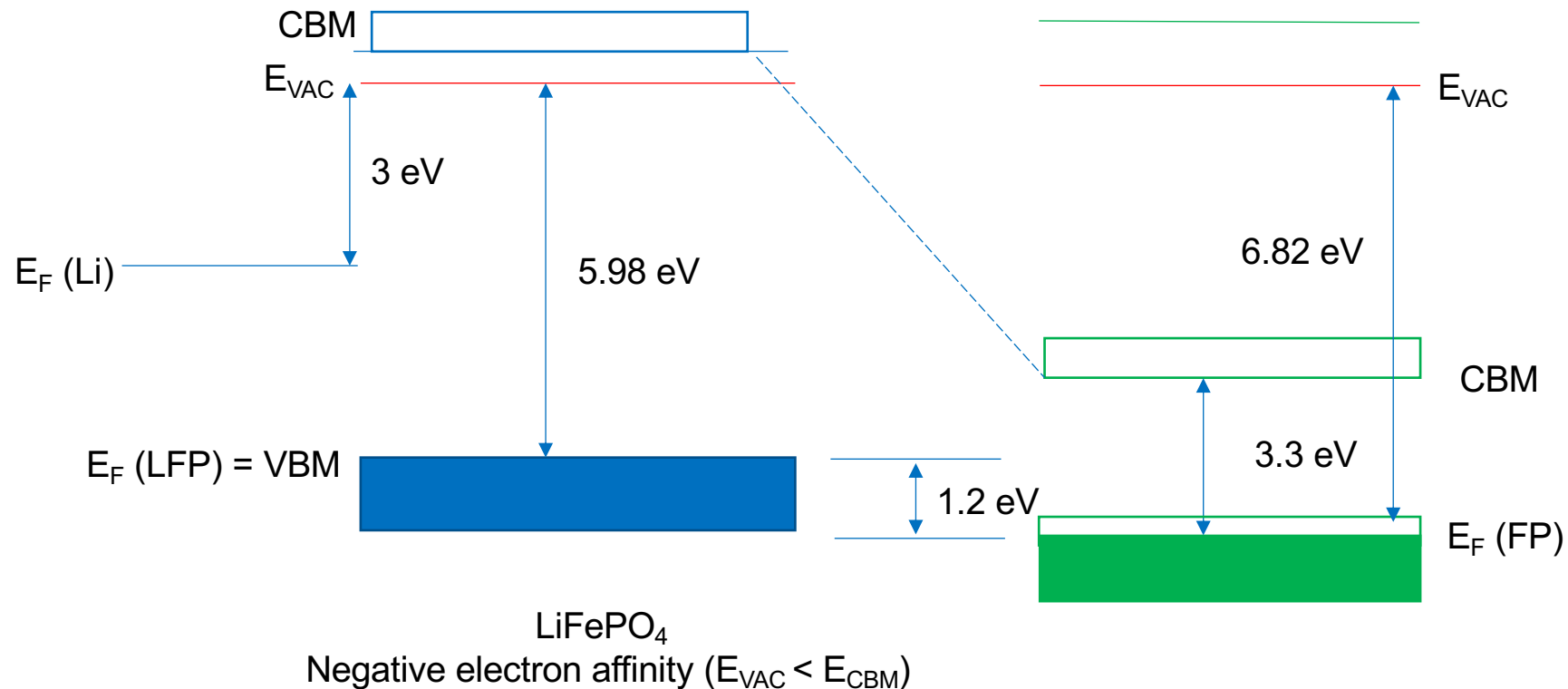


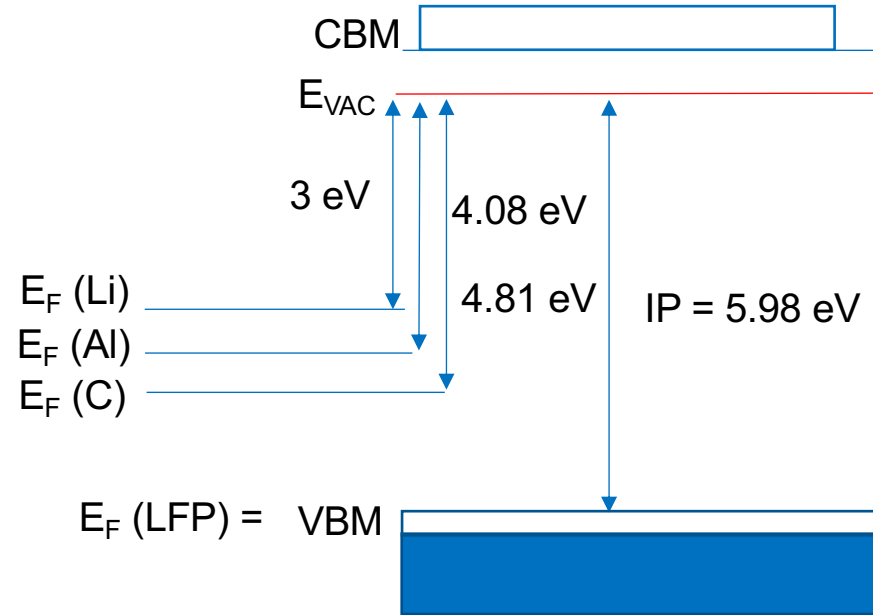
Figure 6. Schematic of the core–shell structure and its effect on the electronic band structure. Reprinted (adapted) with permission from [21]. Copyright (2020) American Chemical Society.

Junction effects

Before Contact



WF (Cu) = 4.7 eV
WF (Al) = 4.08 eV

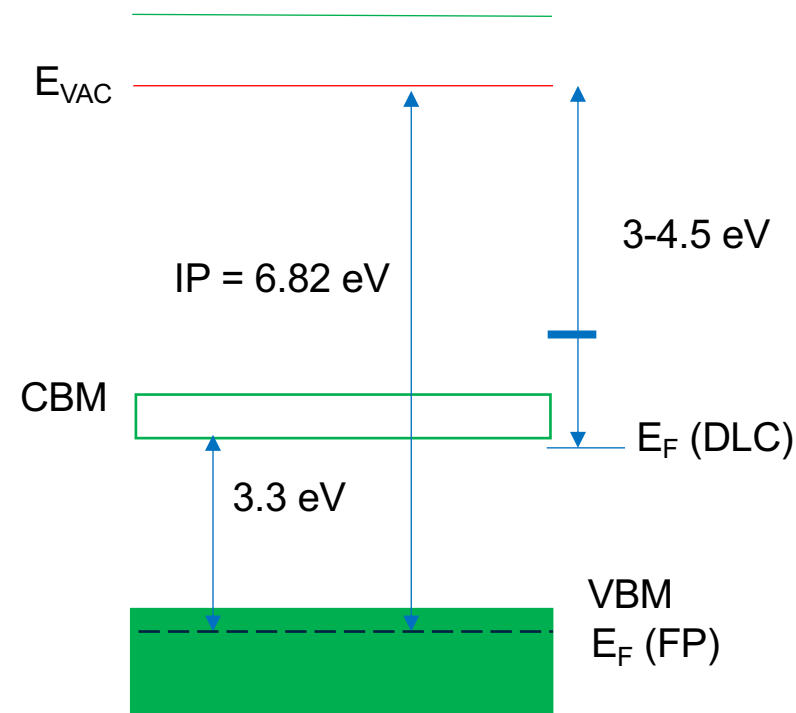


LiFePO₄
Negative electron affinity ($E_{VAC} < E_{CBM}$)

After Contact

WF (Less dense graphitic C) = 3.5 - 6 eV [ref Neuville]

WF (denser DLC) = ~ 2-3 eV [ref Neuville]



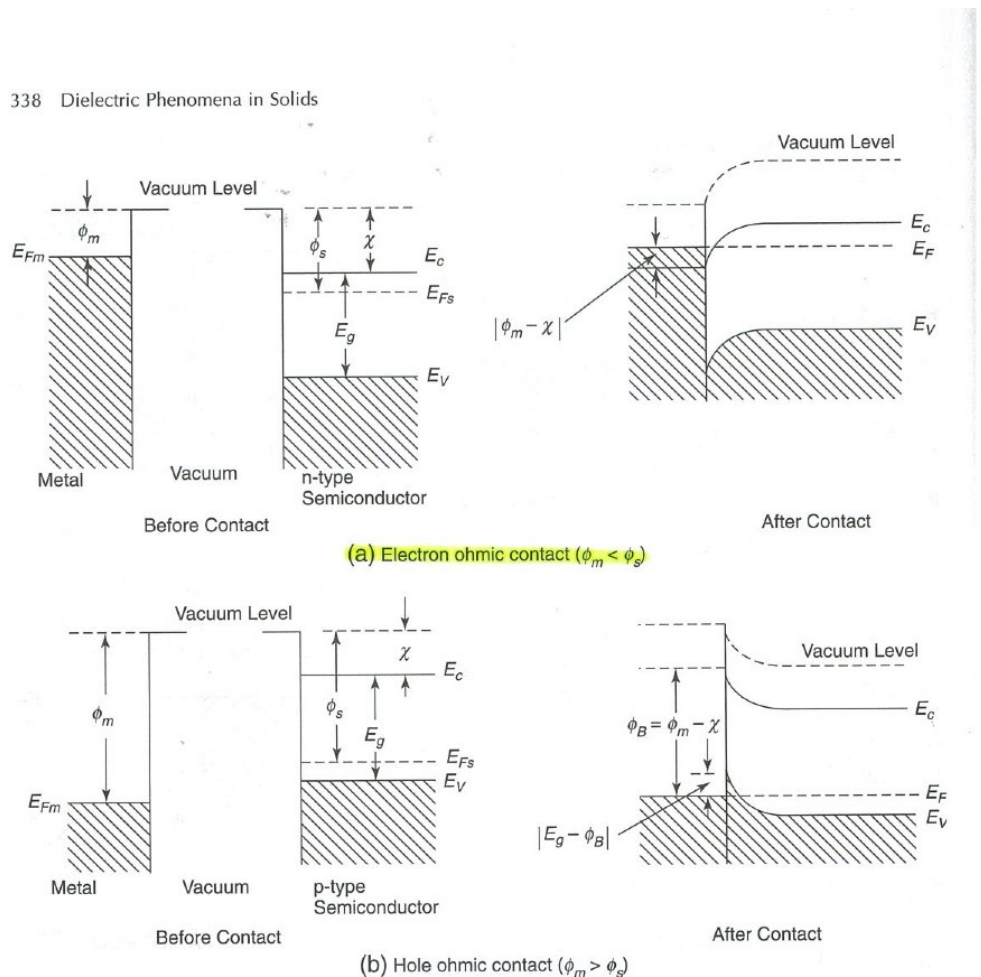


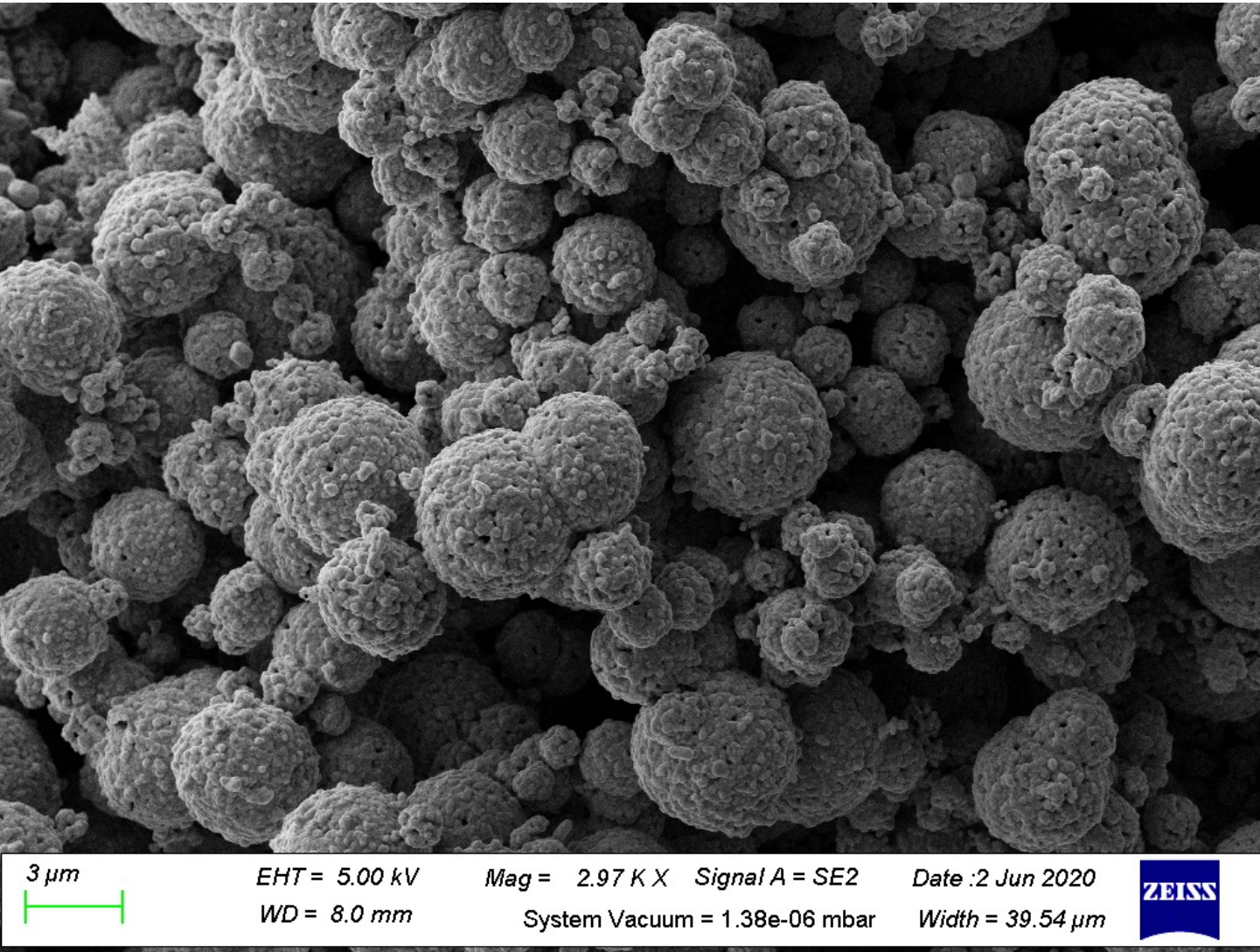
Figure 6-5 Energy level diagrams for an ohmic contact between a metal and an extrinsic semiconductor: (a) n-type, (b) p-type.

It is usually difficult to find a suitable metal with $\phi_m < \phi_s$ for the ohmic contact to n-type semiconductors, or with $\phi_m > \phi_s$ for the ohmic contact to p-type semiconductors. Furthermore, most semiconductors for electronic devices are covalently bonded, so they have surface states. For these reasons, it is not possible to produce an ohmic contact simply based on method 1. Even though it may be possible for other semiconductors, it is still not practical, because the behavior of such ohmic contacts is not reproducible.

The method for obtaining good, reliable ohmic contacts for most semiconductor devices

is based on method 2, that is, producing a very thin layer heavily doped with dopants by either diffusion or ion implantation techniques in order to make this layer become degenerate. Such a layer is called the n^+ layer for n-type semiconductors and the p^+ layer for p-type semiconductors. After this layer has been produced, any metal or alloy can be deposited on the surface of this layer to form a good ohmic contact.

Let us take the ohmic contact for n-type semiconductors as an example. The n^+ layer provides a narrow barrier width for electrons to tunnel quantum-mechanically from the metal

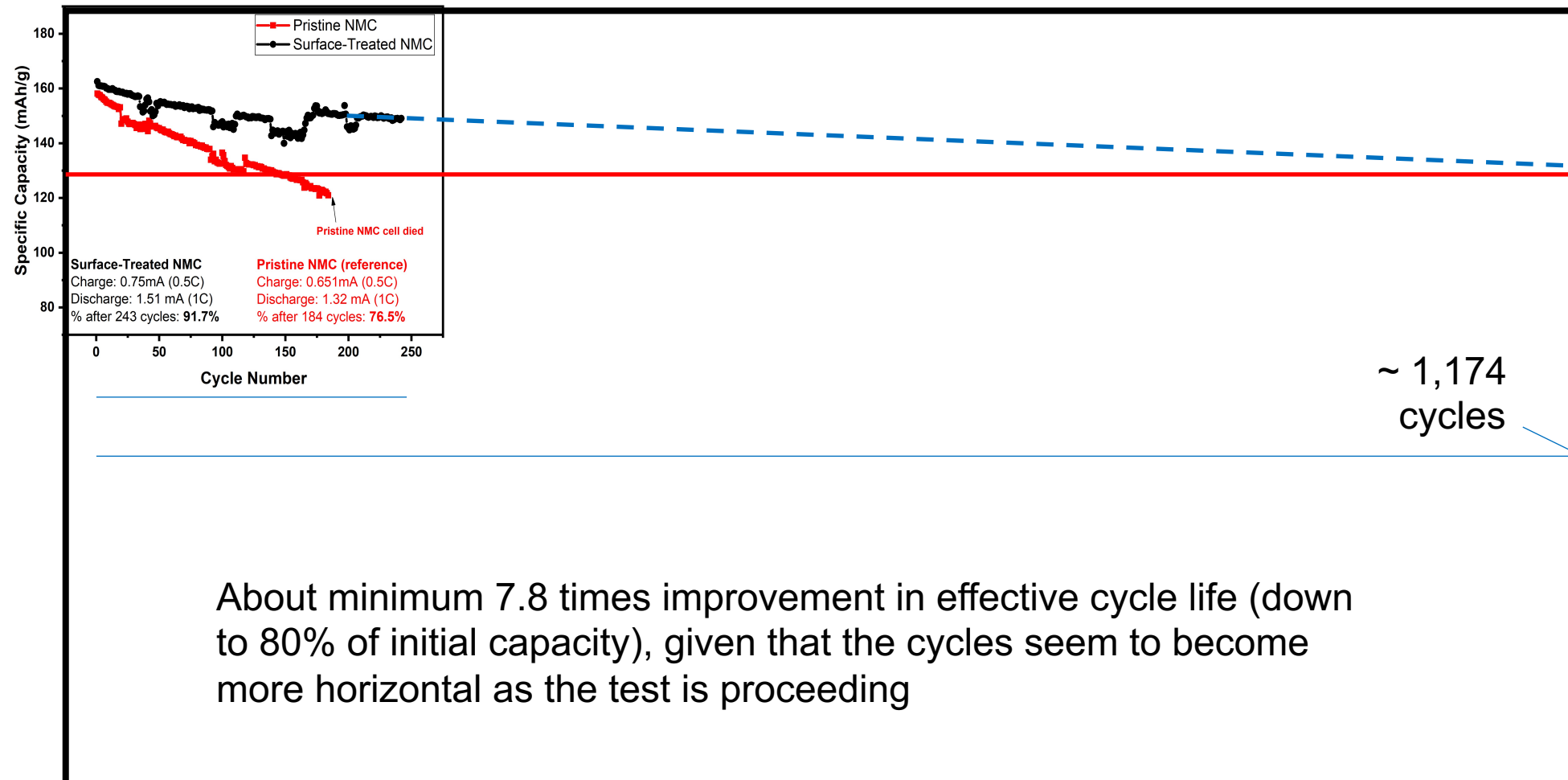


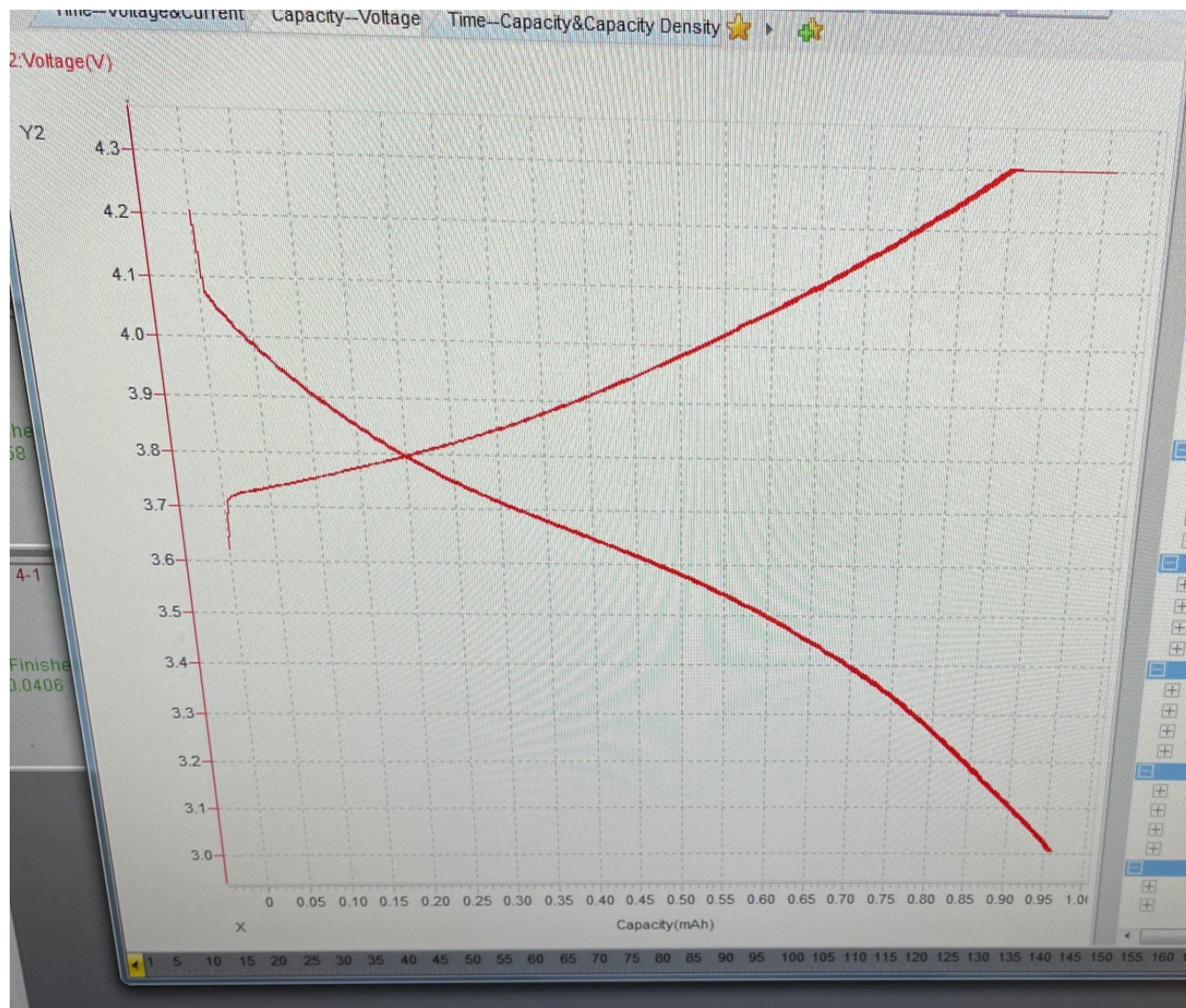
CRICOS No.00213J

jose.alarco@qut.edu.au



Accelerated cycle test (at 1C for discharge)





CRICOS No.00213J

jose.alarco@qut.edu.au

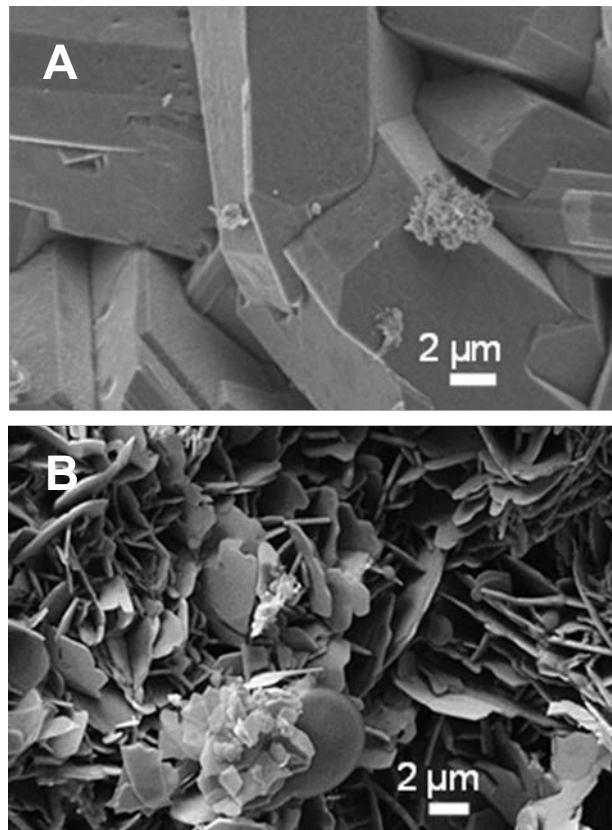


Example of DFT use for improved understanding of superconductor materials symmetry and insight on mechanisms

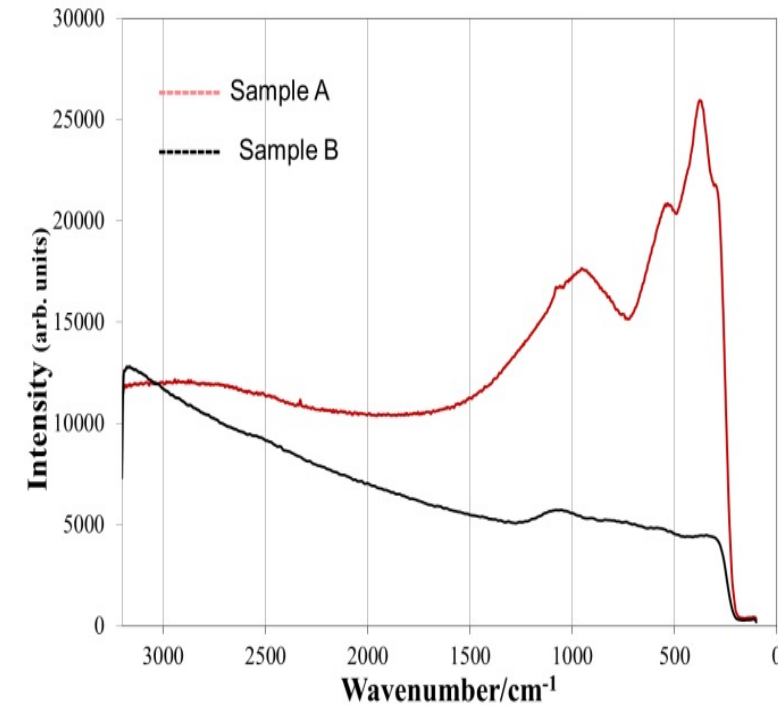
Metal borides synthesis in small Parr reactor

MgB_2 – SEM/Raman

SEM of MgB_2 samples



Raman

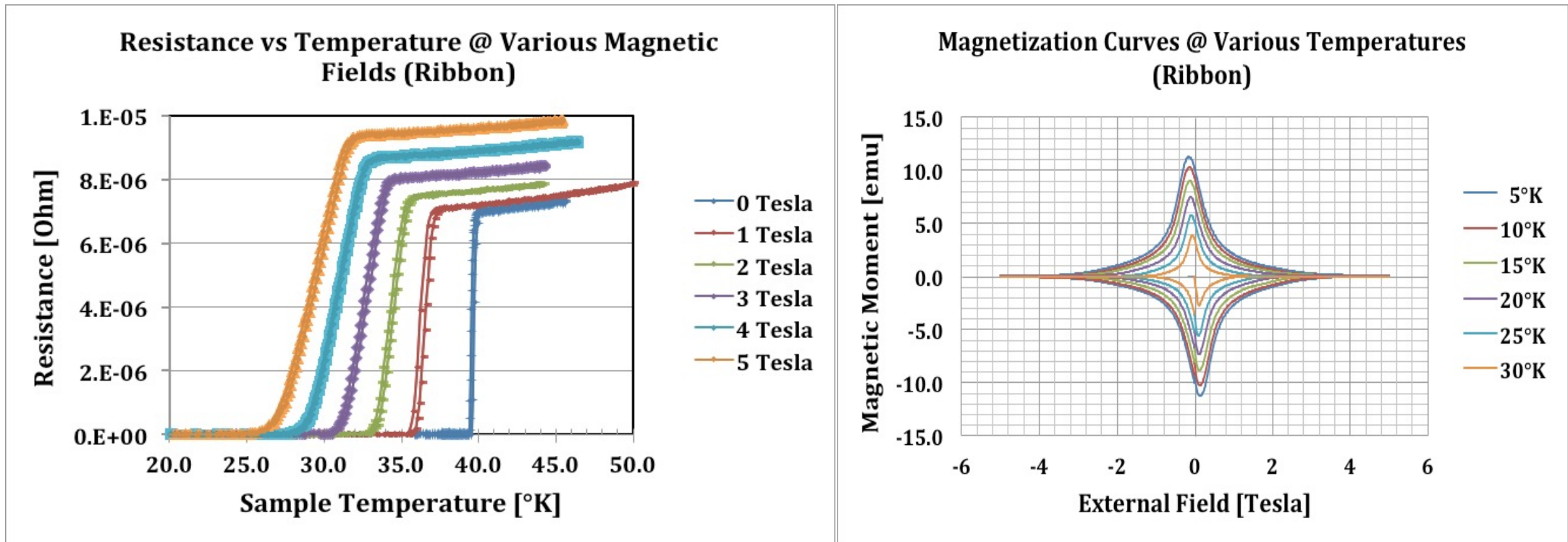


Mackinnon, I.D.R. et al., *Materials*, (2014), 7, 3901-3918.

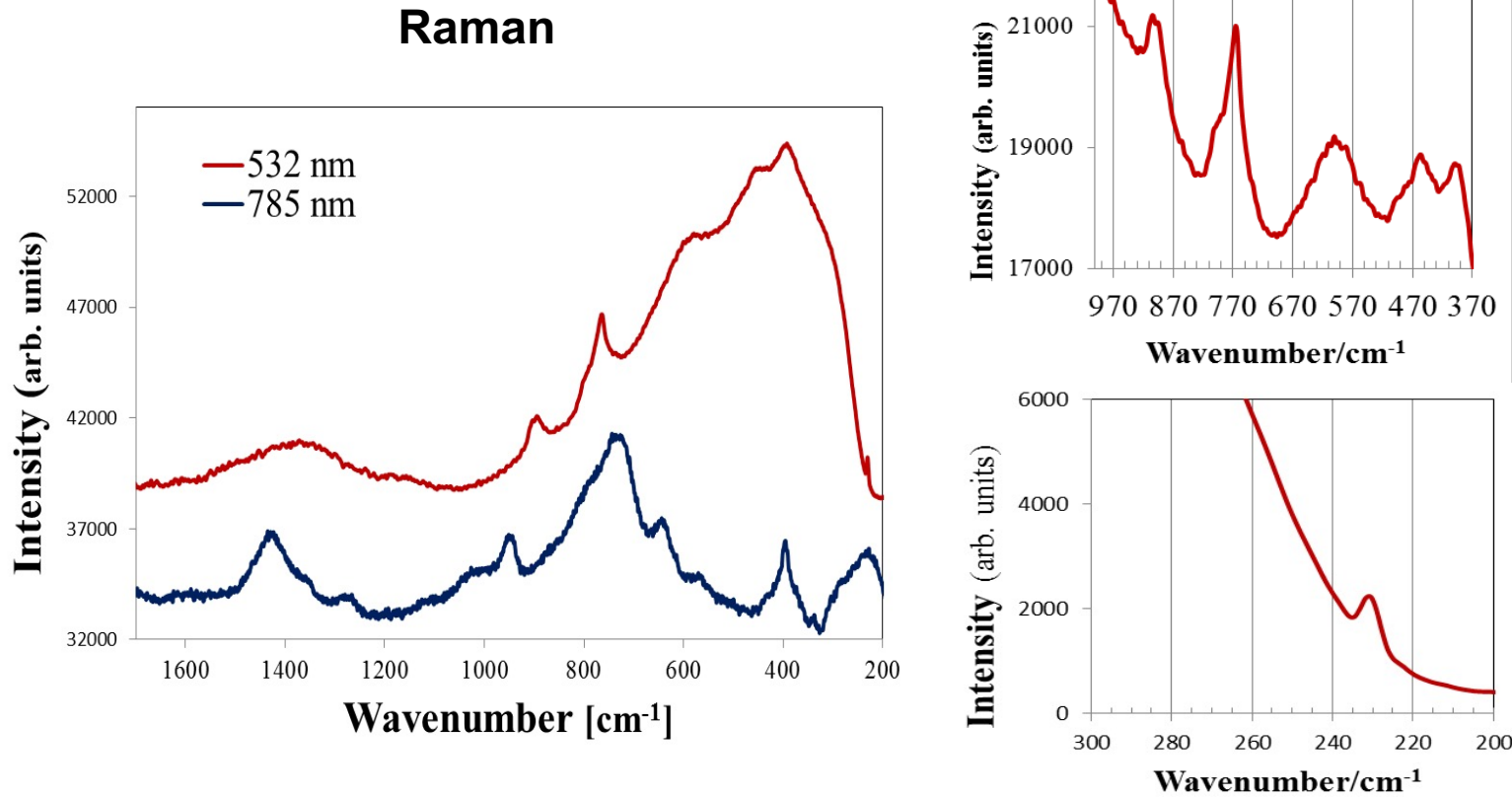
CRICOS No.00213J

Alarco *et al.*, *Phys. Chem. Chem. Phys.*, **16**, 24443-24456, 2014

MgB₂ - Properties



MgB₂ - Raman

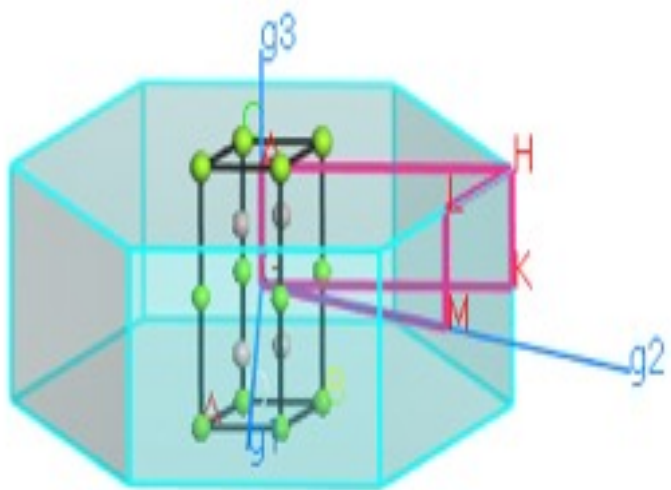


Alarco *et al.*, Phys. Chem. Chem. Phys., **16**, 24443-24456, 2014

MgB₂ – Group Analysis

Frequency (cm ⁻¹)	Group												
	P6		P-6		P6/m		P622		P6mm		P-6m2		P6/mmm
	168		174		175		177		183		187		191
	IR	R	IR	R	IR	R	IR	R	IR	R	IR	R	IR
E _{2g} modes	Y	Y	Y	Y	Y	N	Y	Y	Y	Y	Y	Y	N
	Y	Y	Y	Y	Y	N	Y	Y	Y	Y	Y	Y	N
	Y	Y	Y	N	Y	N	Y	N	Y	Y	N	Y	N
	N	Y	Y	Y	N	Y	N	Y	N	Y	Y	N	Y
	N	Y	Y	Y	N	Y	N	Y	N	Y	Y	N	Y
	N	N	Y	N	N	N	N	N	N	Y	N	N	N

MgB₂ - Super-lattice modes



Frozen phonon technique
results in similar symmetry
reductions

Frequency (cm ⁻¹)	Group							
	P3c1		P-3c1		P63mc		P-6c2	
	158		165		186		188	
	IR	R	IR	R	IR	R	IR	R
233.4	Y	Y	Y	N	N	Y	N	Y
233.4	Y	Y	Y	N	N	Y	N	Y
237.4	Y	Y	N	Y	N	Y	Y	Y
237.4	Y	Y	N	Y	N	Y	Y	Y
336.4	N	N	N	N	N	N	N	N
343.0	Y	Y	Y	N	Y	Y	Y	Y
343.0	Y	Y	Y	N	Y	Y	Y	Y
395.4	N	N	N	N	N	N	N	N
415.9	Y	Y	Y	N	Y	Y	Y	N
534.9	Y	Y	Y	N	Y	Y	Y	Y
534.9	Y	Y	Y	N	Y	Y	Y	Y
426.1-580.8*	Y	Y	N	Y	N	Y	Y	Y
426.1-580.8*	Y	Y	N	Y	N	Y	Y	Y
657.0	N	N	N	N	Y	Y	N	N
712.4	Y	Y	N	Y	N	N	Y	N

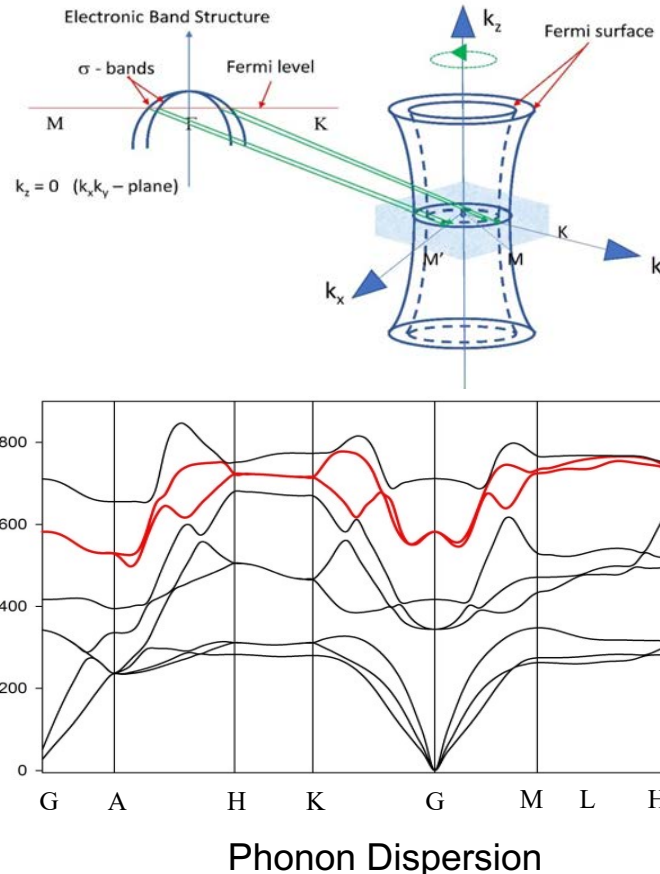
Alarco *et al.*, Phys. Chem. Chem. Phys., **16**, 24443-24456, 2014

Motivation

Density Functional Theory (DFT)



Signatures of superconductivity



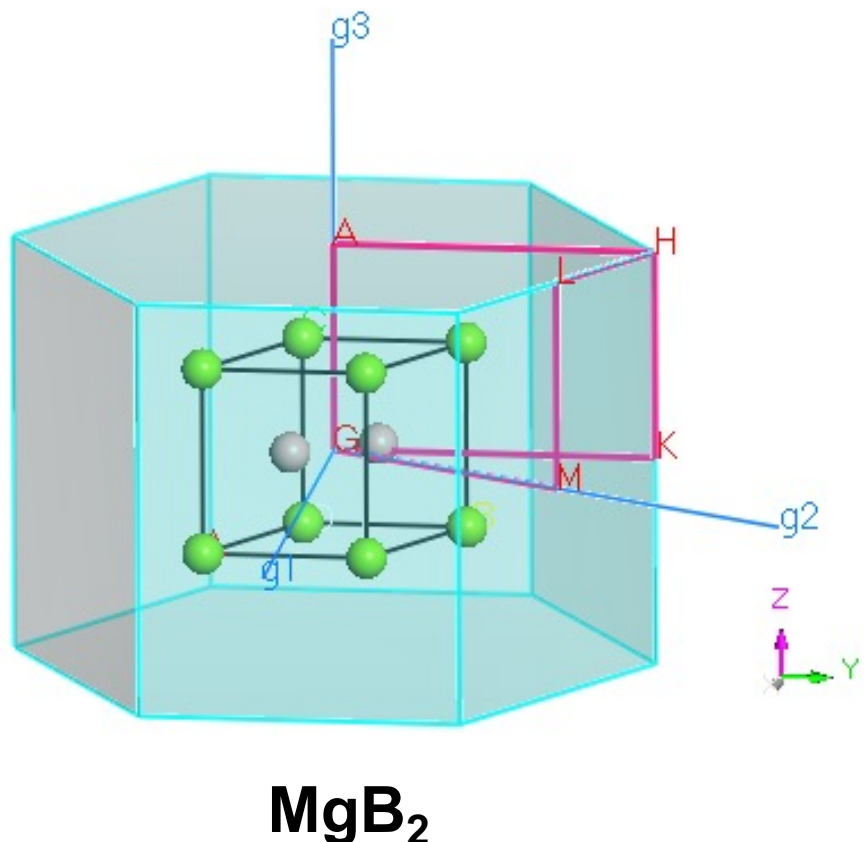
Identify key features in:
Electronic Band Structure
Fermi surface
Phonon dispersion

Complementary to Eliashberg Equations (uses normal state parameters)

Maintain ab-initio approach
Reciprocal geometrical information

Transform back to real space geometry

MgB₂ – choice for benchmarking



Good

Simple structure with few atoms – good for computation
Extensively investigated experimentally and theoretically – good for validation
Multiple effects that influence the superconducting transition temperature (Tc)

- Isotope effects
- Metal substitutions
- Pressure effects

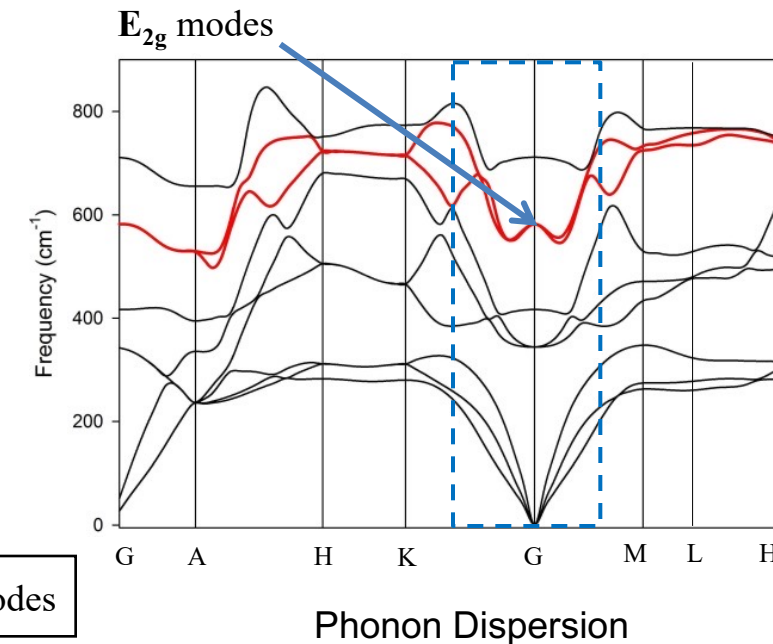
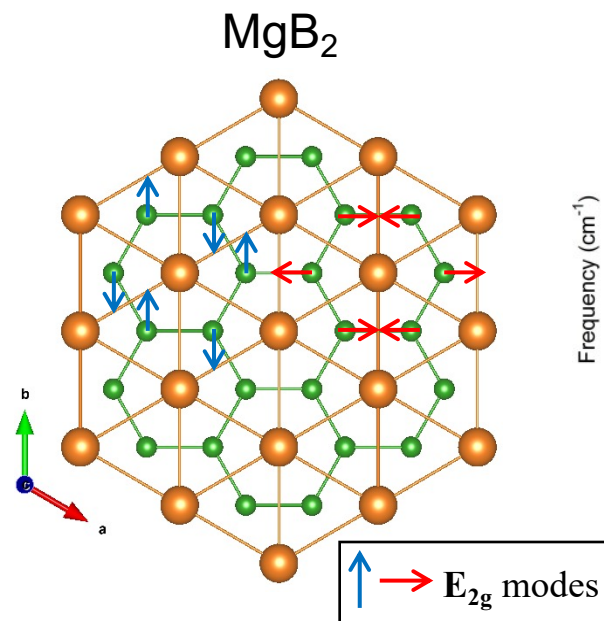
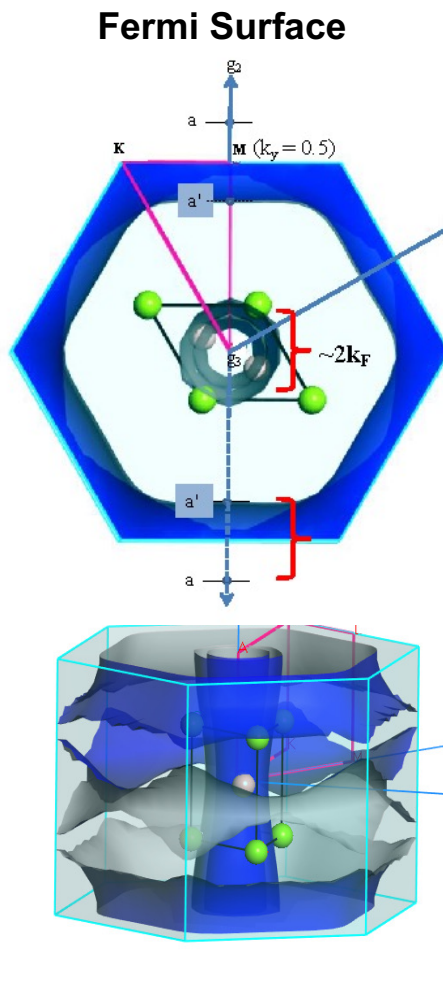
Parent structure hosts superconductors with different elements and Tc's

Bad ??

Out of fashion for publications

Modelling and Simulation

Density Functional Theory – Materials Studio V8.0



- Phonon Dispersion – convergence indicates structural stability
- High computational demand for low values of x
- *Ab initio* models without post-computational corrections

Alarco *et al.*, Phys. Chem. Chem. Phys., **16**, 24443-24456, 2014
Alarco *et al.*, Phys. Chem. Chem. Phys., **16**, 25386-25392, 2014
Alarco *et al.*, Phys. Chem. Chem. Phys., **17**, 25090-25099, 2015

Substitution in AlB₂-type Structures



Solubility of most metals in MgB₂ is low

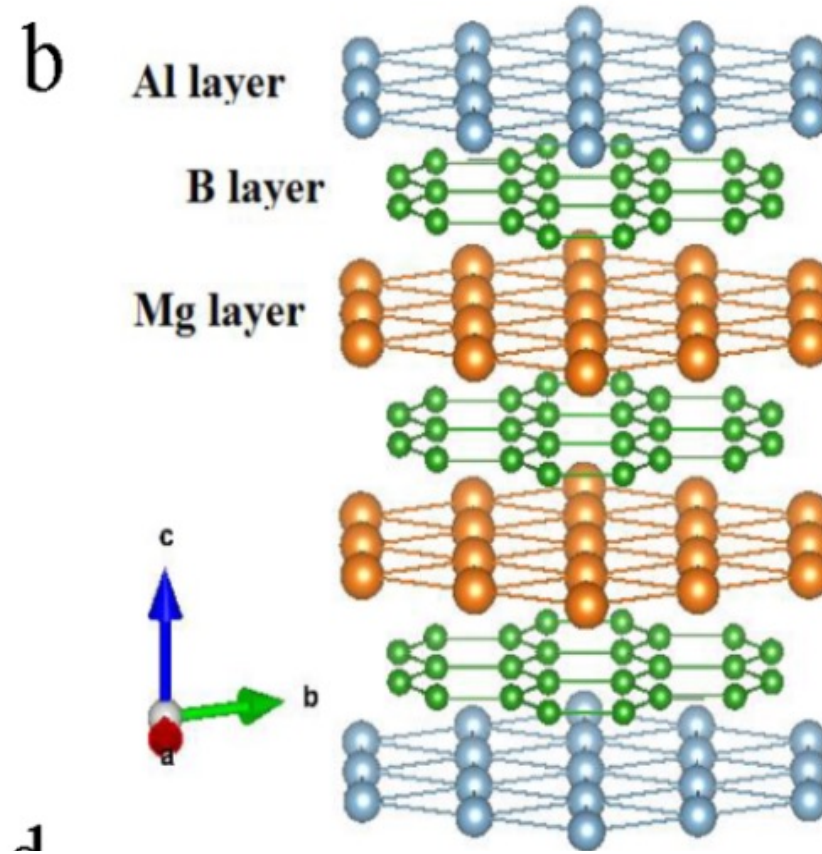
Metal	Max Value (x)	T _c at max x (K)
Li	0.12	~35 ¹
Al	0.90	0 ²
Fe	0.04	~35 ¹
Ti	0.40	~25 ³
Mn	0.05	0 ¹
Sc	0.28	~6 ⁴

Mg(B_{1-x}C_x)₂ x < 0.20; T_c at max x: 0

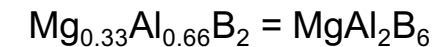
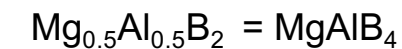
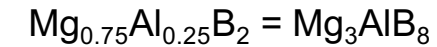
In all cases, T_c is suppressed

1. Karpinski *et al.*, Phys. Rev. B., 2008
2. Lee *et al.*, Physica C, 2007
3. Lee *et al.*, J. Mag. Magnetic Mater., 2008
4. Agrestini *et al.*, J Phys. Chem. Solids, 2004

Substituted Metal Borides



Superlattices



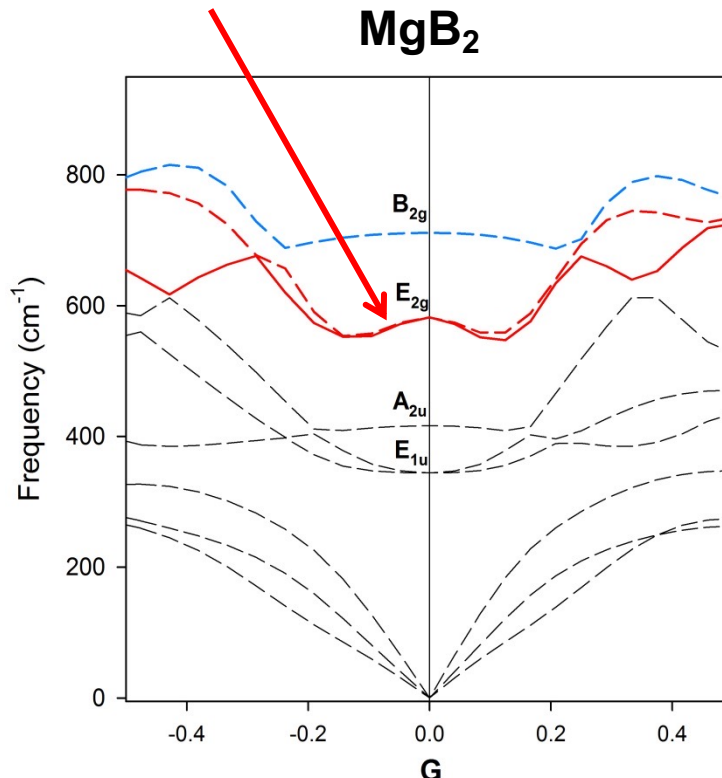
Observed by HREM
Xiang *et al.*, Phys. Rev. B, 2002
Zandbergen *et al.*, Physica C, 2002
Li *et al.*, Phys. Rev. B, 2002

Alarco *et al.*, Phys. Chem. Chem. Phys., **16**, 24443-24456, 2014
Alarco *et al.*, Phys. Chem. Chem. Phys., **16**, 25386-25392, 2014
Alarco *et al.*, Phys. Chem. Chem. Phys., **17**, 25090-25099, 2015

Kohn Anomaly

Centred around \mathbf{G} or Γ
Along $\mathbf{G-K}$ and $\mathbf{G-M}$ directions

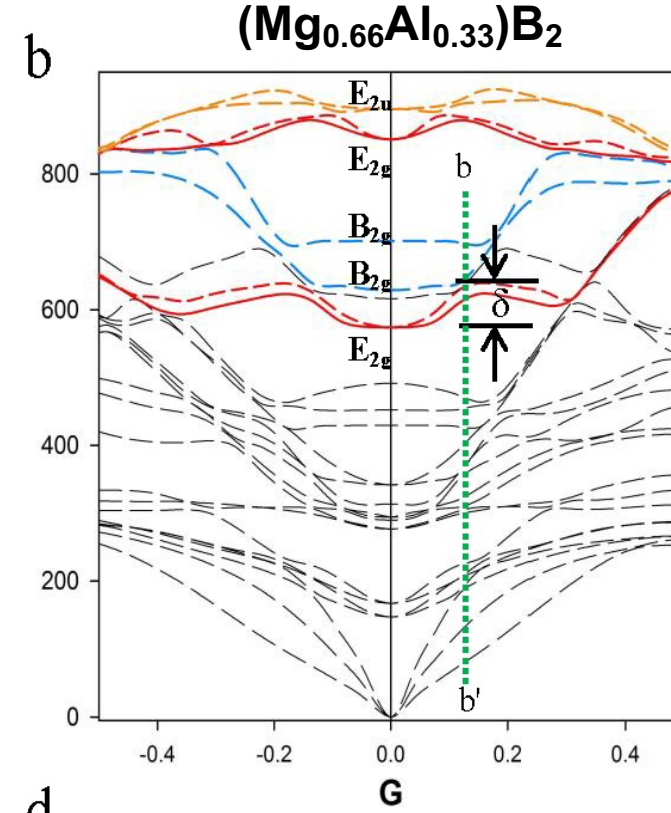
Experimental IXS along G-M (Baron *et al.*,
Phys. Rev. Lett., 92, 2004.) for MgB_2



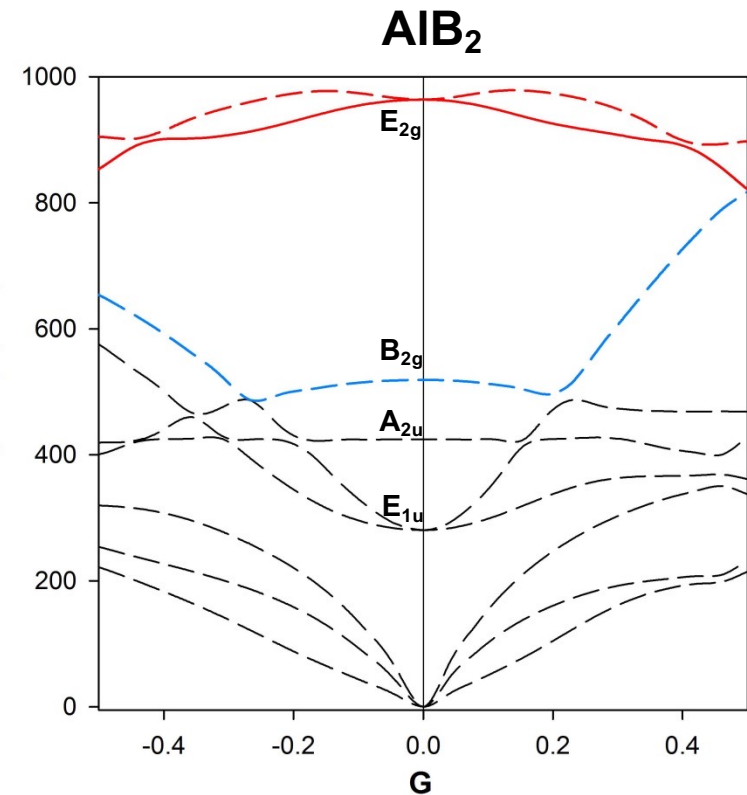
LDA: $k = 0.02 \text{ \AA}^{-1}$

Density Functional Theory

Phonon Dispersions – $\text{Mg}_{1-x}\text{Al}_x\text{B}_2$



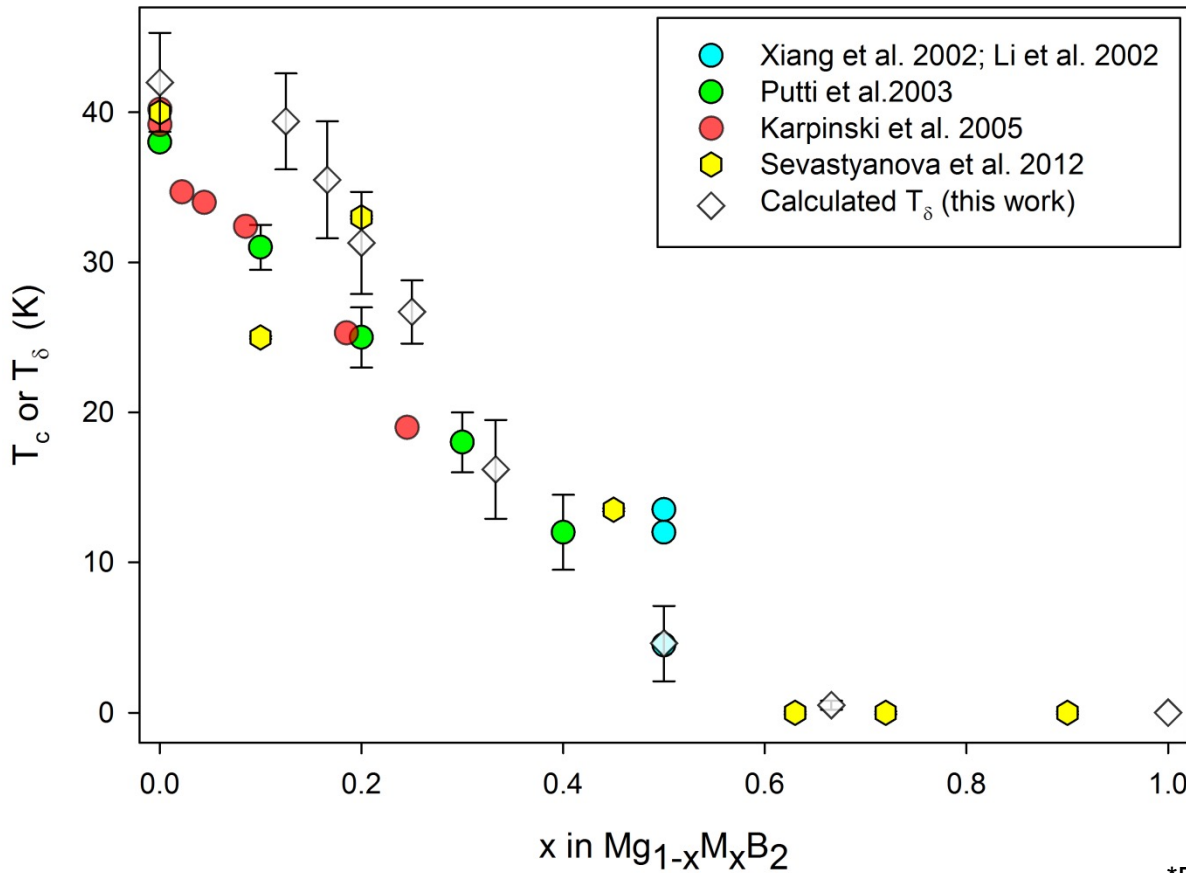
Alarco *et al.*, *Phys. Chem. Chem. Phys.*, **16**, 24443-24456, 2014
Alarco *et al.*, *Phys. Chem. Chem. Phys.*, **16**, 25386-25392, 2014



Superconducting T_c – $Mg_{1-x}Al_xB_2$

Theory and Experiment

$$\delta = (nN/Z)x(k_B T_\delta / 2)$$



$$\delta = (nN/Z)x(k_B T_\delta / 2)$$

δ = height of phonon anomaly (cm $^{-1}$)
 n = degrees of freedom per atom
 N = number of atoms per unit cell
 Z = number of formula units per cell
 k_B = Boltzman's constant
 T_δ = thermal energy of phonon

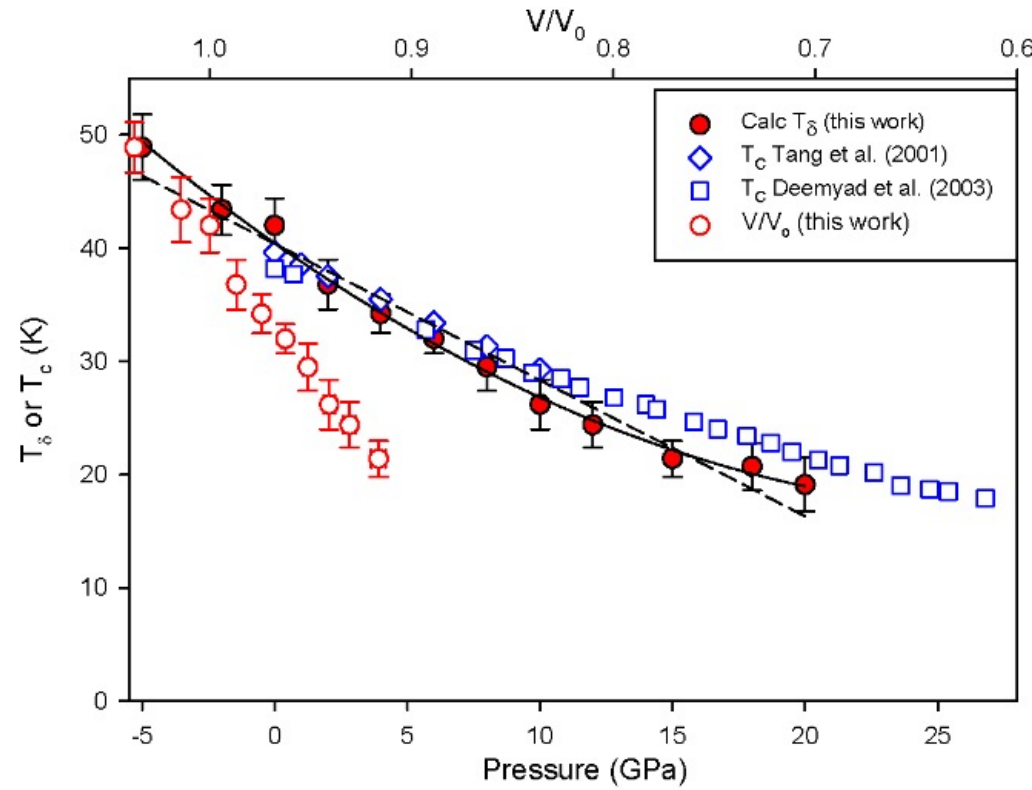
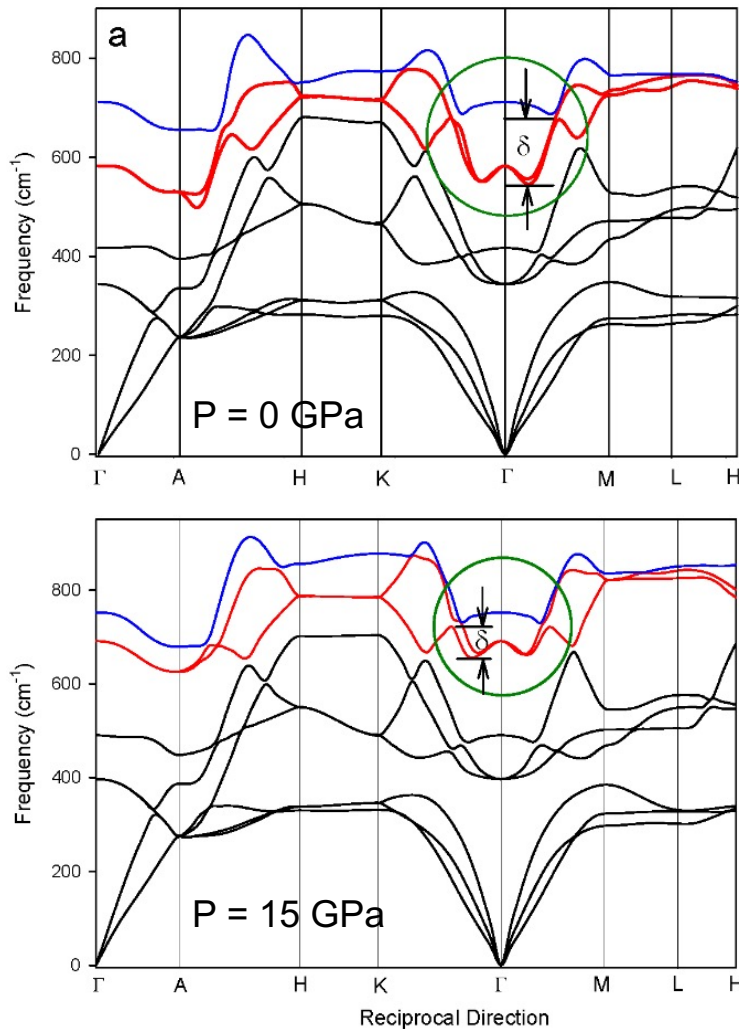
Solve for T_δ

*Experimental values are onset temperatures

Alarco et al., Phys. Chem. Chem. Phys., 17, 25090-25099, 2015

CRICOS No.00213J

MgB₂ - Pressure dependence of T_c



Superconducting T_c – AIB₂-type Structures

Theory and Experiment

Compound	Predicted T_c This work (K)	Experimental T_c By Others (K)
MgB ₂	42.0 (3.0)	39.2 – 40.2
(Mg _{0.8} Al _{0.2})B ₂	31.3 (3.4)	25 (2) – 33.0 (0.1)
(Mg _{0.66} Al _{0.34})B ₂	16.2 (3.3)	13.5 (0.1)
(Mg _{0.5} Al _{0.5})B ₂	4.6 (2.5)	4.0 – 13.5
(Mg _{0.86} Sc _{0.14})B ₂	31.5 (4.4)	23.0 (2.5)**
(Mg _{0.75} Sc _{0.25})B ₂	11.4 (1.0)	~8.2 (5.0)**
AlB ₂	0.0	0.0
BaSi ₂	9.3 (0.5)	8.9
Ca(Al _{0.5} Si _{0.5}) ₂	7.5 (0.5)	7.8

Can we use this approach to design/predict new superconducting materials ?

**peak values from derivative of surface resistance

Superconducting T_c – AIB₂-type Structures

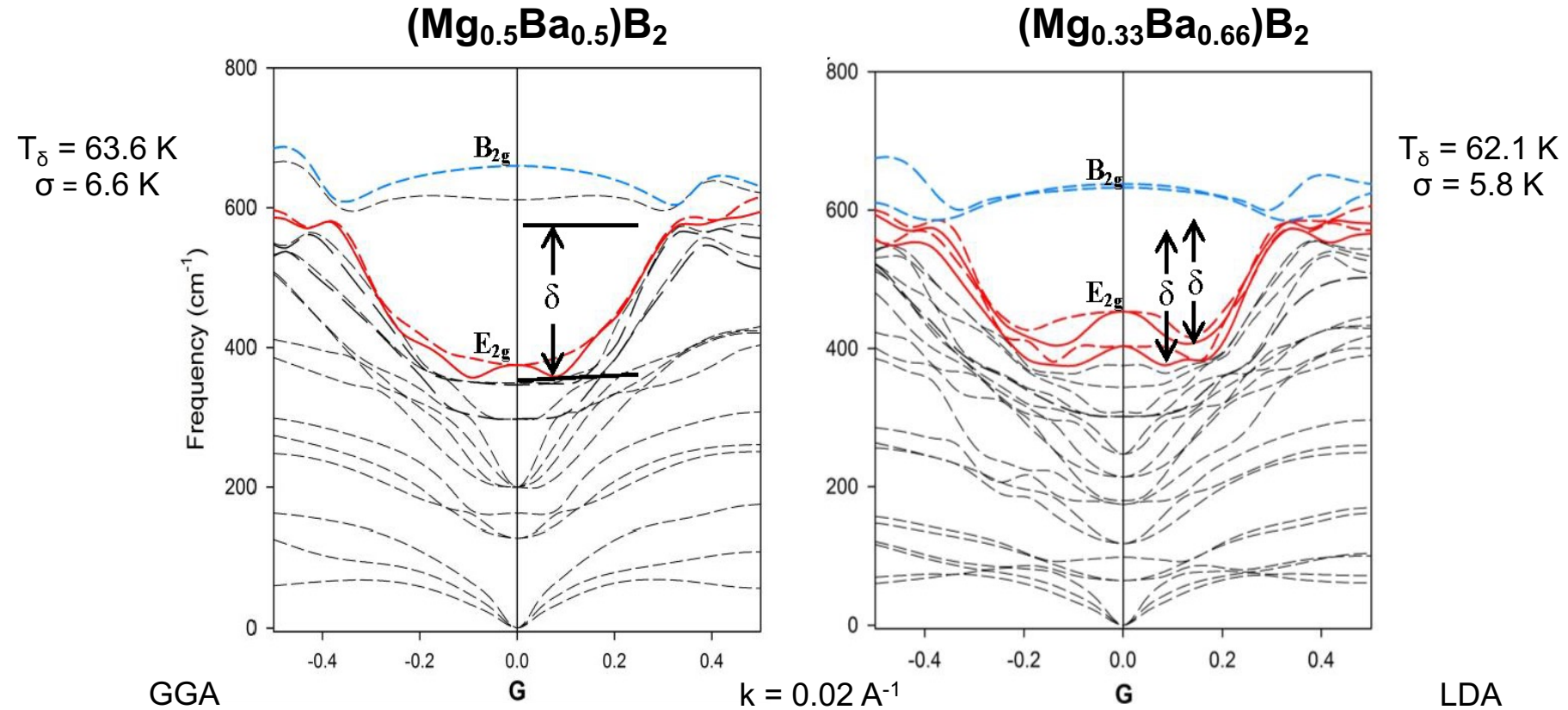
Theory and Experiment

Compound	Predicted T_c This work (K)	Experimental T_c By Others (K)
MgB ₂	42.0 (3.0)	39.2 – 40.2
(Mg _{0.8} Al _{0.2})B ₂	31.3 (3.4)	25 (2) – 33.0 (0.1)
(Mg _{0.67} Al _{0.33})B ₂	16.2 (3.3)	13.5 (0.1)
(Mg _{0.5} Al _{0.5})B ₂	4.6 (2.5)	4.0 – 13.5
(Mg _{0.86} Sc _{0.14})B ₂	31.5 (4.4)	23.0 (2.5)**
(Mg _{0.75} Sc _{0.25})B ₂	11.4 (1.0)	~8.2 (5.0)**
AlB ₂	0.0	0.0
BaSi ₂	9.3 (0.5)	8.9
Ca(Al _{0.5} Si _{0.5}) ₂	7.5 (0.5)	7.8
(Mg _{0.67} Ba _{0.33})B ₂	64.4 (2.2)	n.d.
(Mg _{0.5} Ba _{0.5})B ₂	63.6 (6.6)	n.d.
(Mg _{0.33} Ba _{0.67})B ₂	62.1 (5.8)	n.d.
BaB ₂ (~16GPa)	79.1 (10.2)	n.d.

**peak values from derivative of surface resistance

New Materials: $(\text{Mg}_{1-x}\text{Ba}_x)\text{B}_2$

DFT Predicted T_c



Alarco *et al.*, Phys. Chem. Chem. Phys., **17**, 25090-25099, 2015

CRICOS No.00213J

MgB₂ substituted with Ba, Rb and Cs

Magnetic susceptibility T_c

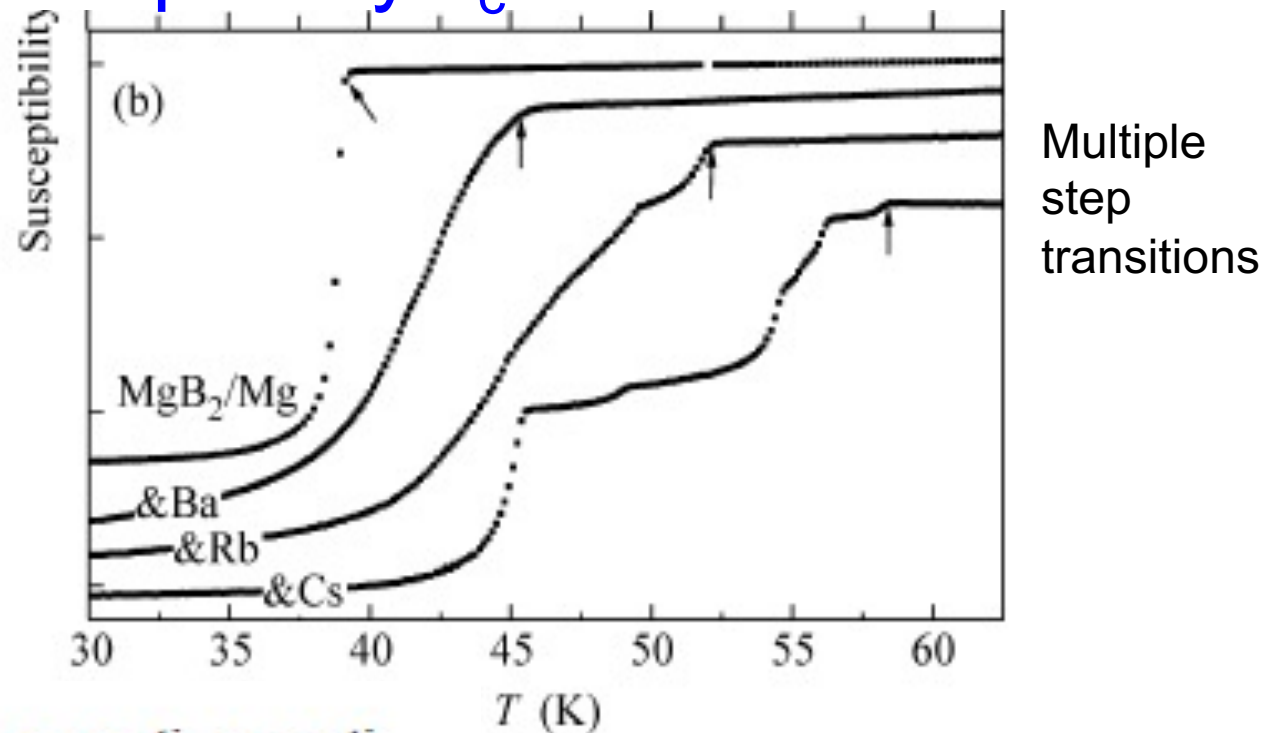
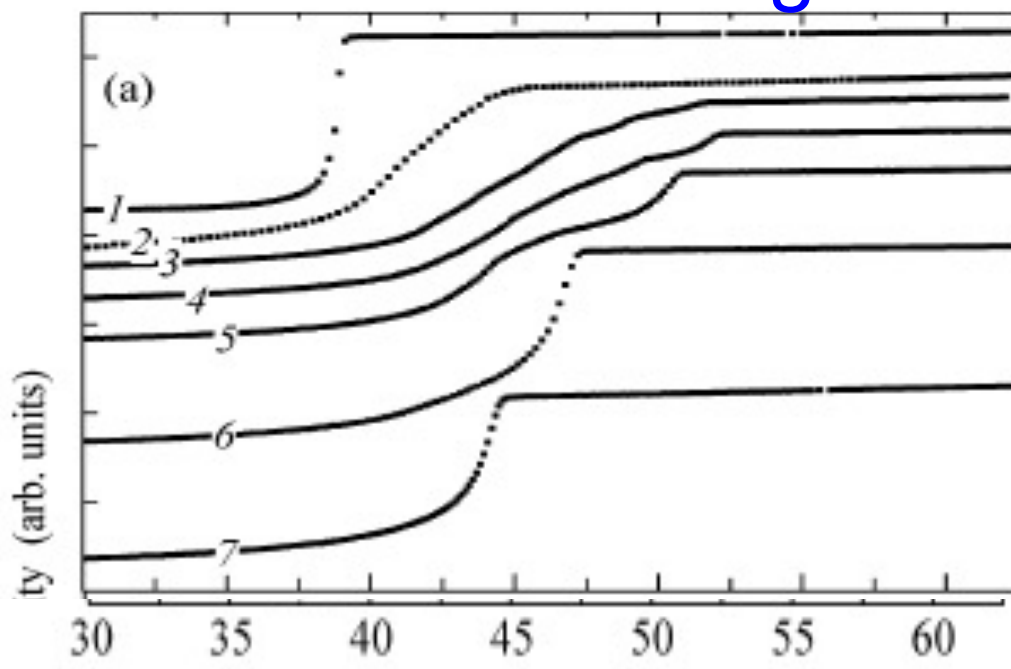
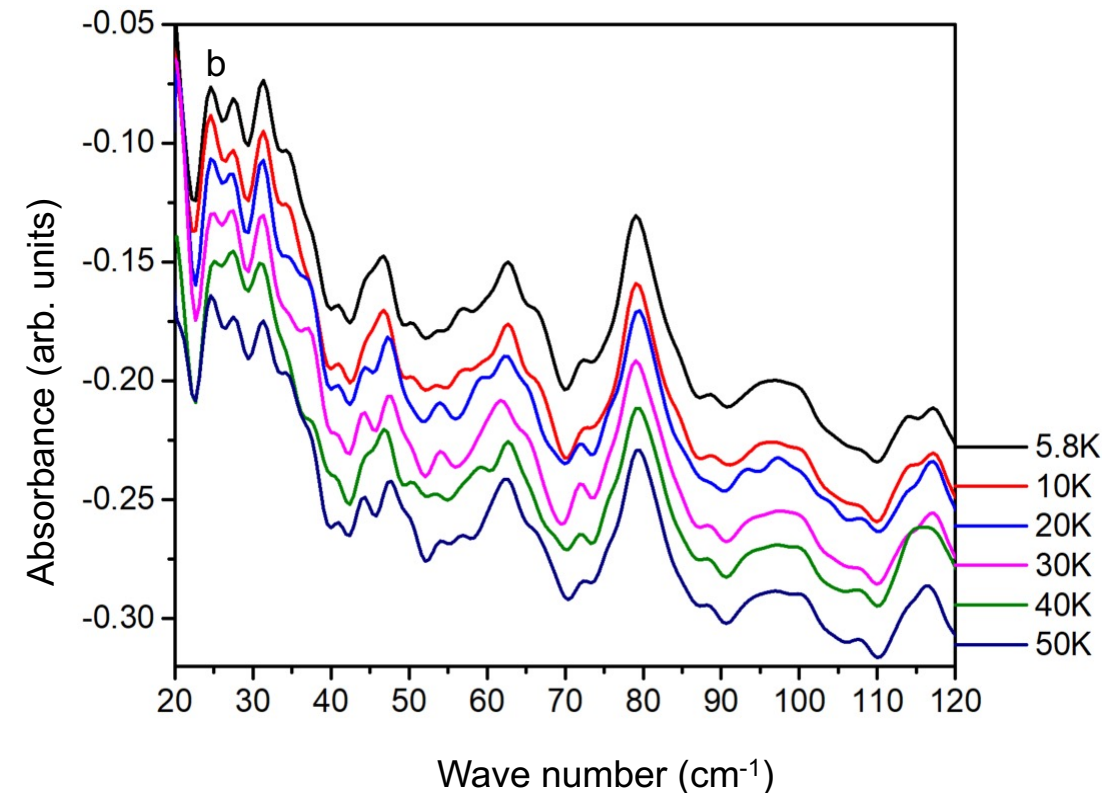
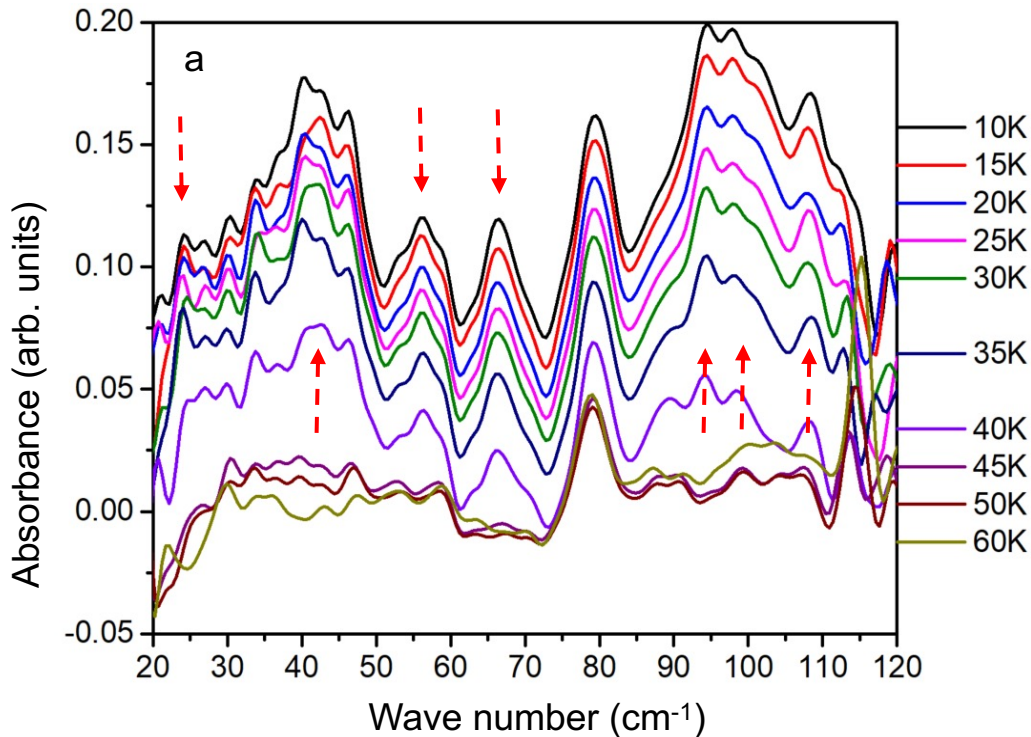


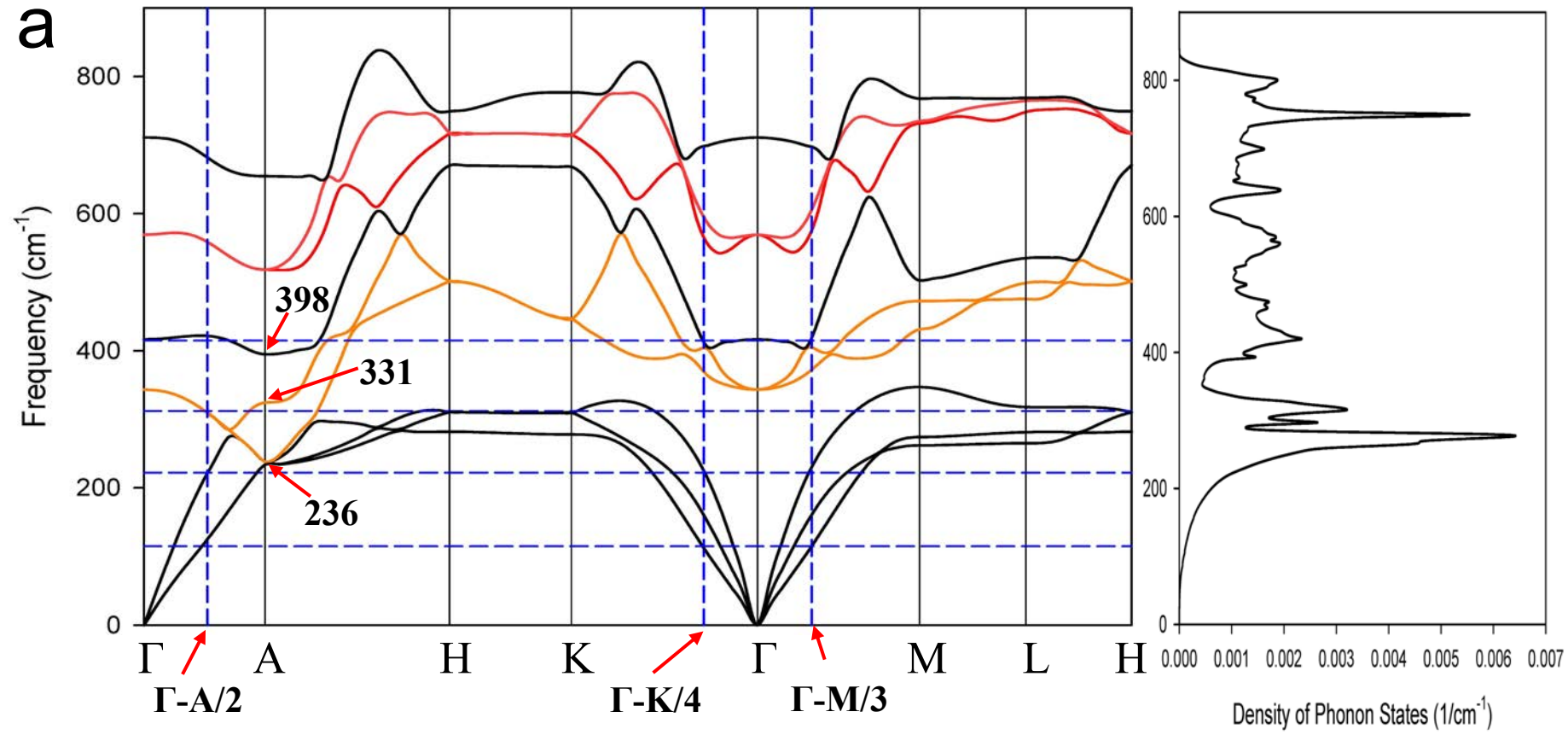
Fig. 1. Temperature dependencies of the magnetic susceptibility: (a) measured between consecutive heat treatments of MgB_2/Mg with Rb, 1—initial sample, 2—10 hours at 180°C , 3—13 hours at 190°C , 4—15.5 hours at 200°C , 5—36 hours at 200°C , 6—56 hours at 200°C , 7—18 hours at 300°C ; (b) the initial MgB_2/Mg , the one reacted with Ba (5 min at 700°C), with Rb (17 hours at 200°C), and with Cs (20 hours at 160°C followed by 100 hours annealing at 100°C). The arrows indicate the onsets of superconducting transitions.

A. Prof. Alexei Kolmogorov alerted us on
Palnichenko *et al.*, JETP Letters **86** (4), 272-274, 2007

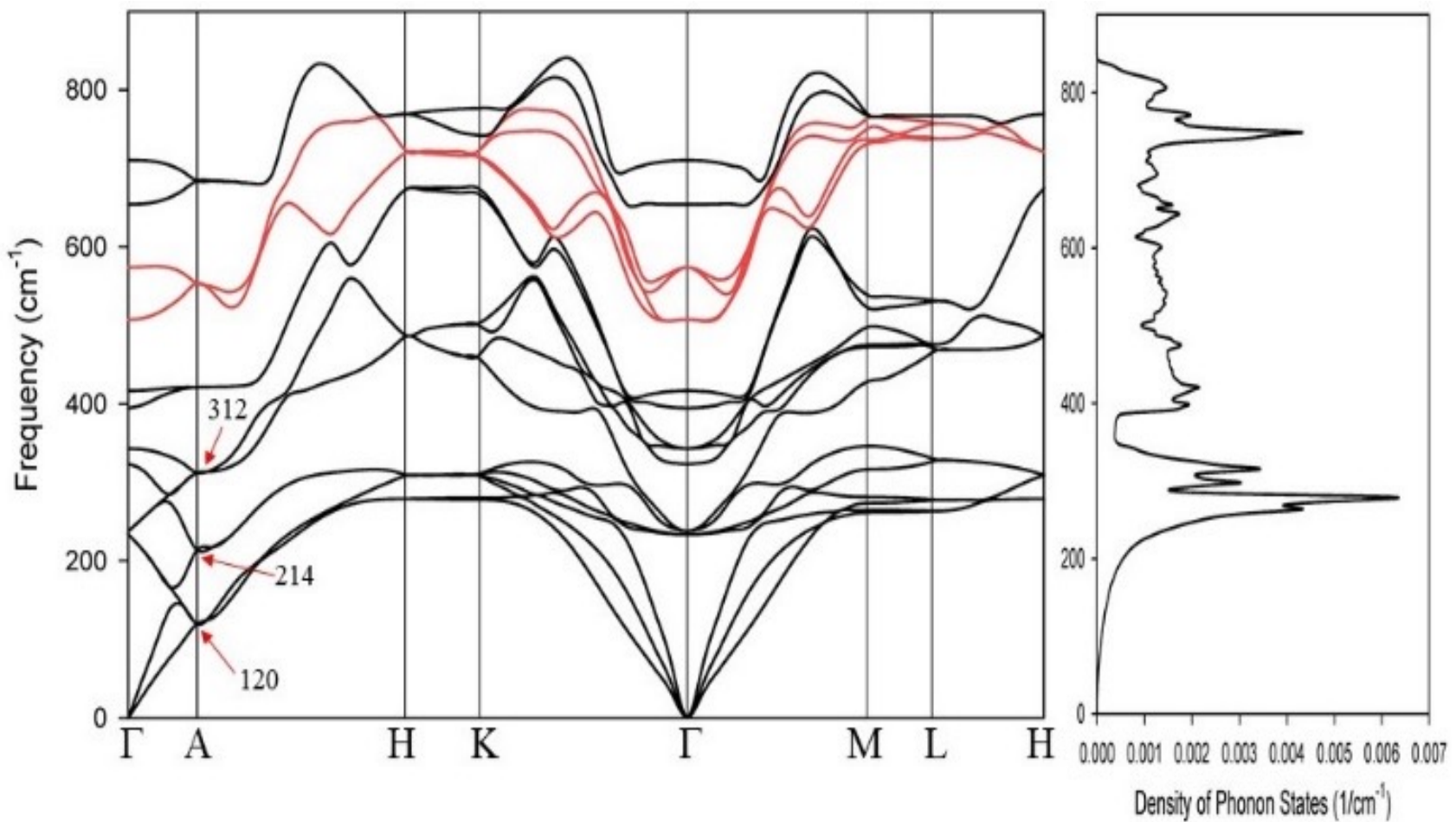
THz/Far Infrared synchrotron absorption

C-doped MgB₂

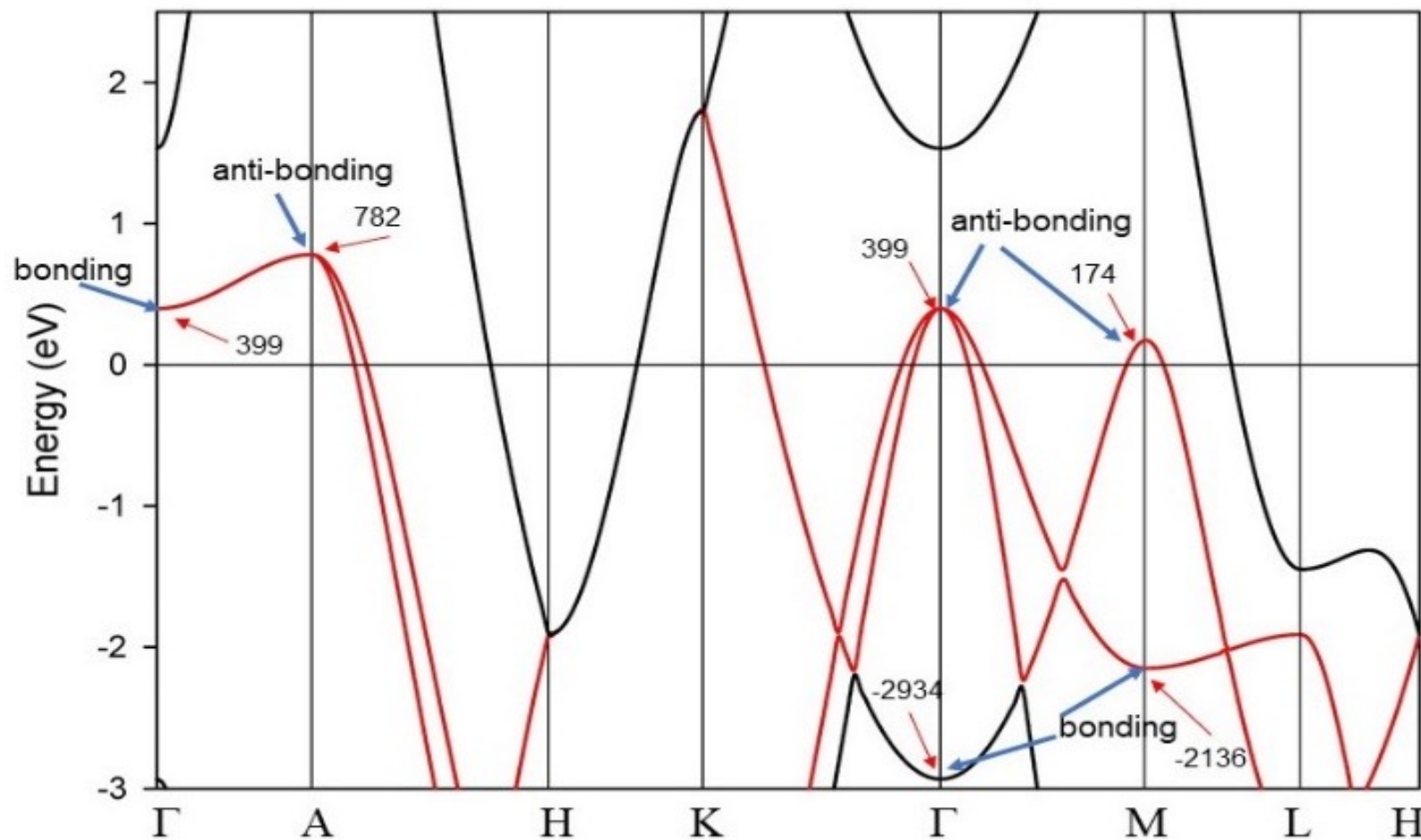




Alarco *et al.*, submitted to Phys. Chem. Chem. Phys., Jul 2021

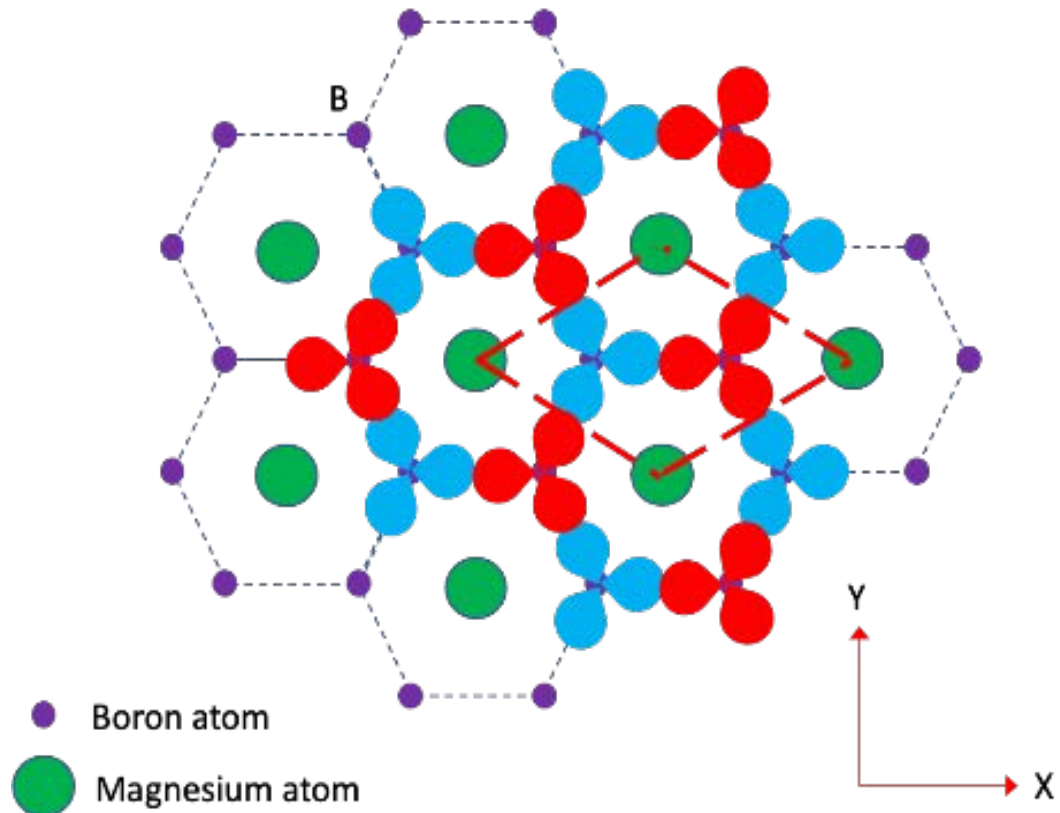


Alarco *et al.*, submitted to Phys. Chem. Chem. Phys., Jul 2021



Alarco *et al.*, submitted to Phys. Chem. Chem. Phys., Jul 2021

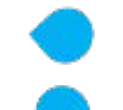
Anti-symmetric (Ungarde) combination (at k=0)



Positive sp^2 hybrid orbitals



Negative sp^2 hybrid orbitals



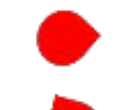
$$(1/\sqrt{3}) S + (\sqrt{2}/3) P_x$$



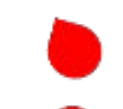
$$(1/\sqrt{3}) S - (1/\sqrt{6}) P_x + (1/\sqrt{2}) P_y$$



$$(1/\sqrt{3}) S - (1/\sqrt{6}) P_x - (1/\sqrt{2}) P_y$$



$$- [(1/\sqrt{3}) S - (\sqrt{2}/3) P_x]$$



$$- [(1/\sqrt{3}) S + (1/\sqrt{6}) P_x - (1/\sqrt{2}) P_y]$$

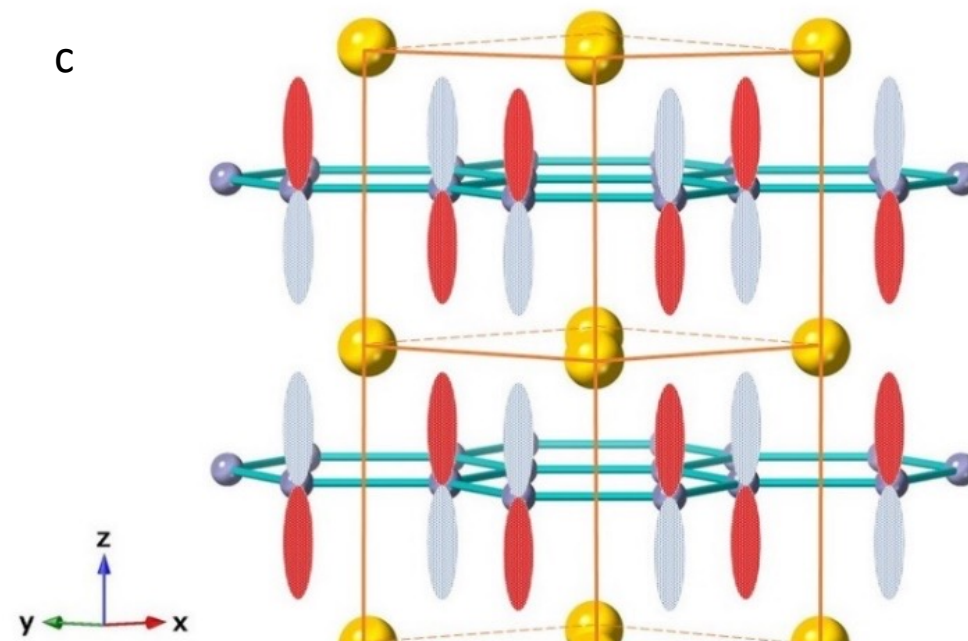
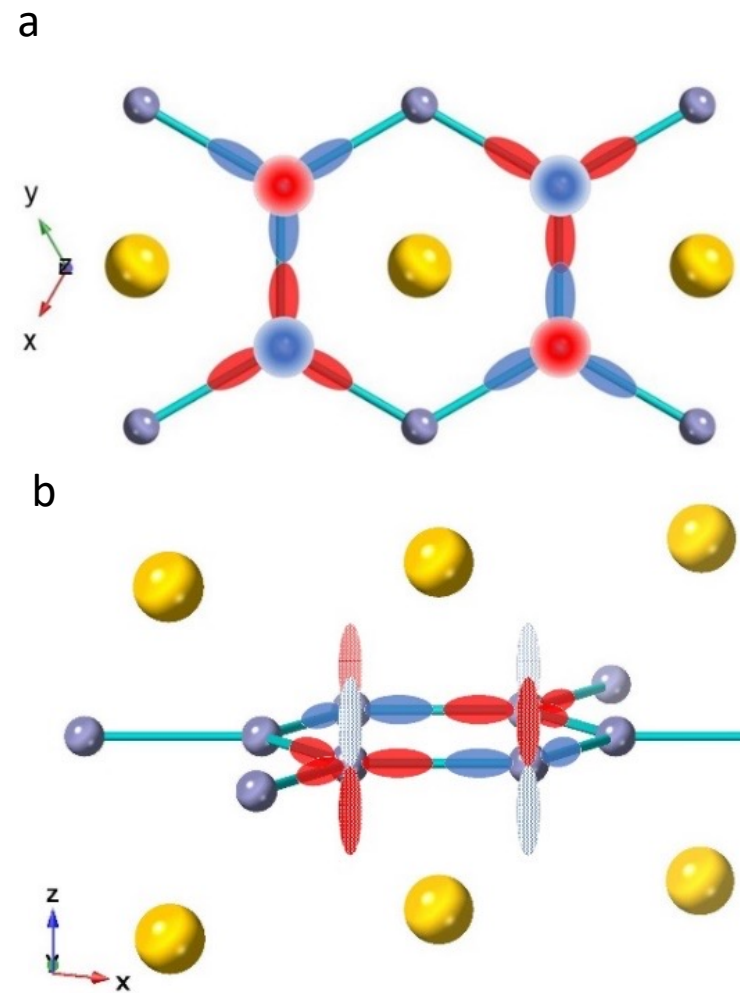


$$- [(1/\sqrt{3}) S + (1/\sqrt{6}) P_x + (1/\sqrt{2}) P_y]$$

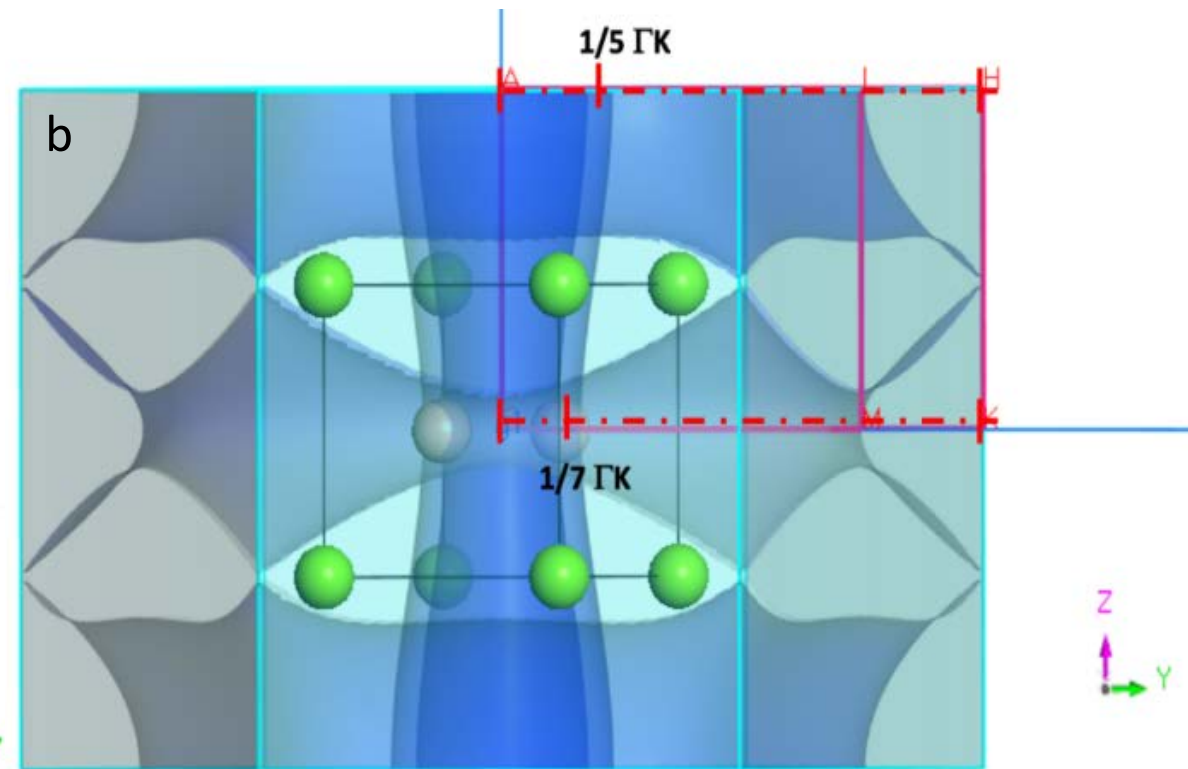
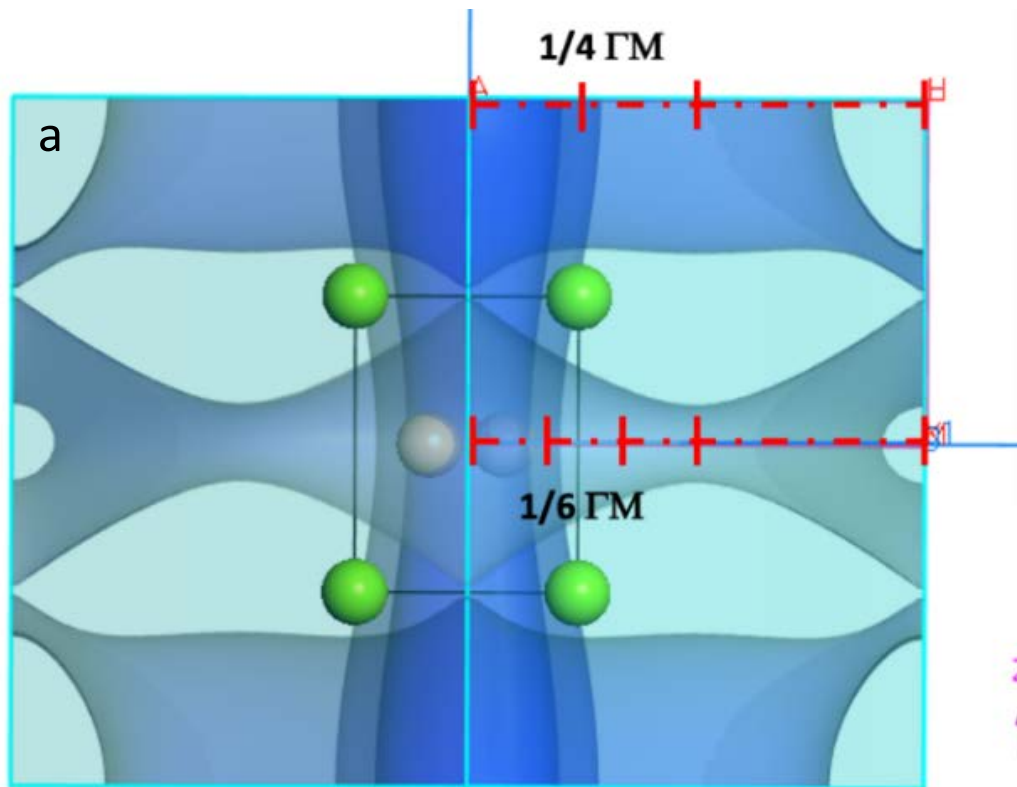
$$\text{Blue} + \text{Red} = 2 (\sqrt{2}/3) P_x$$

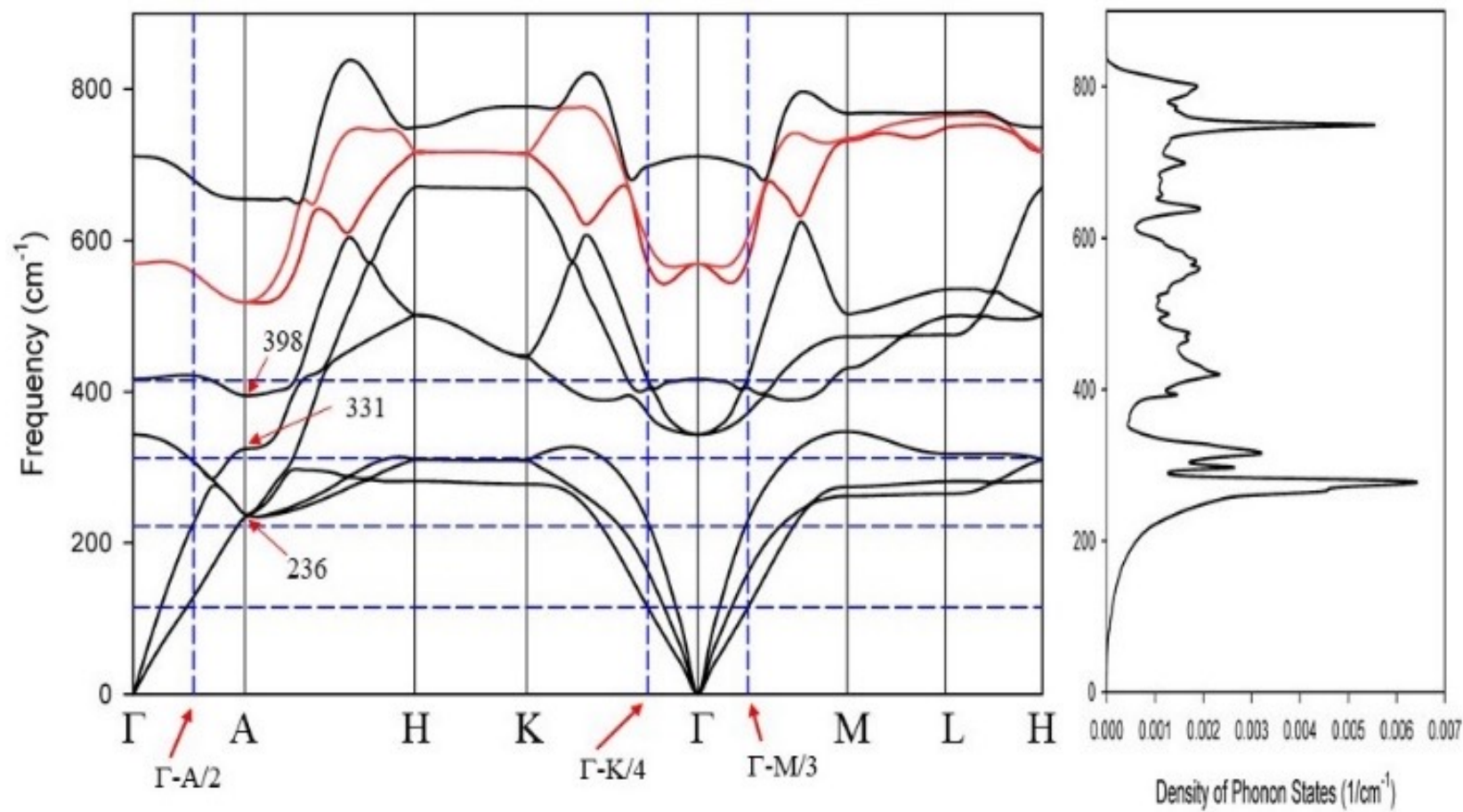
$$\frac{\sqrt{2}/3}{(1/\sqrt{6})} = 2$$

Ratio of effective masses



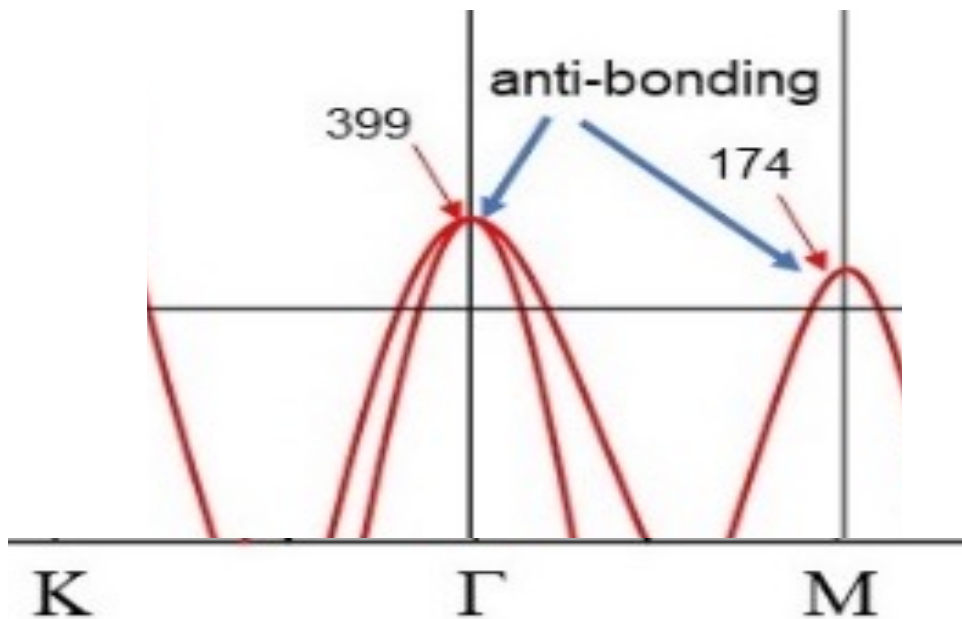
Alarco *et al.*, submitted to Phys. Chem. Chem. Phys., Jul 2021





$$E_n(k_x, k_y, k_z) = E_0 - 2t_{\perp} \cos(ck_z) - \hbar^2 (k_x^2 + k_y^2) / 2m_n$$

$m_{eff}^H = 0.53 - 0.59$,
 $m_{eff}^L = 0.20 - 0.28$,
 $E_0 = 0.58 - 0.6$ and
 $t_{\perp} = 0.092 - 0.094$ eV



Alarco *et al.*, submitted to Phys. Chem. Chem. Phys., Jul 2021

Collaboration opportunities

LIST OF PUBLICATIONS

Publication in refereed journals:

1. Intermetallic MP_3 ($M = Ti, Zr, Hf$): Elastic, electronic, optical and thermal properties
S. K. Mitro, M. A. Rahman, F. Parvin, and A. K. M. A. Islam
International Journal of Modern Physics B (**World scientific publishing, IF: 1.219**),
<https://doi.org/10.1142/S0217979219501893>

2. Zirconium trigallide polymorphs with tetragonal and cubic structures: Optical and thermodynamic properties
M. A. Rahman, **S. K. Mitro**, F. Parvin, and A. K. M. A. Islam
Indian Journal of Physics (**Springer, IF: 1.947**), <https://doi.org/10.1007/s12648-020-01716-4>

3. Comprehensive first-principles calculations on physical properties of ScV_2Ga_4 and ZrV_2Ga_4 in comparison with superconducting HfV_2Ga_4
Mirza HK Rubel, K. M. Hossain, **S. K. Mitro**, M. M. Rahaman, M. A. Hadi, and A. K. M. A. Islam
Materials Today Communications (**Elsevier, IF: 3.383**), <https://doi.org/10.1016/j.mtcomm.2020.100935>

4. Newly synthesized A-site ordered cubic-perovskite superconductor $(Ba_{0.54}K_{0.46})_4Bi_4O_{12}$: A DFT investigation
M. H. K. Rubel, **S. K. Mitro**, B. K. Mondal, M. M. Rahaman, Md Saiduzzaman, J. Hossain, A. K. M. A. Islam, and N. Kumada
Physica C: Superconductivity and its Applications (**Elsevier, IF: 1.241**),
<https://doi.org/10.1016/j.physc.2020.1353669>

5. Influence of metalloid antimony on the physical properties of palladium-based half-Heusler compared to the metallic bismuth: A first-principle study

R. Majumder, **S. K. Mitro**, and B. Bairagi

Journal of Alloys and Compounds (**Elsevier, IF: 5.316**), <https://doi.org/10.1016/j.jallcom.2020.155395>

6. Insights into the physical properties and anisotropic nature of ErPdBi with an appearance of low minimum thermal conductivity

S. K. Mitro, R. Majumder, K. M. Hossain, Md Zahid Hasan, Md Emran Hossain, and M. A. Hadi
Chinese Physics B (**IOP publishing, IF: 1.494**), <https://doi.org/10.1088/1674-1056/abaf9d>

7. Effect of the negative chemical pressure on physical properties of doped perovskite molybdates in the framework of DFT method

S. K. Mitro, K. M. Hossain, R. Majumder, and Md Zahid Hasan

Journal of Alloys and Compounds (**Elsevier, IF: 5.316**), <https://doi.org/10.1016/j.jallcom.2020.157088>

8. Justification of crystal stability and origin of transport properties in ternary half-Heusler ScPtBi

R. Majumder, and **S. K. Mitro***

RSC Advances (**Royal Society of Chemistry, IF: 3.361**), [10.1039/D0RA06826H](https://doi.org/10.1039/D0RA06826H)

9. Structural, mechanical, thermal, and optical properties of inverse-Heusler alloys Cr₂CoZ (Z = Al, In): A first-principles investigation

Md Rasheduzzaman, Khandaker Monower Hossain, **S. K. Mitro**, M. A. Hadi, Jibon Krishna Modak, and Md Zahid Hasan

Physics Letters A (**Elsevier, IF: 2.654**), <https://doi.org/10.1016/j.physleta.2020.126967>

10. Structural, mechanical, electronic, and anisotropic properties of niobium-doped strontium ferrite: first-principle calculations

Md Zahid Hasan, Khandaker Monower Hossain, **S. K. Mitro**, Md Rasheduzzaman, Jibon Krishna Modak, and M. A. Rayhan

Applied Physics A (Elsevier, IF: 2.584), <https://doi.org/10.1007/s00339-020-04219-5>

11. Influences of antimony on the structural, electronic, mechanical, and anisotropic properties of cubic Barium stannate

Khandaker Monower Hossain, **S. K. Mitro***, Md Anwar Hossain, Jibon Krishna Modak, Md asheduzzaman, and Md Zahid Hasan

Materials Today Communications (Elsevier, IF: 3.383), <https://doi.org/10.1016/j.mtcomm.2020.101868>

12. Effect of boron incorporation into the carbon-site in Nb₂SC MAX phase: Insights from DFT

S. K. Mitro, M. A. Hadi, F. Parvin, R. Majumder, S. H. Naqib, and A. K. M. A. Islama

Journal of Materials Research and Technology (Elsevier, IF: 5.039),

<https://doi.org/10.1016/j.jmrt.2021.02.031>

13. Comprehensive study on the physical properties of tetragonal LaTGe₃ (T = Rh, Ir, or Pd) compounds: An ab initio investigation

Md Khokon Miah, Khandaker Monower Hossain, Md Atikur Rahman, Md Rasheduzzaman, **S. K. Mitro**, Jibon Krishna Modak, and Md Zahid Hasan

Journal of AIP (American Institute of Physics) Advances, (AIP, IF: 1.627),

<https://doi.org/10.1063/5.0042924>

*Corresponding author

Conclusions

Conclusions

- DFT can be an exceptional tool to advance the understanding of fundamental physical properties and for prediction of the properties of new materials.
- Examples from two areas at the frontier of R&D and practical applications have been discussed.
- The importance of calibration for accurate and realistic DFT approaches to modelling, combined with regular experimental validation, cannot be overstated.
- DFT is suited to long-distance collaboration, where there may be experimental limitations at one of the locations.

Acknowledgements

- Hamish Macintosh, Chris Williams - members of the HPC support team, e-Research Office, QUT

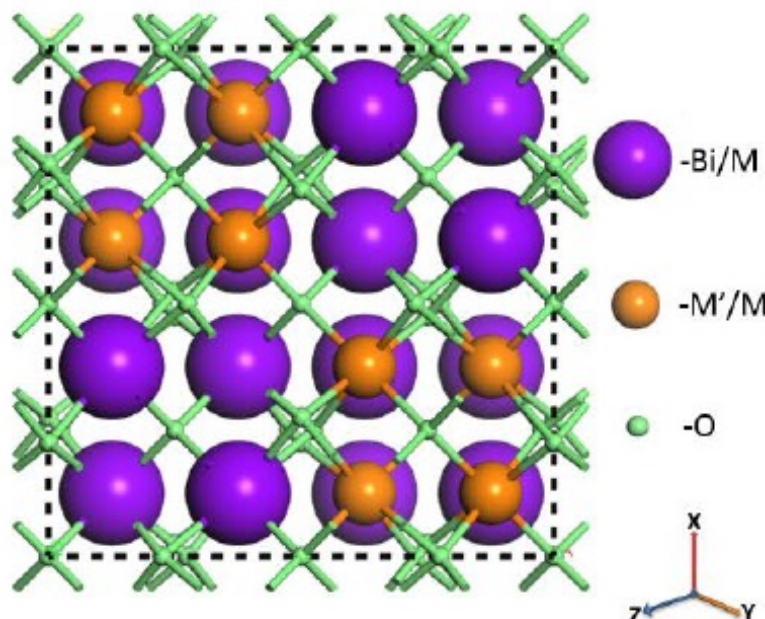
THANK YOU!

Electronic Band Structure of Bi-oxide based photocatalysts

Electronic Band Structure of Bi-oxide based photocatalysts

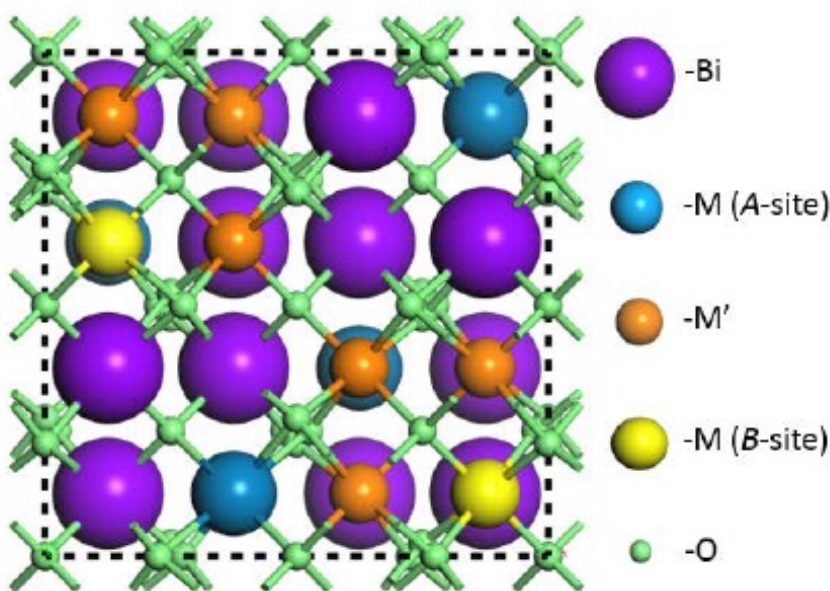
$A_2B_2O_7$ pyrochlores

Cubic CIF, random substitution
(fractional occupation)
→ No band gap

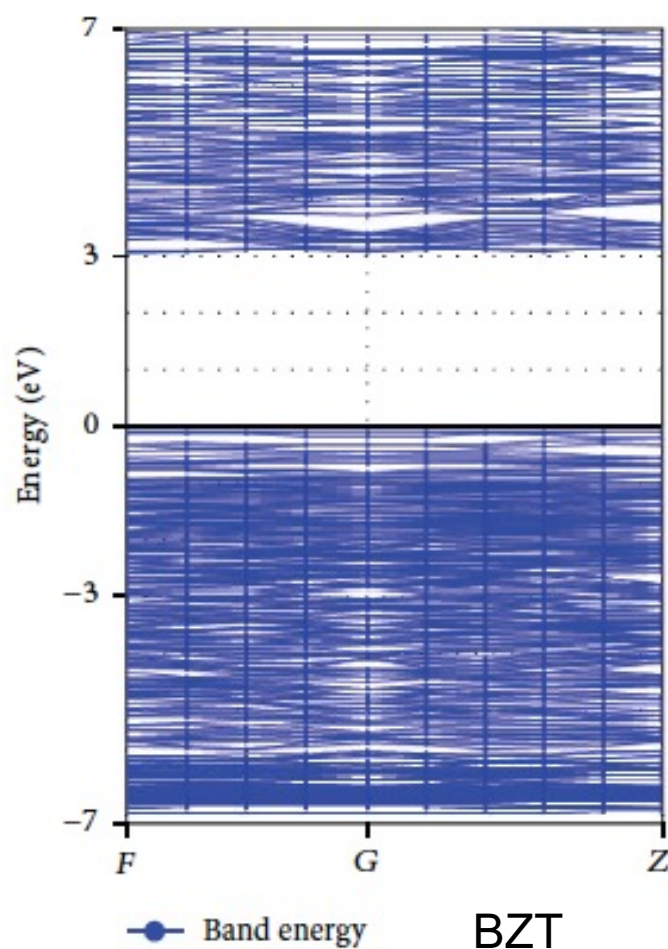


$Bi_{1.5}M'M_{1.5}O_7$ ($M' = Zn, Cd$, $M = Nb, Ta$)

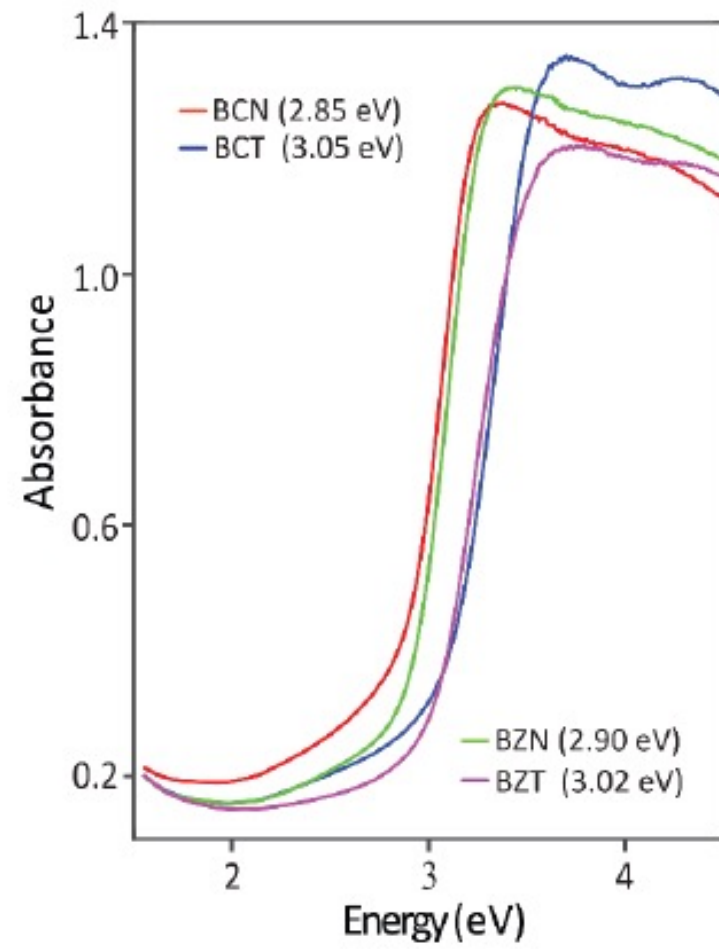
Ordered substitution,
rhombohedral structure → Band
gap close match to experiment



Band Structure



Optical Absorption



Summary of calculated lattice parameters

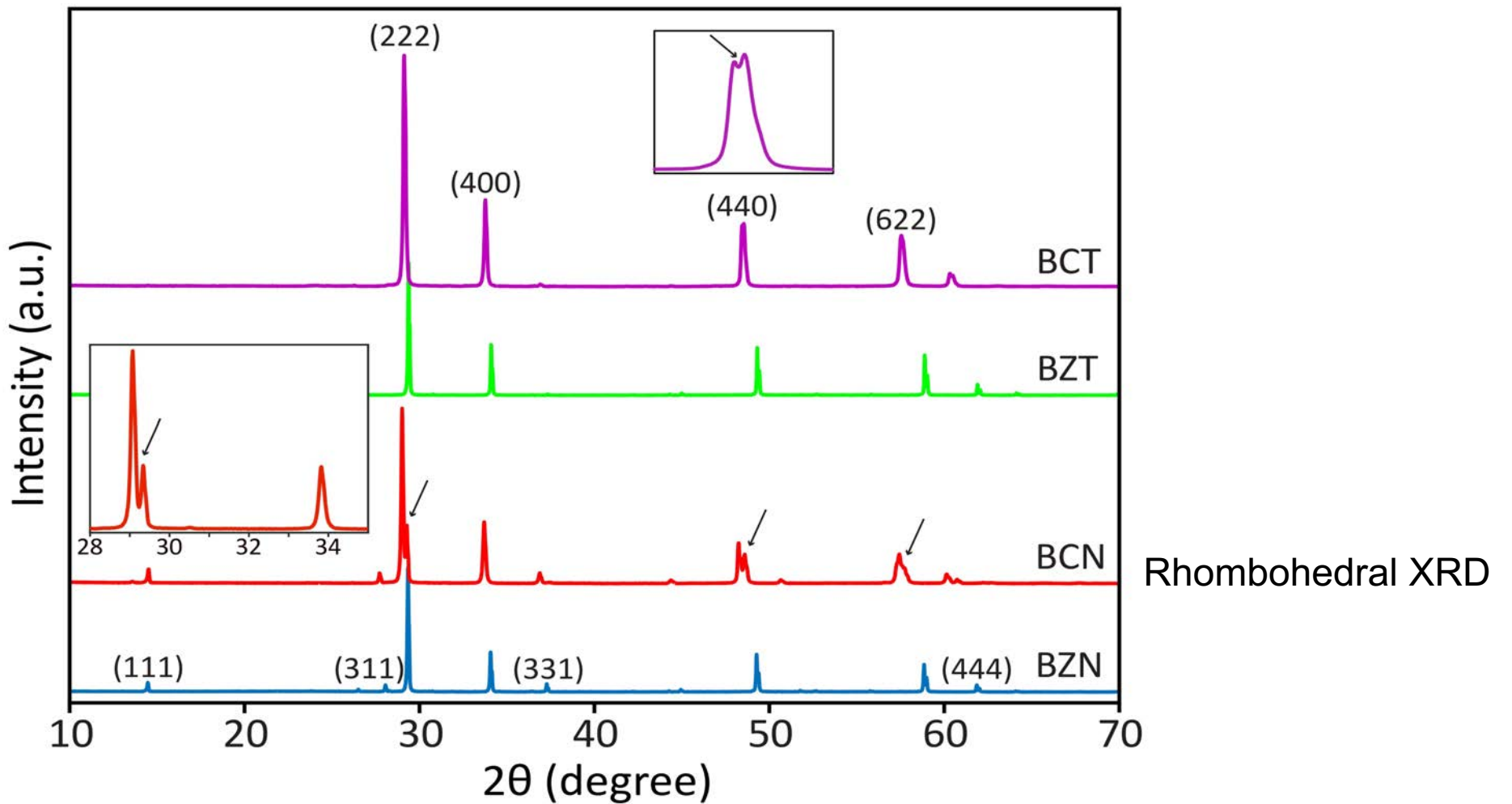
Table 3 Lattice parameters calculated from BCN and BCT with different cation substitutional order, along with those for BZN and BZT structures.

Structure	DFT calculated (geometry optimized) lattice parameters				Refined lattice parameters from XRD data		
	Random	Partially ordered (A-site)	Partially ordered (B-site)	Ordered	a (Å)	α (°)	
	a (Å)	a (Å)	a (Å)	a (Å)	α (°)	a (Å)	α (°)
BCN	10.532	10.495	10.895	10.867	90.33	10.627	90.37
BCT	10.273	10.173	10.536	10.520	90.25	10.623	89.98
BZN	10.492	10.566	10.822	10.767	90.11	10.558	90.00
BZT	10.223	10.214	10.442	10.418	90.13	10.555	90.00

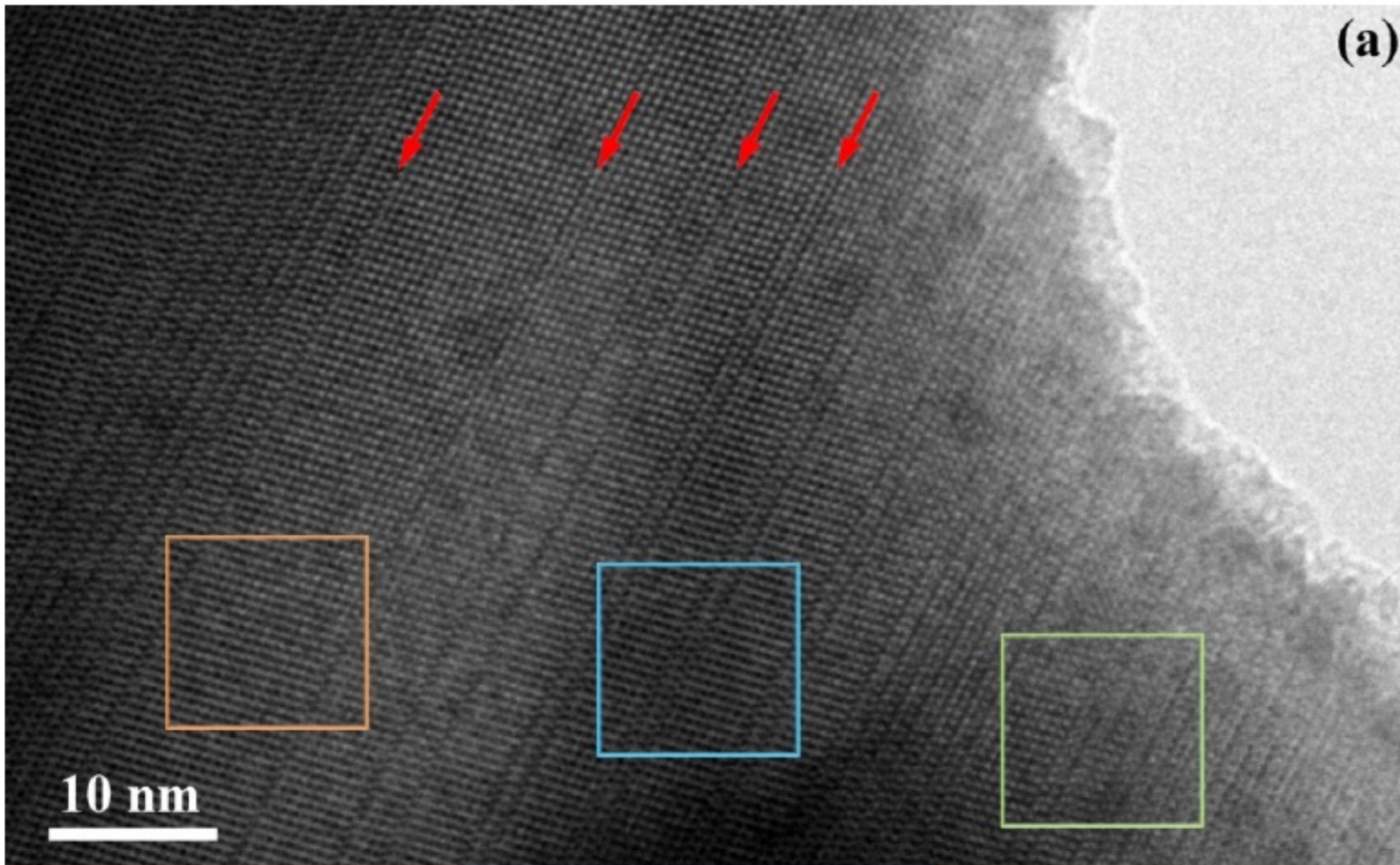
Enthalpies of Formation

Struc- ture	Enthalpy (eV)			
	Random	Partially ordered (A-site)	Partially ordered (B-site)	Ordered
BCN	-55605.61	-55812.94	-57363.54	-57570.16
BCT	-55523.88	-55729.18	-57381.29	-57590.19
BZN	-56059.83	-56278.83	-58209.31	-58427.47
BZT	-55972.85	-56188.72	-58228.60	-58449.02

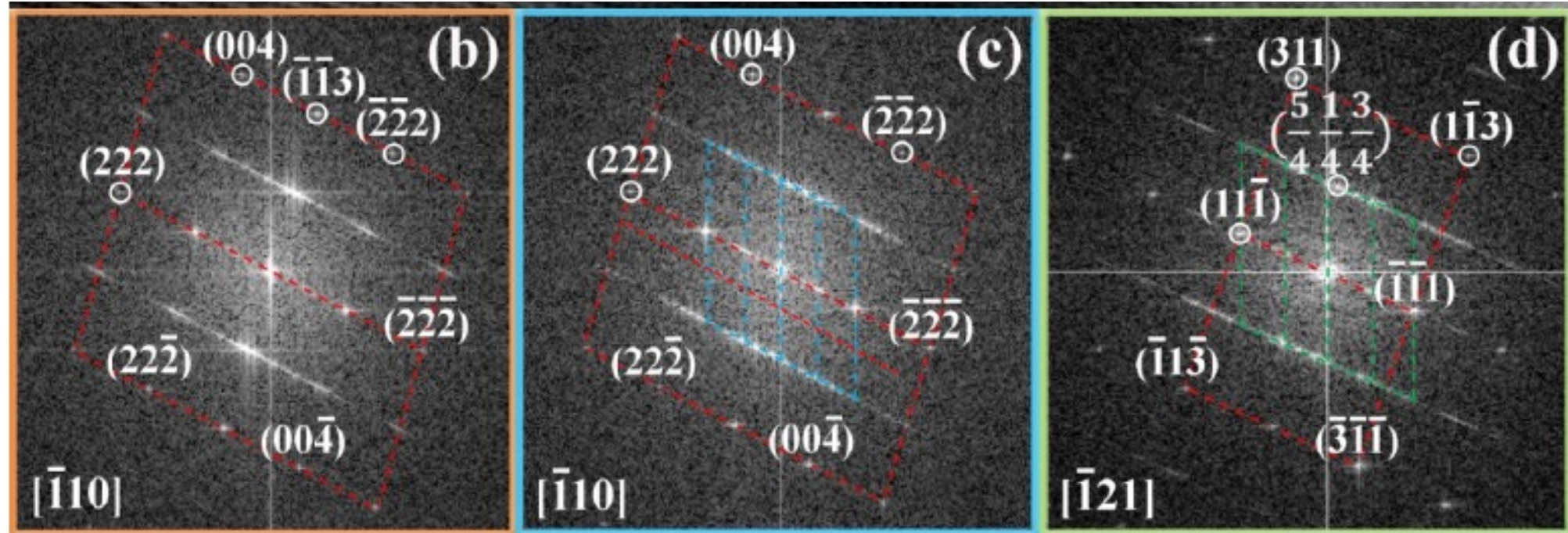
X-ray diffraction



Transmission electron microscopy

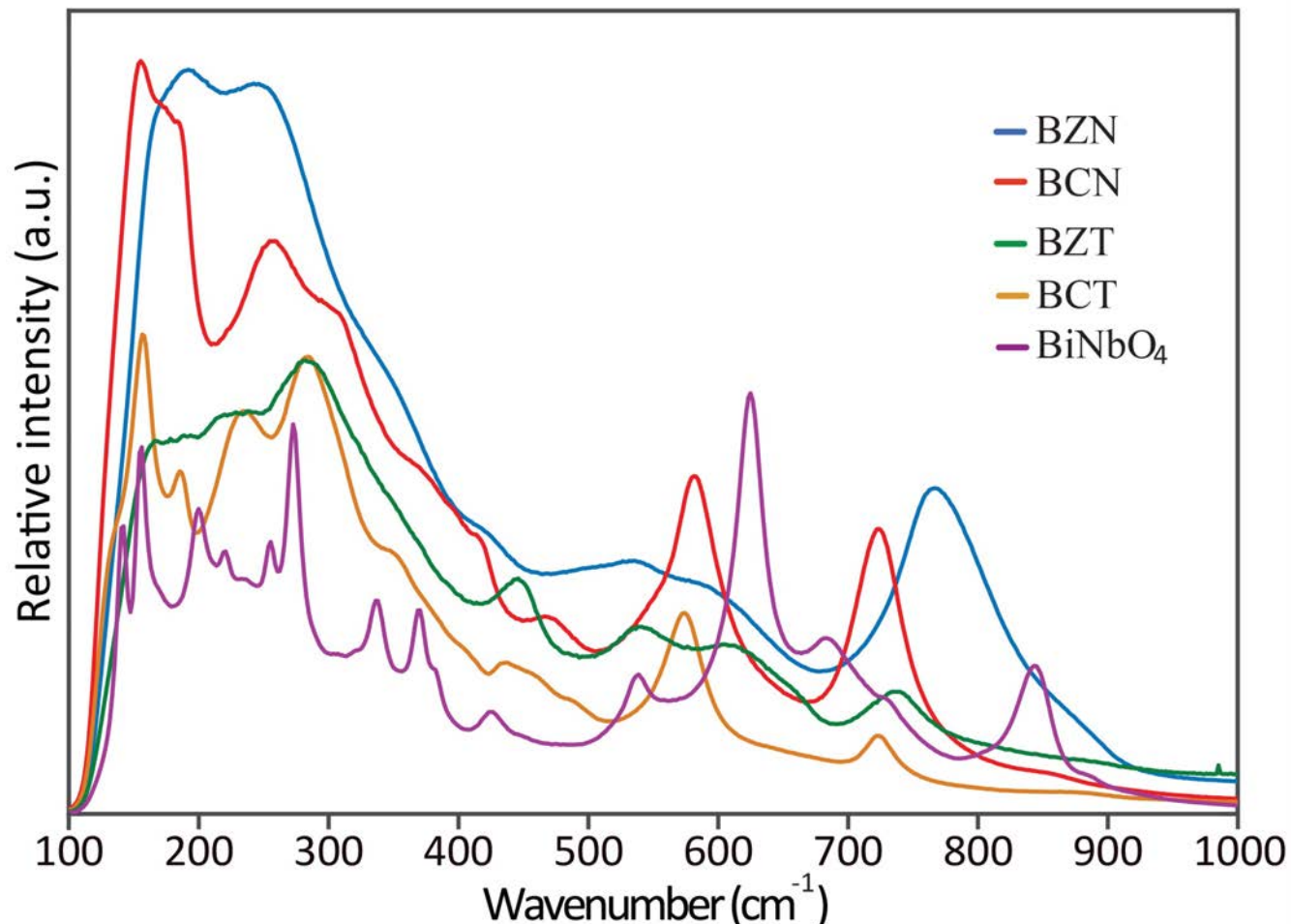


Selected area micro-diffraction



Superlattice diffraction in BCN

Raman spectrometry



BiNbO₄
Orthorhombic →
sharp peaks

All others, similar
broad peaks →
Raman (and IR)
activity governed
by group symmetry
and degeneracy
breaking

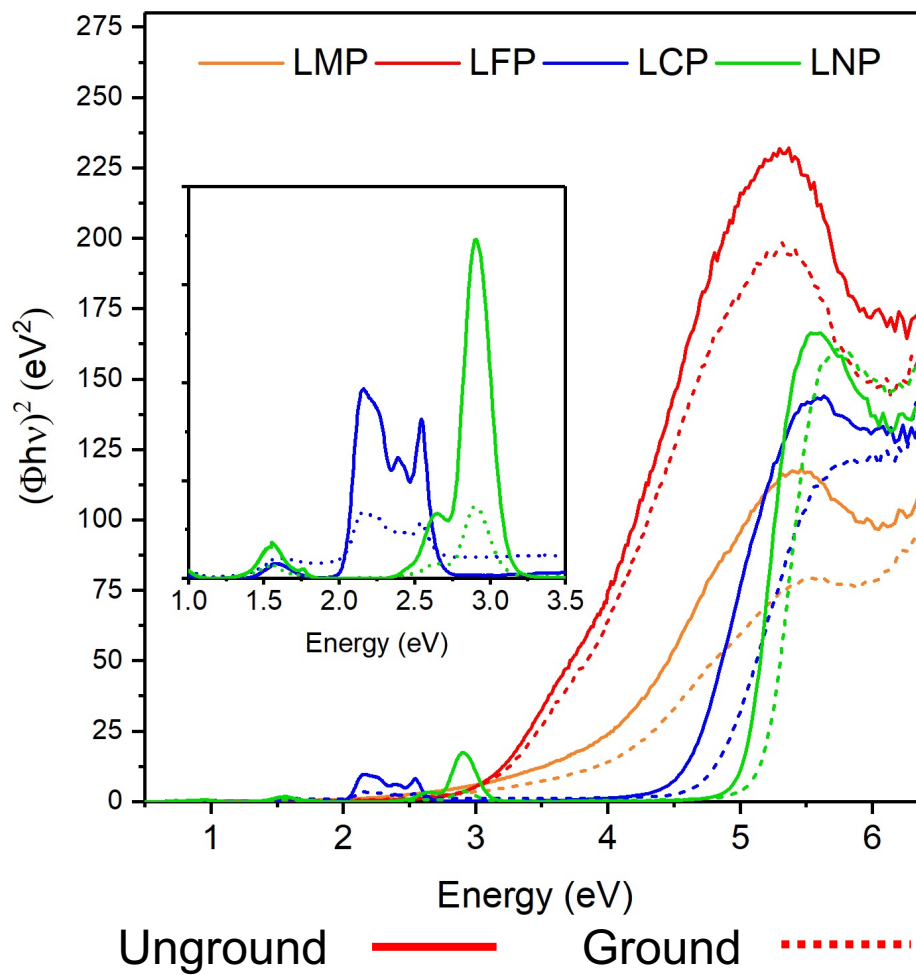
Effect of pseudopotential

Table 5 Comparison of DFT calculated and experimentally observed lattice constants and band gaps.

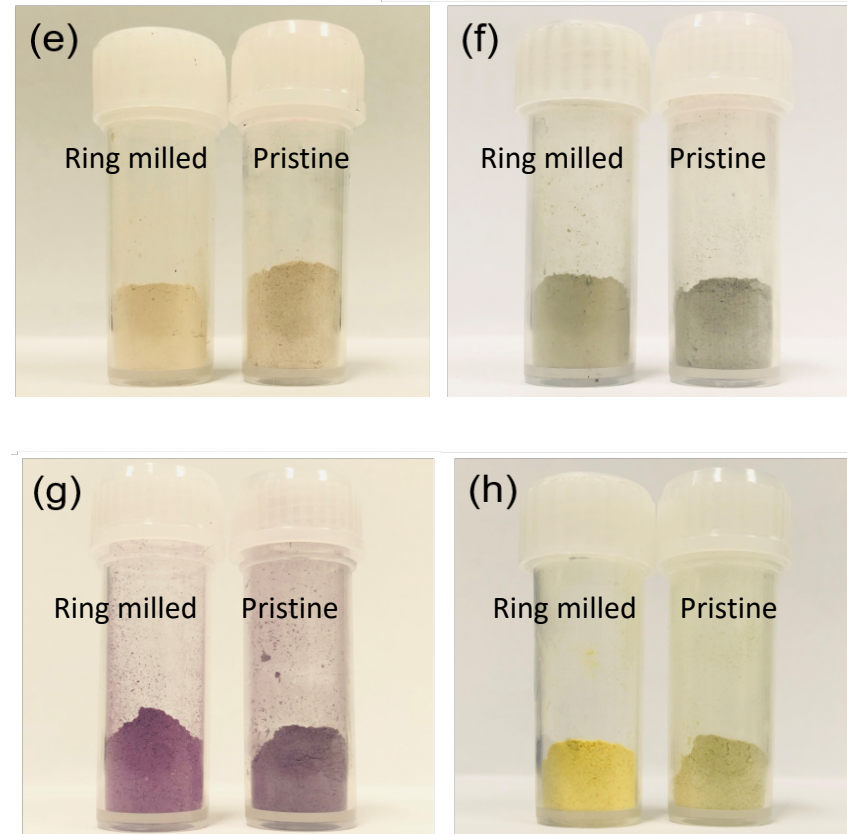
Structure	Computational data (DFT calculated)				Experimental data	
	Norm-conserving pseudopotential		Ultrasoft pseudopotential		Lattice constant (Å)*	Band gap (eV)
	Lattice constant (Å)	Band gap (eV)	Lattice constant (Å)	Band gap (eV)		
BCN	10.867	1.73	10.766	2.55	10.627	2.85
BCT	10.520	3.06	10.989	2.40	10.623	3.05
BZN	10.767	1.76	10.582	2.96	10.558	2.90
BZT	10.418	3.12	10.809	2.71	10.555	3.02

*TOPAS refined values

Tauc plots for LTMP



CRICOS No.00213J

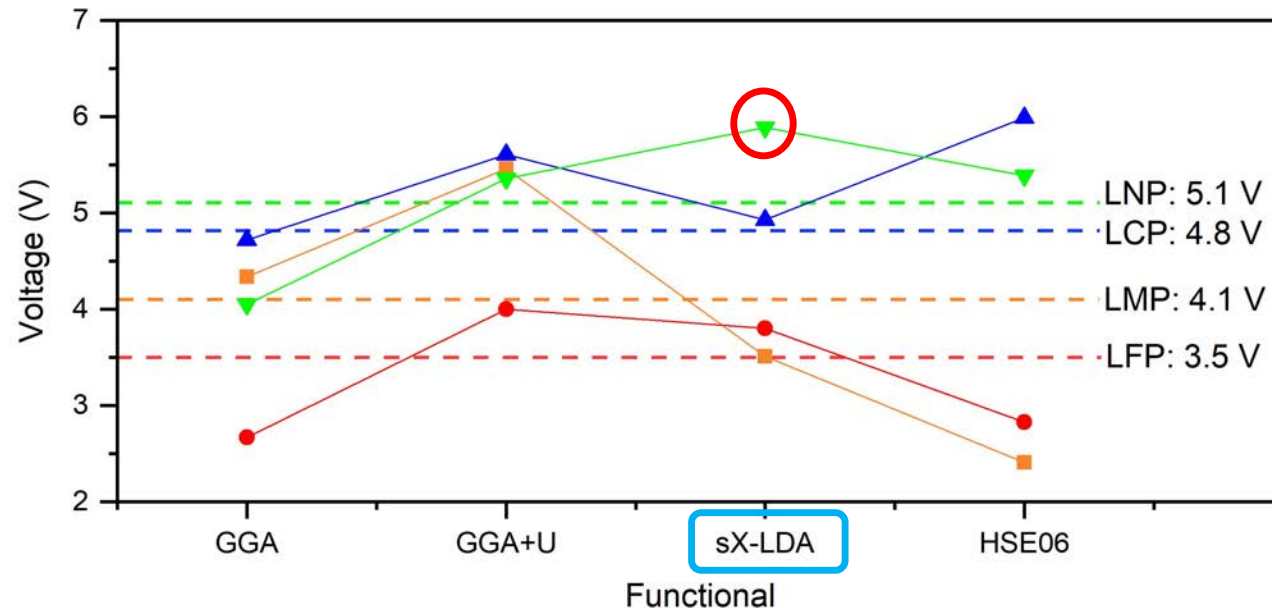


Conclusions

Open circuit voltage from calculated enthalpies

- sX-LDA outperforms all other functional in EBS determination for phosphate materials.

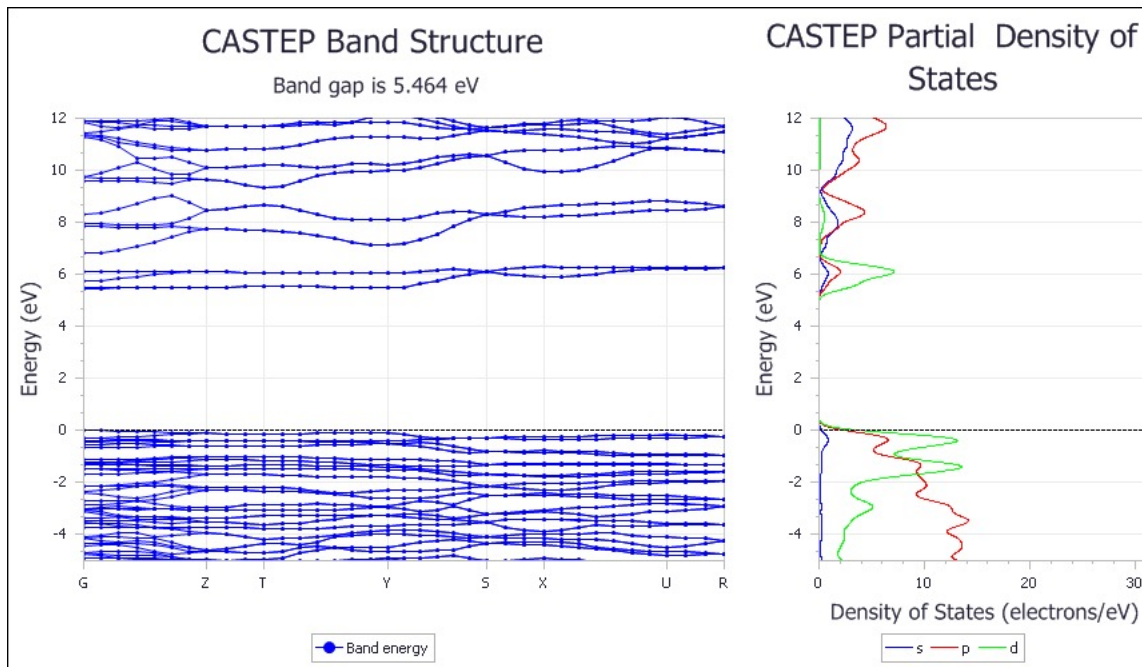
$$V = \frac{G[\text{Li}_{x_2} \text{ Host}]-G[\text{Li}_{x_1} \text{ Host}]-(x_2-x_1)G[\text{Li}]}{x_2-x_1}$$



Estimated Li intercalation voltage with GGA, GGA+U, HSE06 and sX-LDA.

Peak fitting refinement vs Geometry Optimization

LiNiPO₄ (CIF 72929)



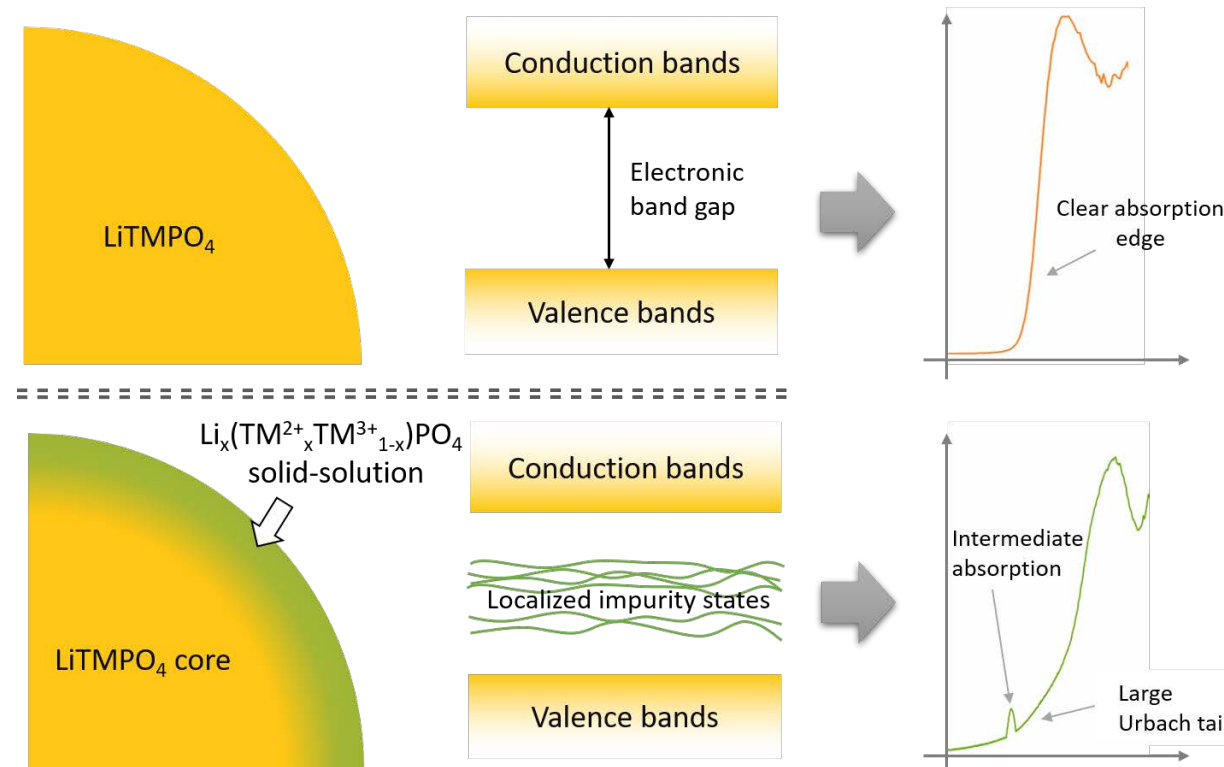
$$V = -\frac{G[\text{Li}_{x_2} \text{Host}] - G[\text{Li}_{x_1} \text{Host}] - (x_2 - x_1)G[\text{Li}]}{x_2 - x_1}$$

Geometry optimised
mode (no spin)
Enthalpy -24760.02 eV
More stable
Band gap 5.464 eV
Closer to exp.
Reduced forces
Equilibrium positions

Conclusions

Localised impurity states

- Phosphate cathode materials surfaces are different from their cores.



Soft X-ray Absorption Spectroscopy (Australian Synchrotron)



CRICOS No.00213J

Density Functional Theory

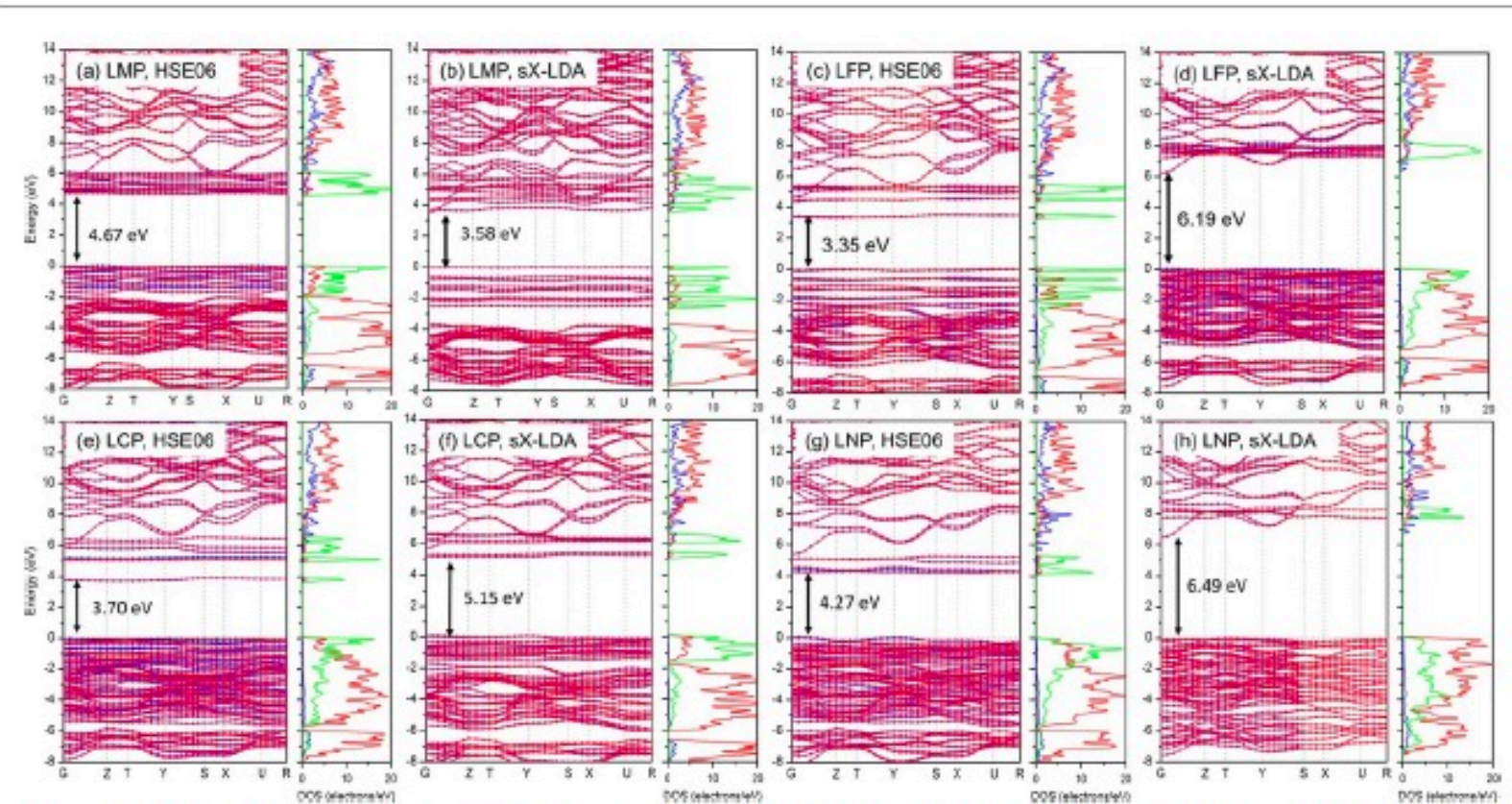
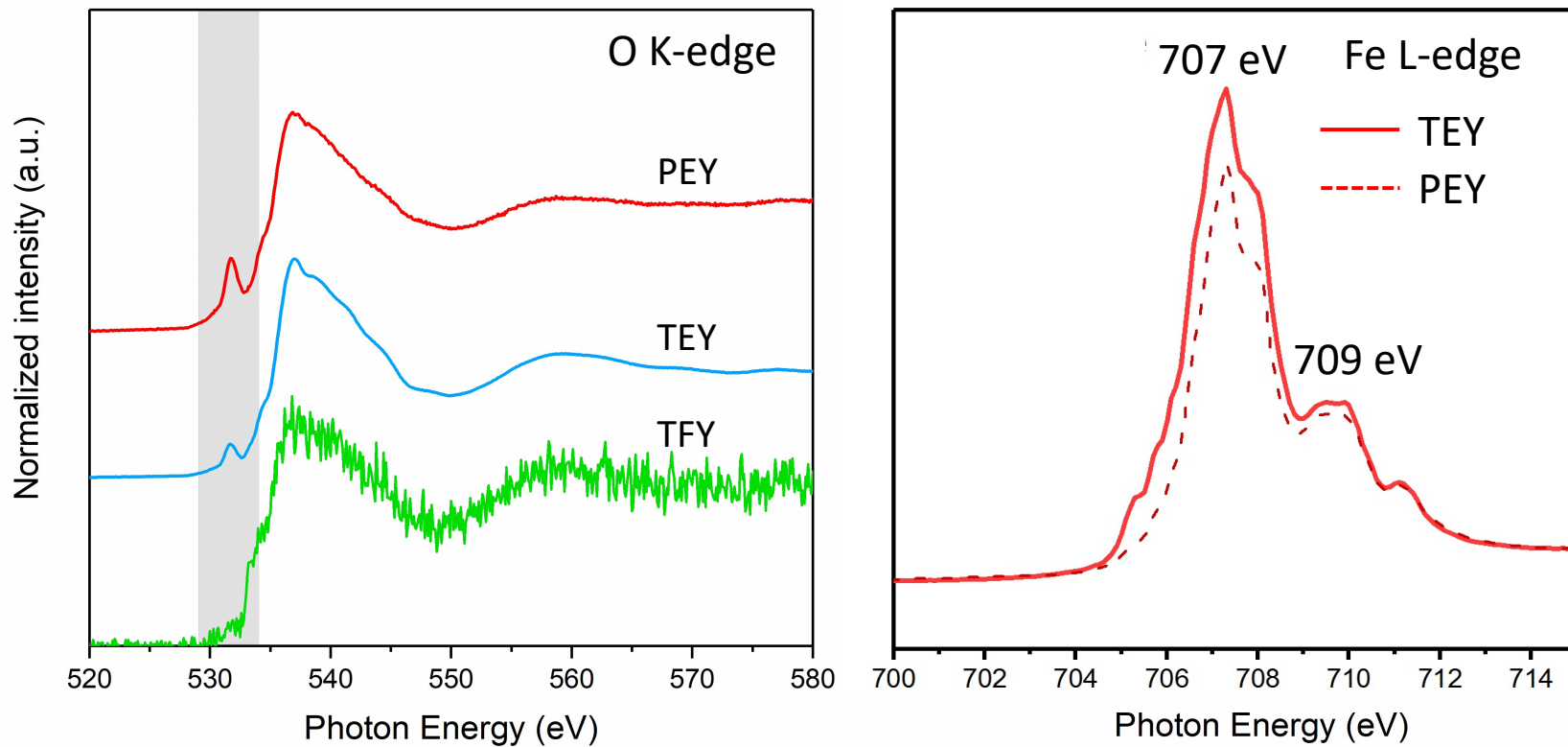


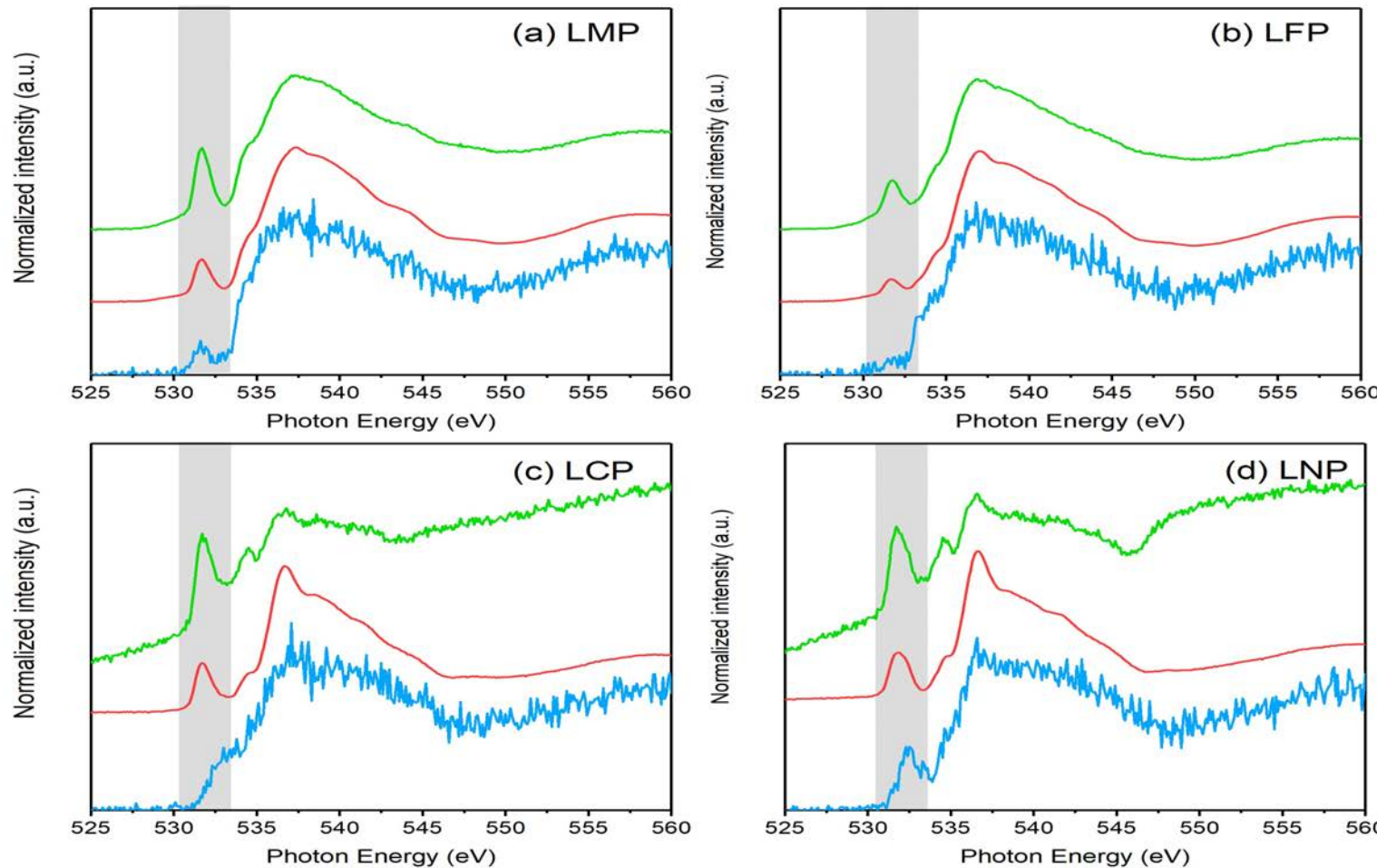
Figure 4. Calculated electronic band structure (left panels) and DOS (right panels) for LiMPO_4 with HSE06 and sX-LDA. (a) and (b) $M = \text{Mn}$; (c) and (d) $M = \text{Fe}$; (e) and (f) $M = \text{Co}$; (g) and (h) $M = \text{Ni}$. The blue, red and green lines on the right panels represent the s, p and d density of states. Reprinted (adapted) with permission from [23]. Copyright (2020) American Chemical Society.

O K-edge and Fe L-edge vs escape depth

- Partial electron yield (PEY): surface sensitive
- Total electron yield (TEY): $\sim 50 \text{ \AA}$
- Total fluorescence yield (TFY): $\sim 3000 \text{ \AA}$



O K-edge of LTMP

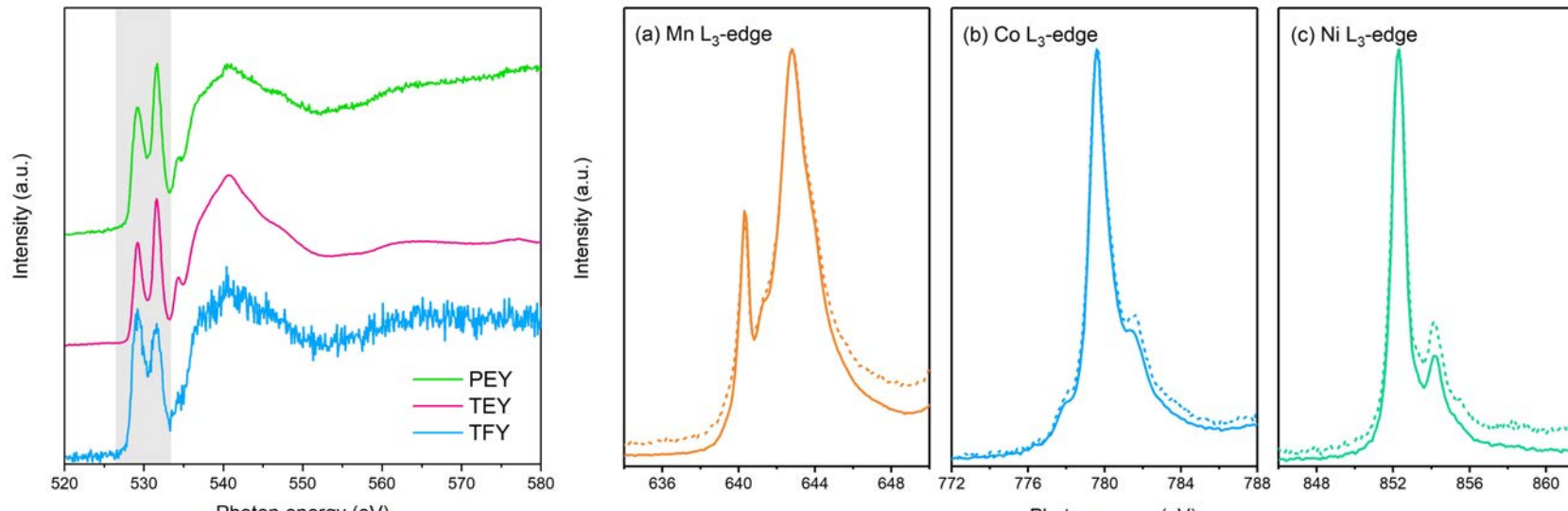


O K-edge spectra of the as prepared LiMPO_4 .

Conclusions

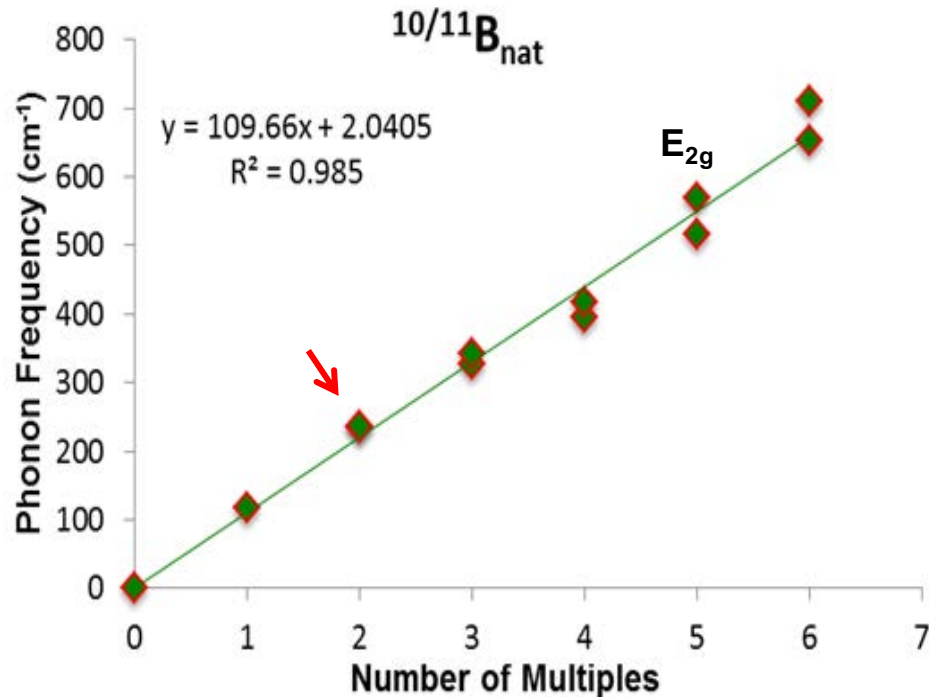
Preliminary results for NMC materials

- Differentiation between surfaces and cores may be more general than for only phosphates.



O K-edge and TM L-edge spectra for NMC.

MgB₂ – Frequency Harmonics



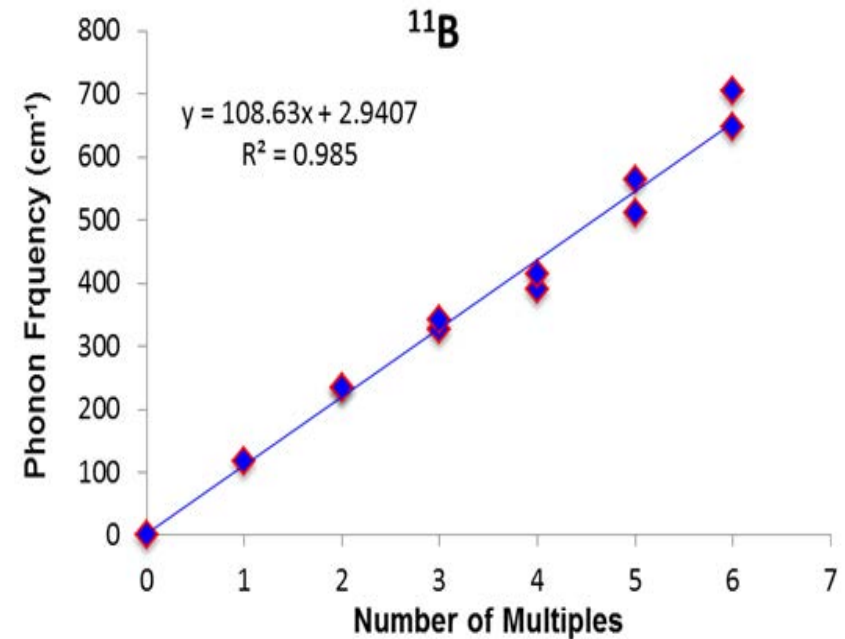
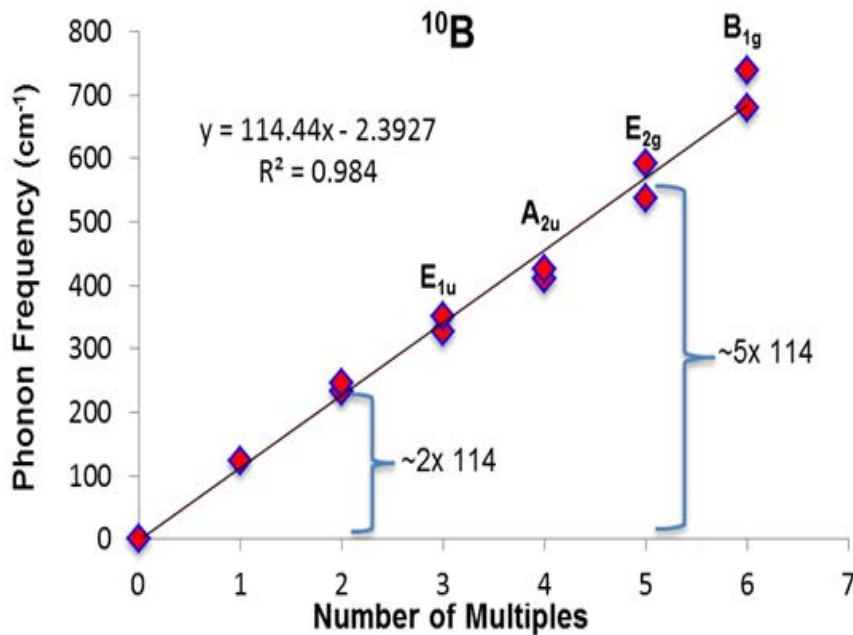
$$\text{Slope} \sim 4k_B T_c$$

Slope \propto Isotope effect

$$A_{1g} (= B_{1g}) = E_{2g} + 116 \text{ cm}^{-1}$$

Alarco et al., Phys. Chem. Chem. Phys., 16, 25386-25392, 2014

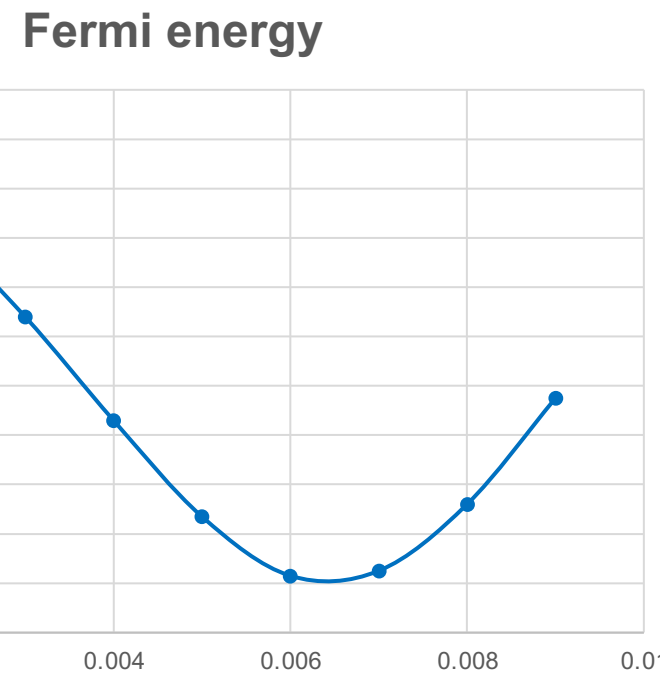
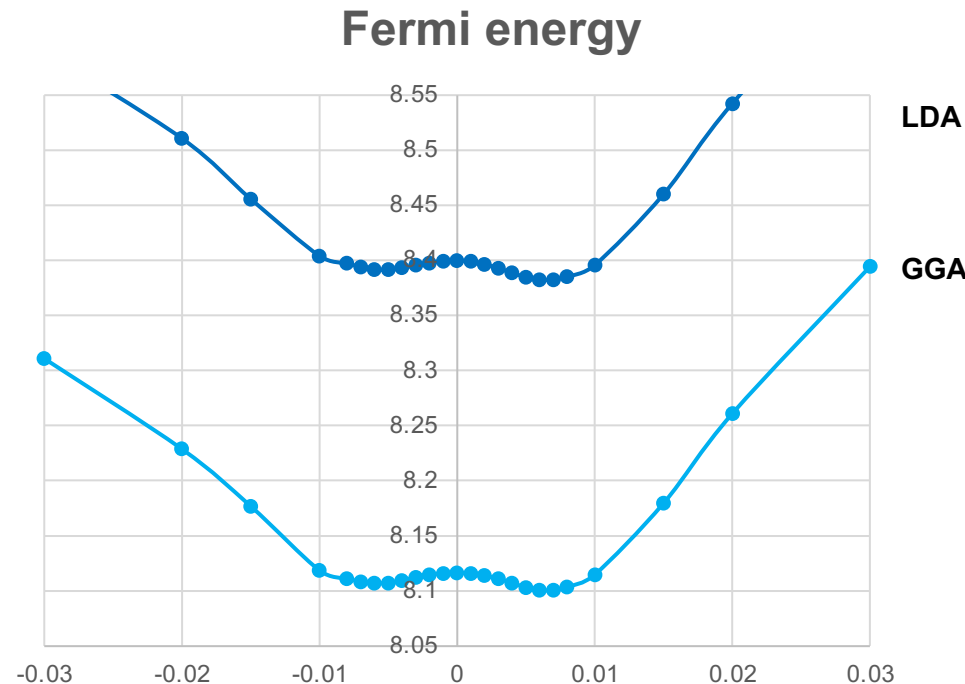
MgB₂ – Isotope Effect



Slope $\sim 4k_B T_c$

Slope \propto Isotope effect

Electron density response— MgB₂ with Frozen displaced atoms



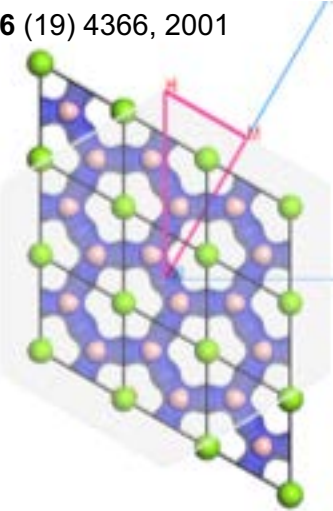
Alarco *et al.*, MNSMS **8**, 21-46, 2018

CRICOS No.00213J

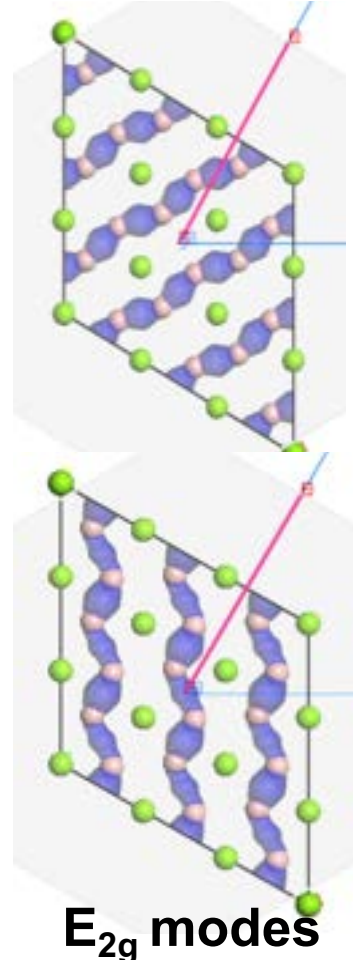
Electron density response—MgB₂ with Frozen displaced atoms

E_{2g} modes → 25 times stronger contribution to e-ph coupling than other modes

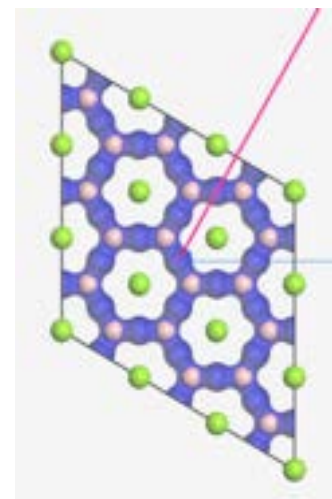
An and Pickett, PRL 86 (19) 4366, 2001



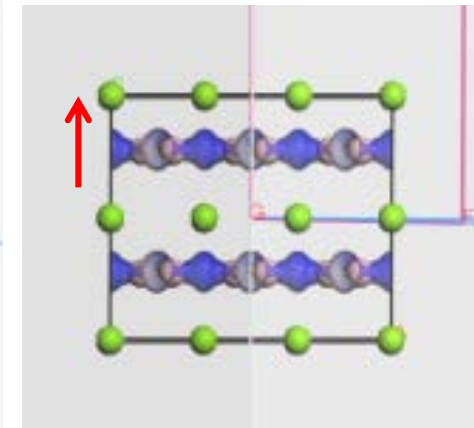
MgB₂
symmetric
Geometry
optimized



E_{2g} modes



E_{1u} mode



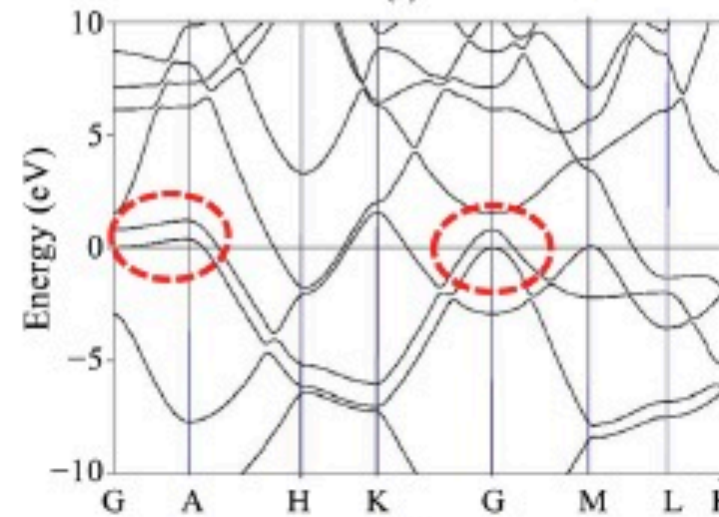
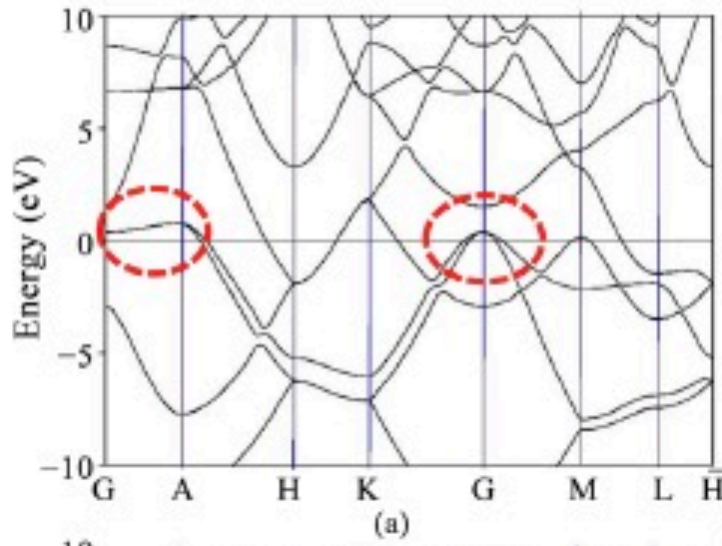
A_{2u} mode

Relative
displacement
 $Dx = 0.05$

Alarco *et al.*, MNSMS 8, 21-46, 2018

Frozen displaced atoms

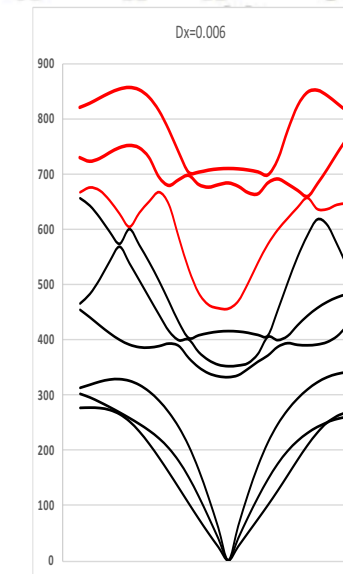
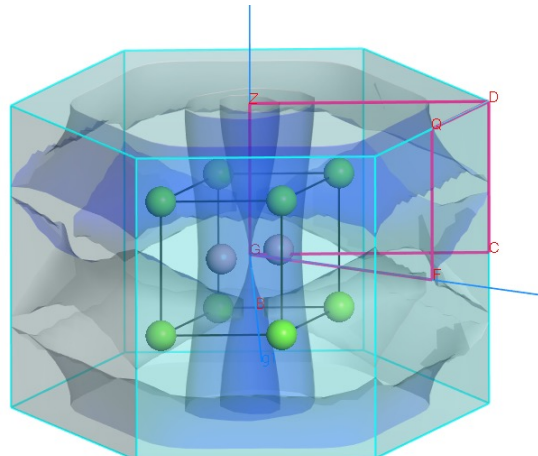
Dx = -0.000



Dx = -0.006

Dx = 0.006

Fermi surface topological changes

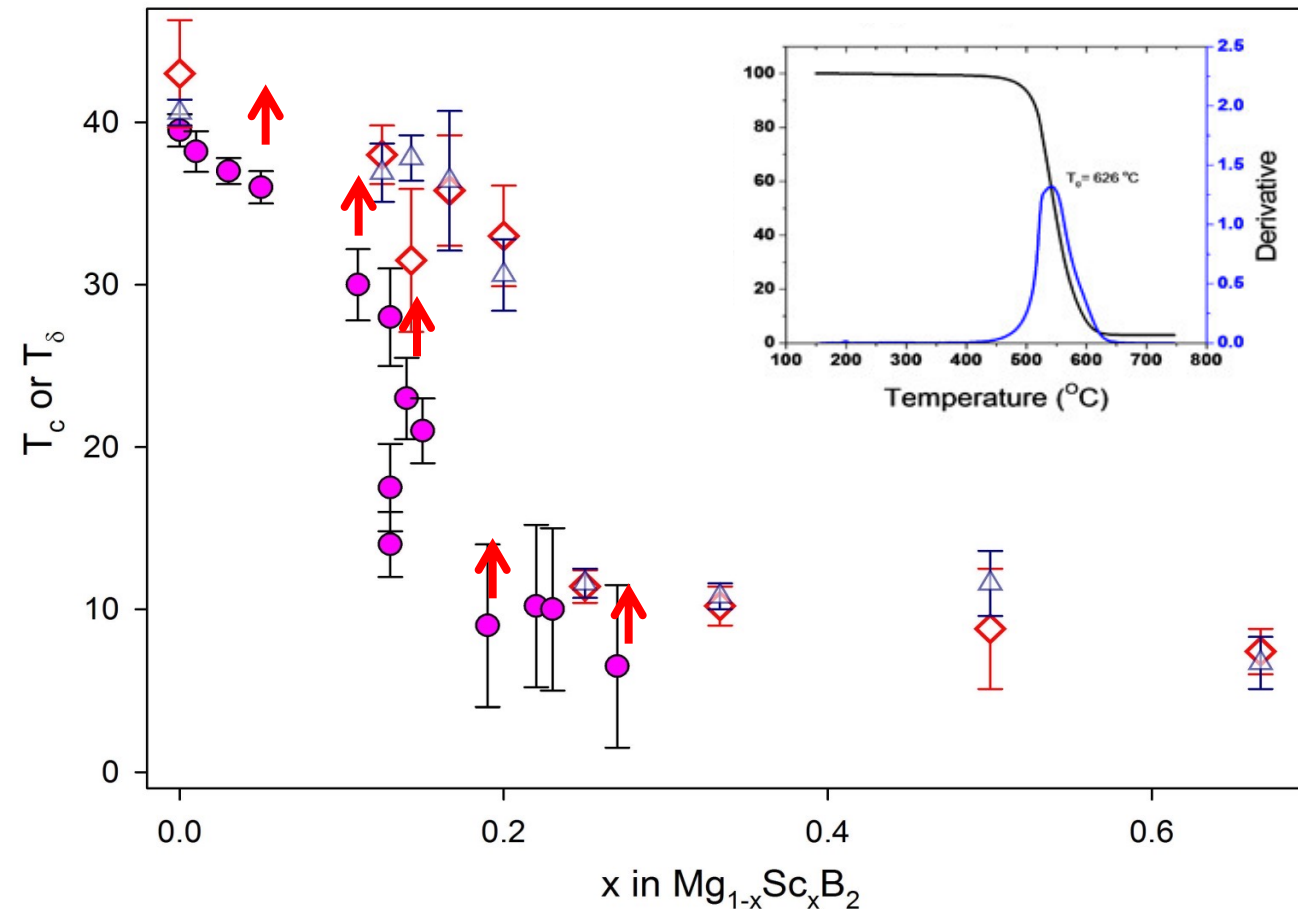


Dx = 0.006

Alarco *et al.*, MNSMS **8**, 21-46, 2018

Superconducting T_c – $Mg_{1-x}Sc_xB_2$

Theory and Experiment



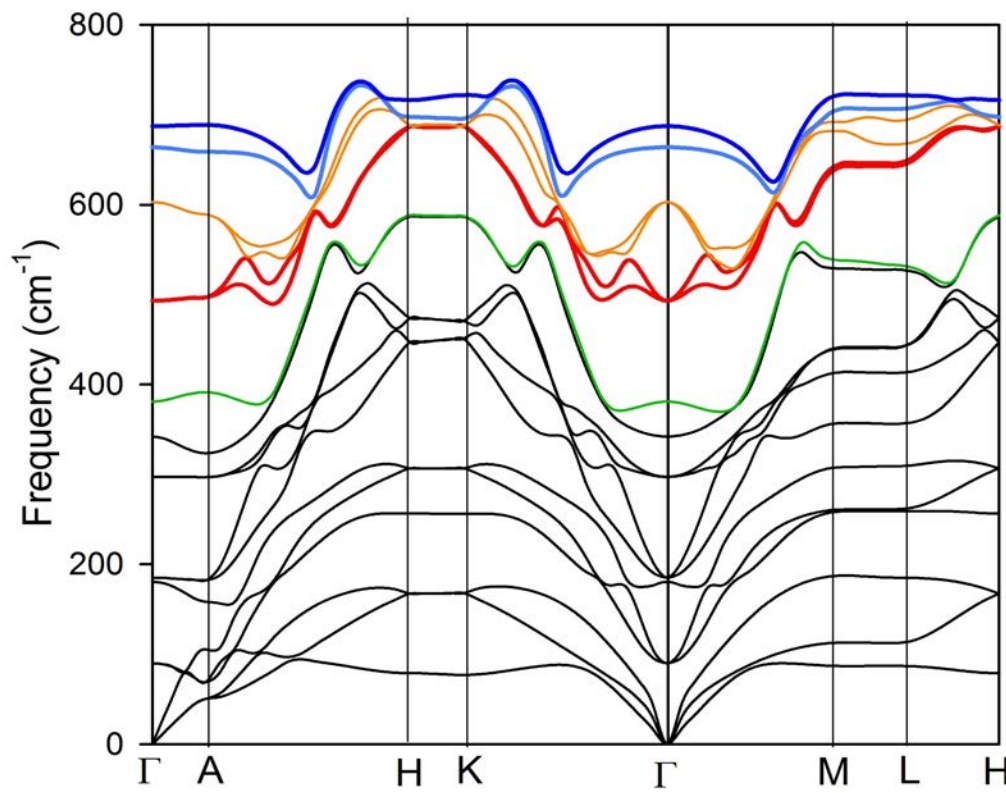
**Agrestini et al. 2004 use peak values from derivative of surface resistance measurements

CRICOS No.00213J

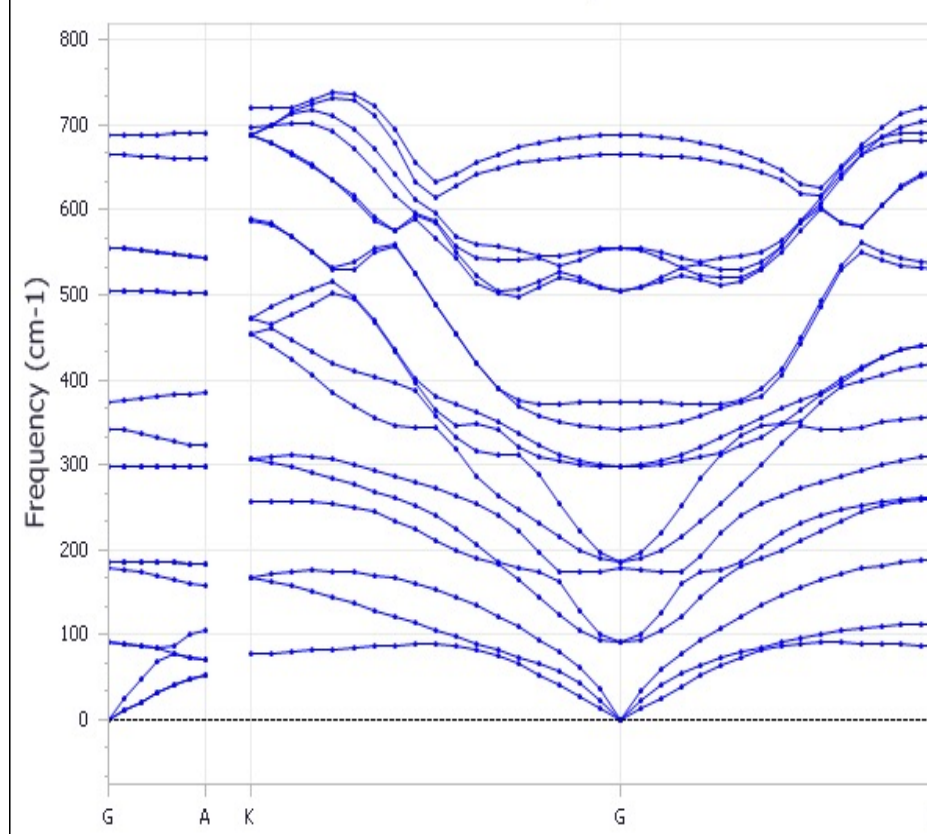
MgB₂ substituted with Rb

Phonon Dispersions

MgRbB4 LDA 0.017



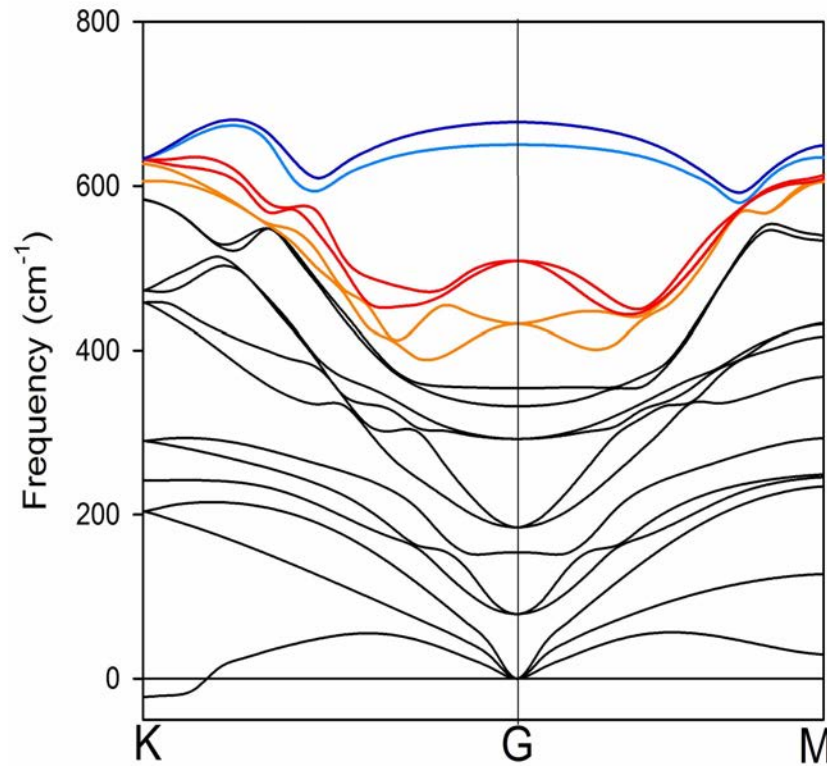
MgRbB4 LDA k=0.012



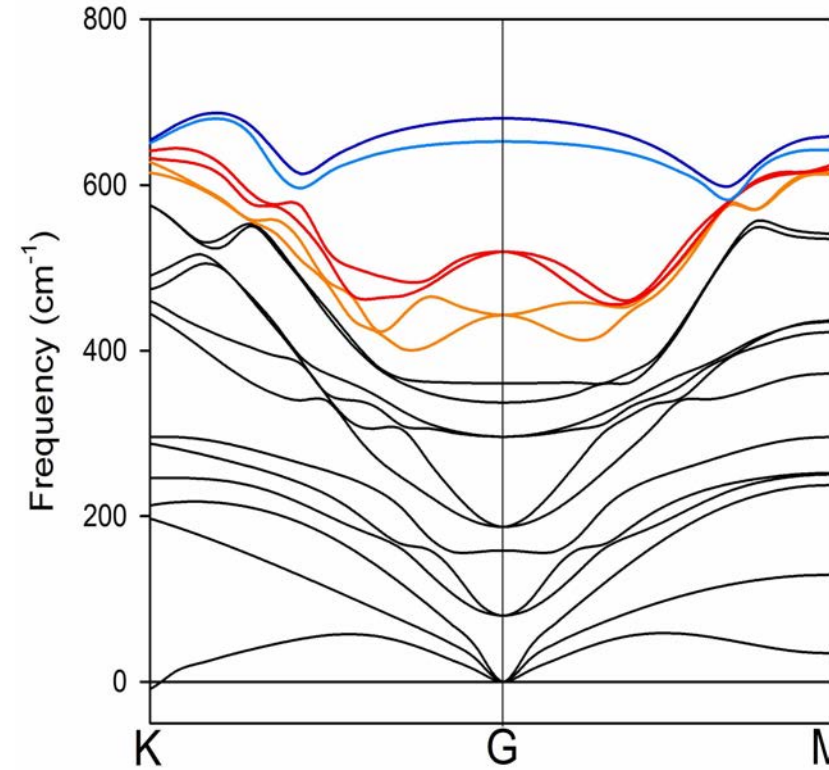
Asymmetric
and
Multiple
level
anomaly

MgB₂ substituted with Cs Phonon Dispersions

MgCsB4 LDA k=0.015 0GPa



MgCsB4 LDA k=0.015 1GPa



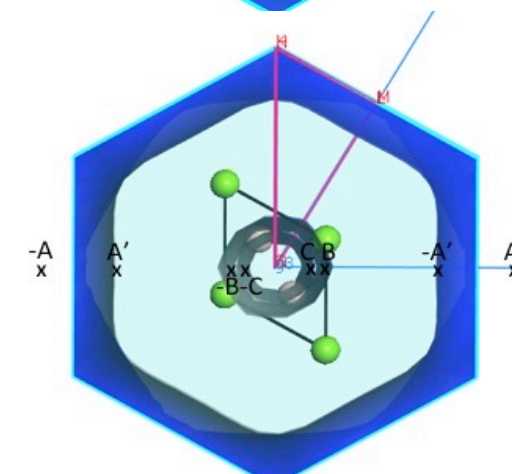
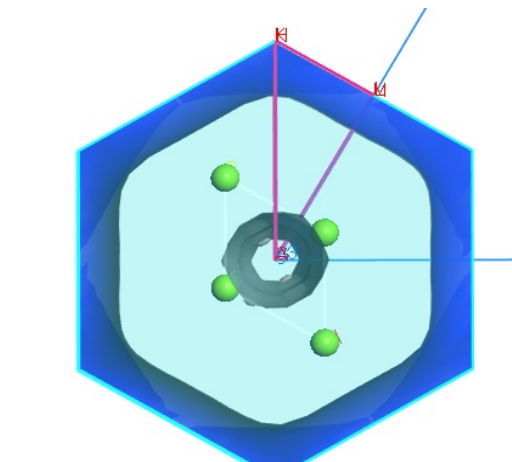
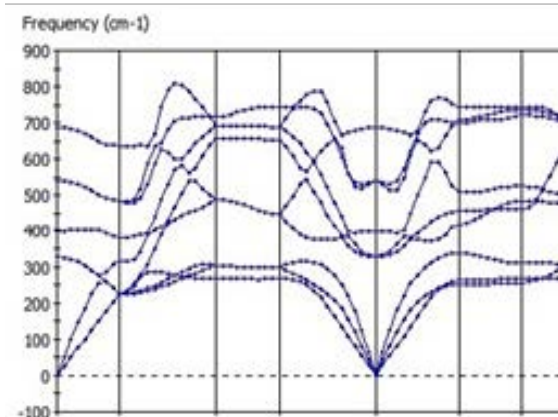
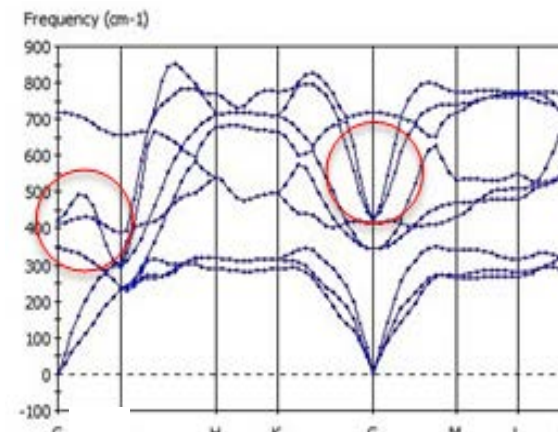
Asymmetric
and
Multiple
level
anomaly

Density Functional Theory

Phonon Dispersions – MgB₂

Key Factors:

- Optimise cell parameters
- Use dense k-grid mesh
(optimise for lowest k-value)
- Avoid negative phonon frequencies
- Fractional occupancies for metal substitutions are limited
- Mean relative error $\pm 5\%$



Alarco *et al.*, Phys. Chem. Chem. Phys., **16**, 24443-24456, 2014

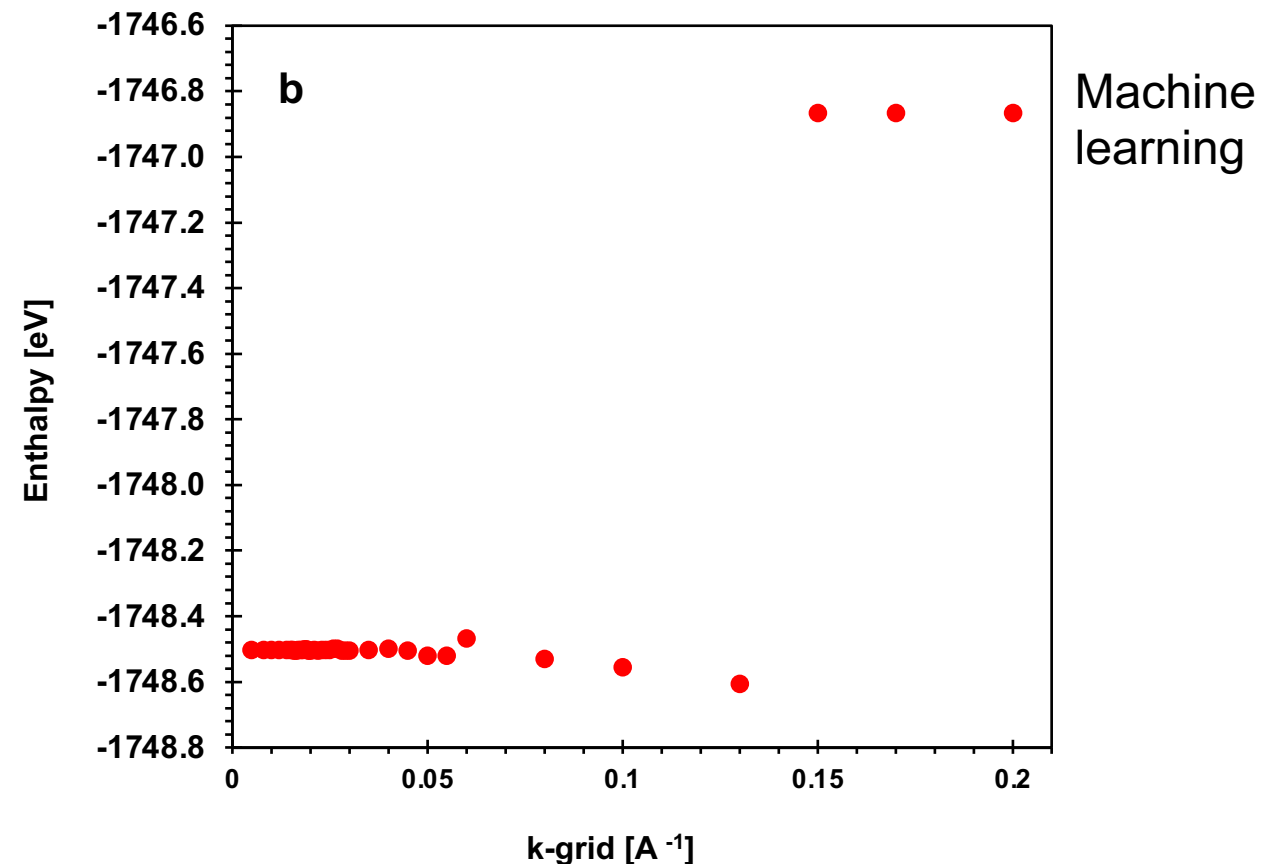
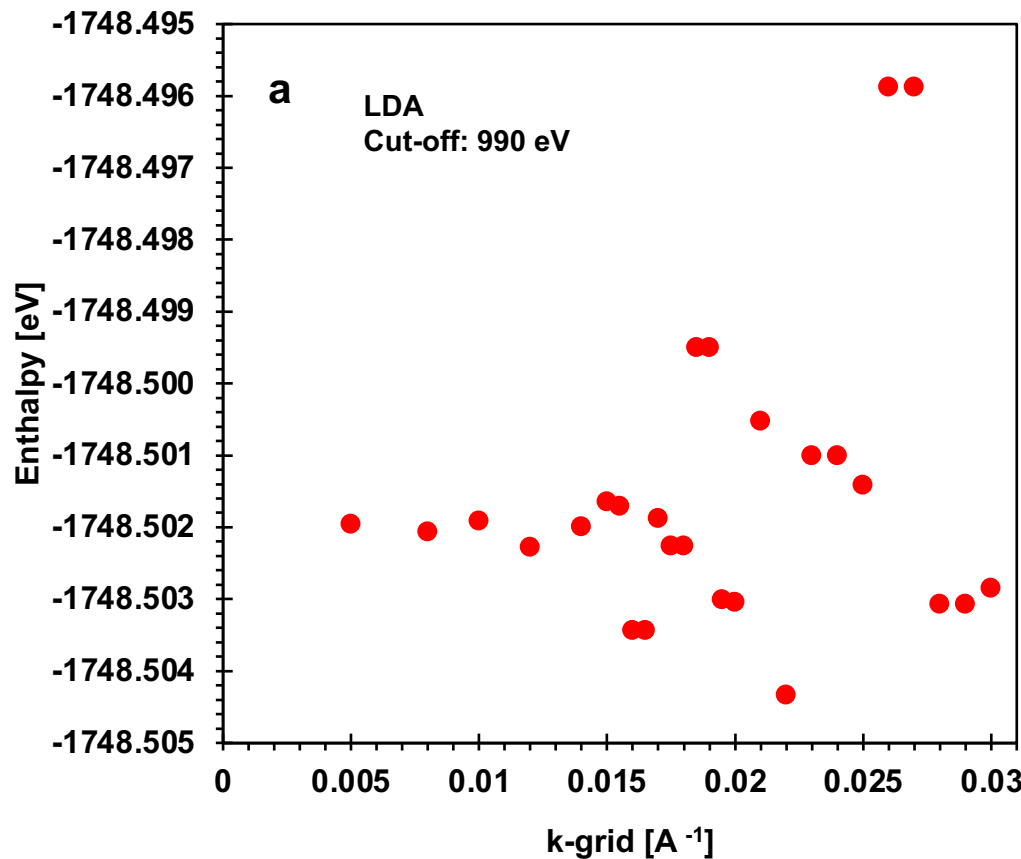
CRICOS No.00213J

K-grid optimization

DFT Code	Δk value (\AA^{-1})	Grid Equivalent	No. of k-points	Energy Cut-off (eV)	Fermi Energy (eV)	ΔE_v [eV]	Funct'l
CASTEP	0.100	4x4x4	8	990	8.8103	-0.097	LDA
CASTEP	0.060	6x6x6	21	990	8.2110	0.636	LDA
CASTEP	0.050	8x8x6	30	990	8.5190	0.419	LDA
CASTEP	0.040	9x9x8	48	990	8.4706	0.328	LDA
CASTEP	0.030	12x12x10	95	990	8.3773	0.383	LDA
CASTEP	0.020	19x19x14	280	990	8.3976	0.348	LDA
CASTEP	0.015	25x25x20	650	990	8.3991	0.352	LDA
CASTEP	0.008	47x47x36	3744	990	8.4038	0.343	LDA
CASTEP	0.005	75x75x58	14703	990	8.4040	0.343	LDA
CASTEP	0.005	75x75x58	14703	500	7.3295	0.371	LDA
CASTEP	0.008	47x47x36	3744	500	7.3285	0.372	LDA
CASTEP	0.020	19x19x14	280	500	7.3218	0.370	LDA
CASTEP	0.030	12x12x10	95	500	7.2449	0.475	LDA

All k-grid values are geometry optimized and converged to the same ultrafine tolerance.

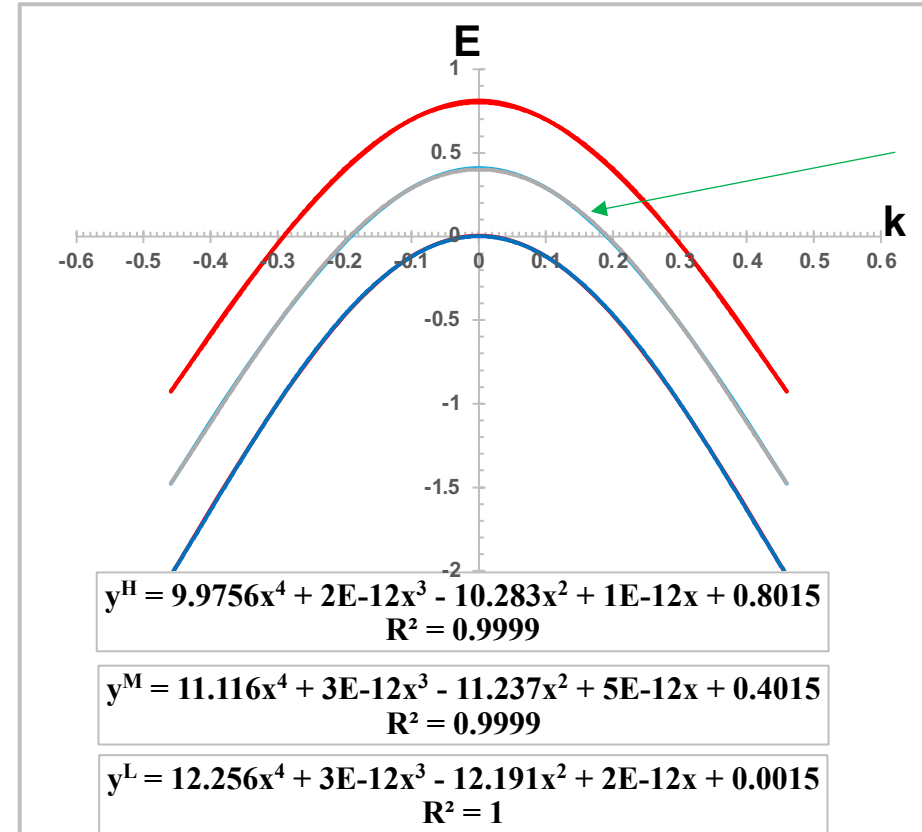
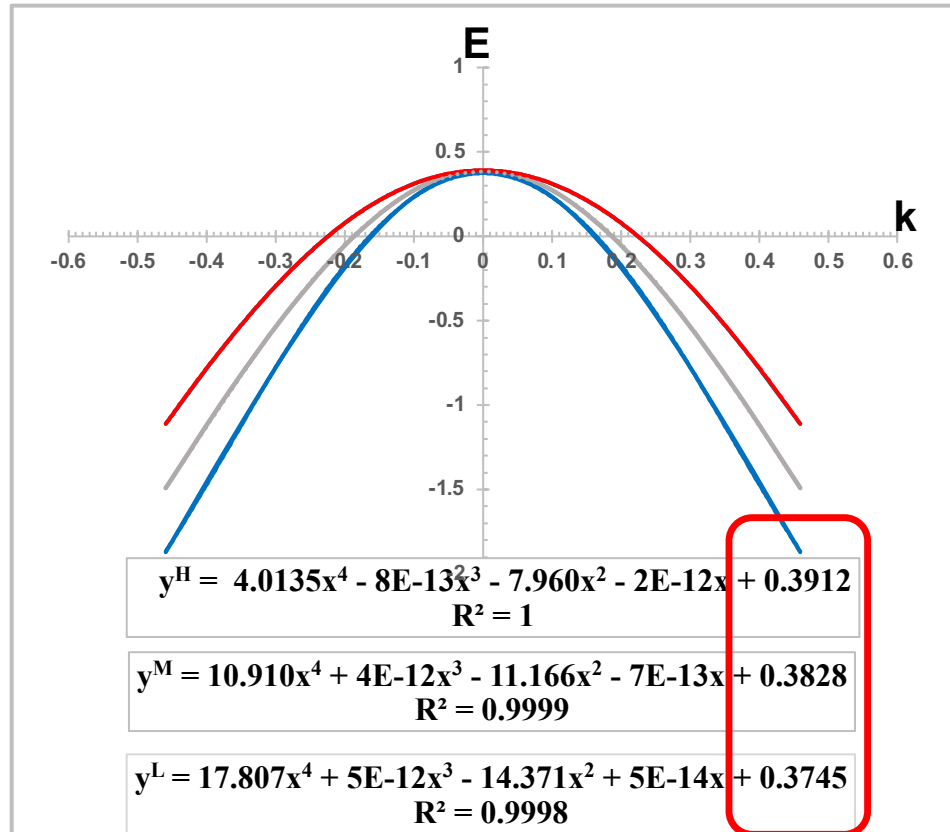
K-grid optimization



All k-grid values are geometry optimized and converged to the same ultrafine tolerance!

Trendline fittings EBS

Heavy
—
Light
—



Approximate Constant of Movement

Average or Medium

Fig.1 σ bands (heavy (y^H) - red, light (y^L) - blue and average (y^M) - gray) for the EBS of MgB₂ along the Γ -K-direction at atmospheric pressure (0 GPa), calculated with the LDA functional using k-grid $\Delta k = 0.01 \text{ \AA}^{-1}$: (a) for equilibrium B – atom positions and (b) for displaced B –atom positions along E_{2g} modes.

Trendline fittings EBS

Table 2. Trendline fittings along Γ K for the σ bands of MgB₂ calculated using LDA and different k-grids*.

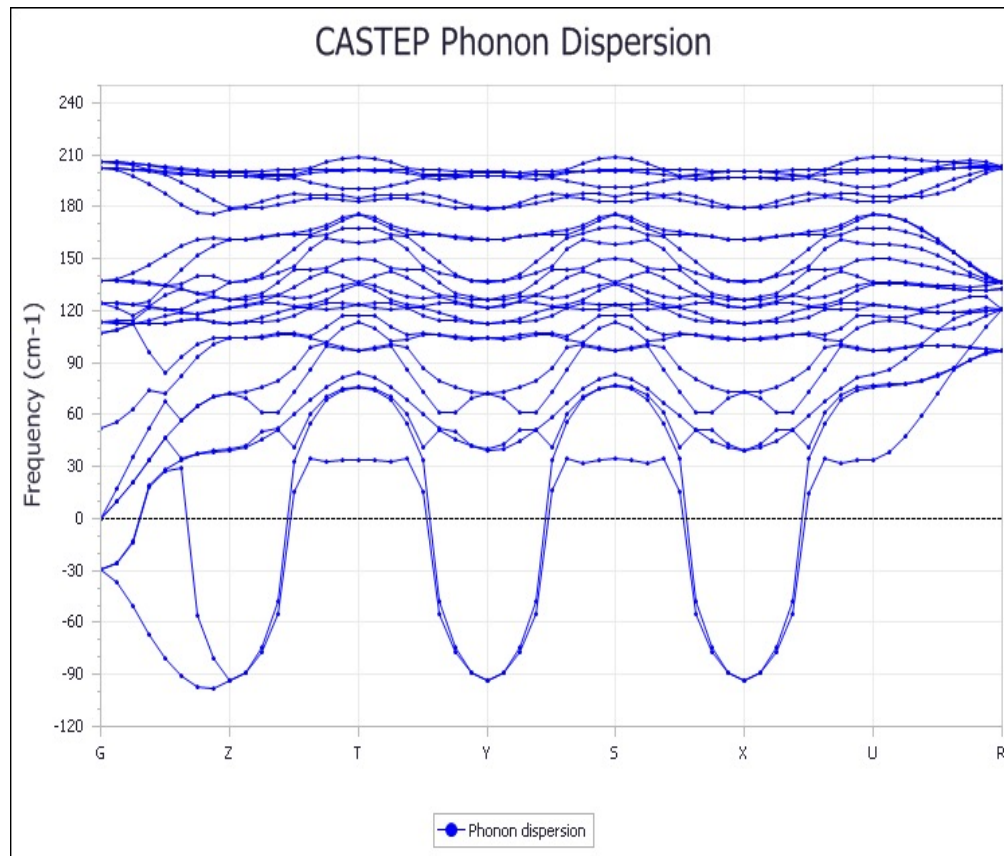
k-grid	Coefficient X ⁴			Coefficient X ² (-1)			Coefficient X ⁰			Estimated gap energy (eV)
	H	M	L	H	M	L	H	M	L	
0.005	4.2955	11.434	18.572	8.161	11.455	14.749	0.3441	0.3354	0.3266	0.0175
0.008	8.0342	23.341	36.301	11.159	15.864	20.344	0.3441	0.3375	0.3287	0.0154
0.01	4.0135	10.91	17.807	7.96	11.166	14.371	0.3912	0.3828	0.3745	0.0167
0.022	6.8879	21.451	36.014	10.381	14.929	19.477	0.3377	0.3333	0.3289	0.0088
0.03	6.4614	24.477	42.492	10.33	15.271	20.213	0.383	0.383	0.383	0.000

*Tables present the coefficients in front of the even powers of the quartic polynomials (X⁴, X² and X⁰). Smearing was 0.001eV for k-grids 0.005 and 0.008A⁻¹, and 0.1eV for k-grids 0.01, 0.022 and 0.03A⁻¹.

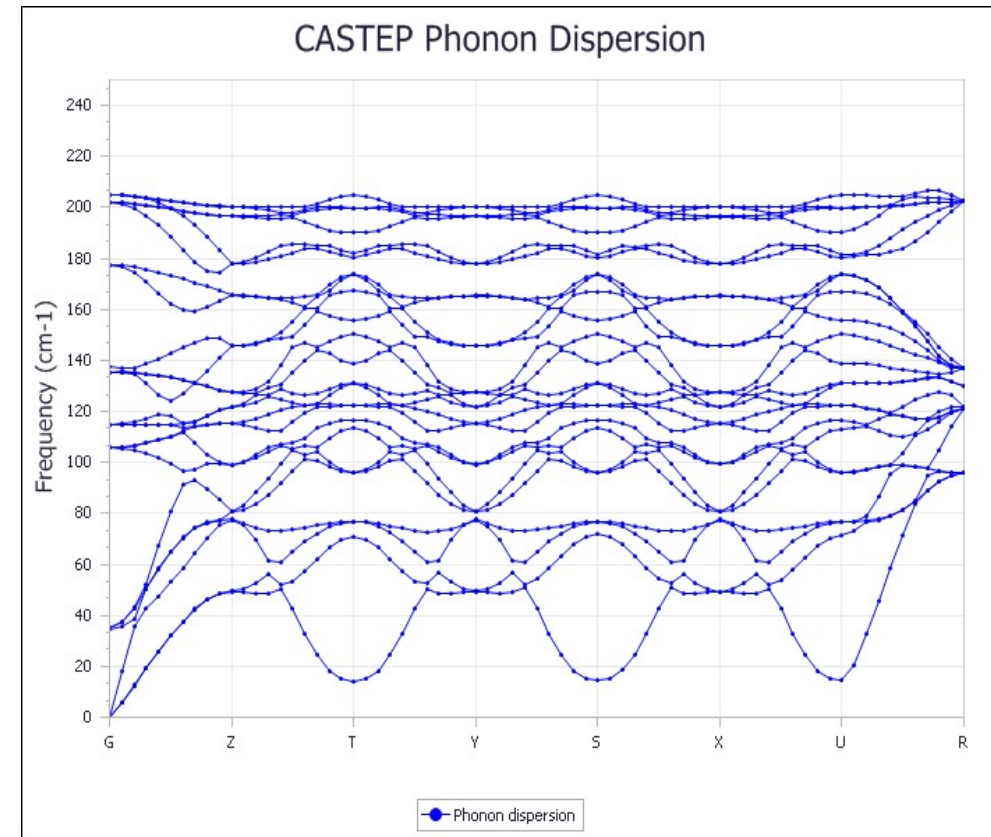
A15-superconductors

Nb_3Ga Tc ~ 20.3K

Negative Frequencies
Soft modes
Phase instability



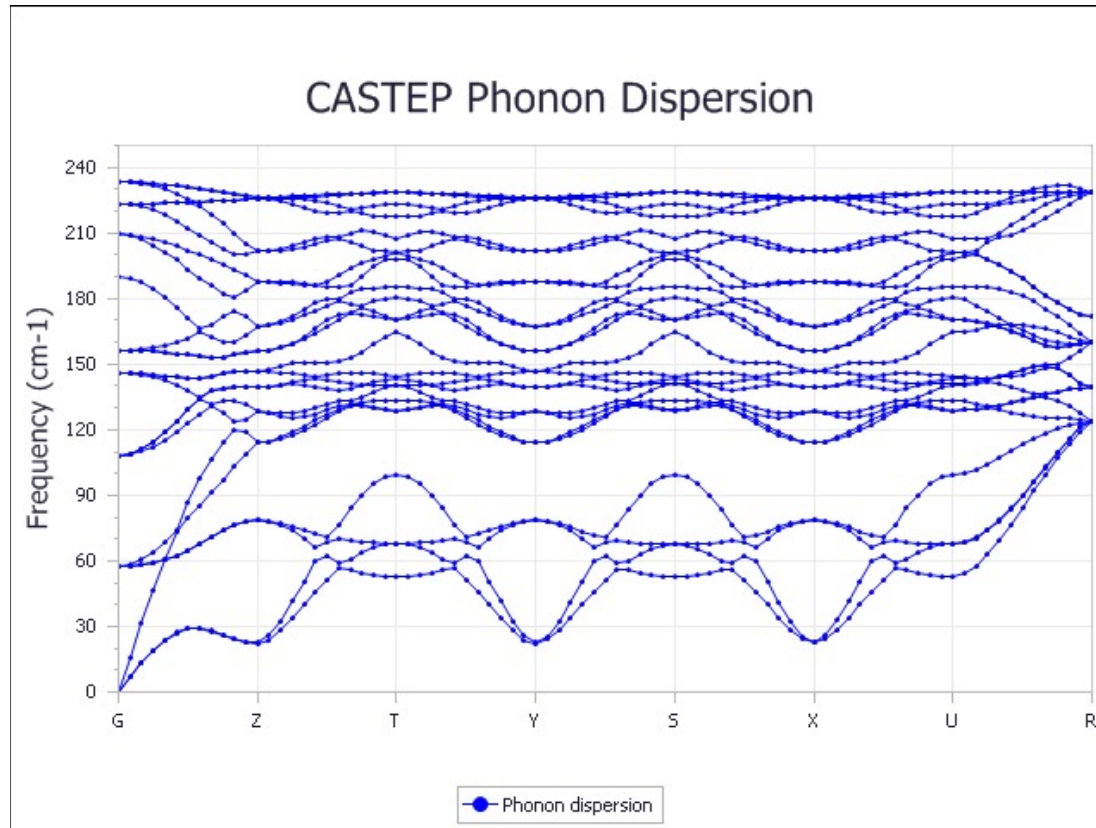
$$k = 0.016 \text{ \AA}^{-1} \rightarrow 0.012 \text{ \AA}^{-1}$$



$$k = 0.01 \text{ \AA}^{-1}$$

A15-superconductors

Nb_3In $T_c \sim 9.2\text{K}$



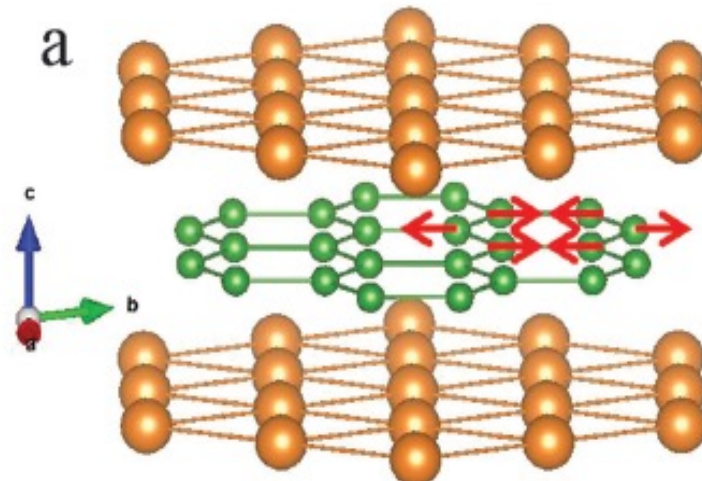
At 20 GPa, $k = 0.008 \text{ \AA}^{-1}$

At 0 GPa,
 $k = 0.01 \text{ \AA}^{-1} \rightarrow k = 0.005 \text{ \AA}^{-1}$
Soft modes

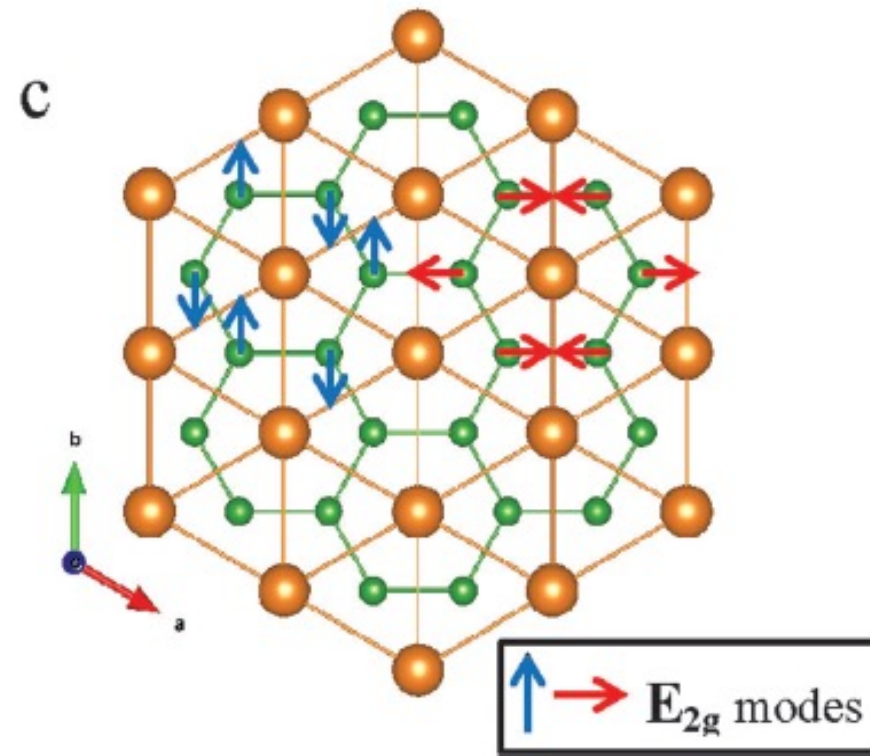
At 20 GPa,
increased T_c

Better resolved
reciprocal space
features

MgB₂ – E_{2g} Phonon Modes



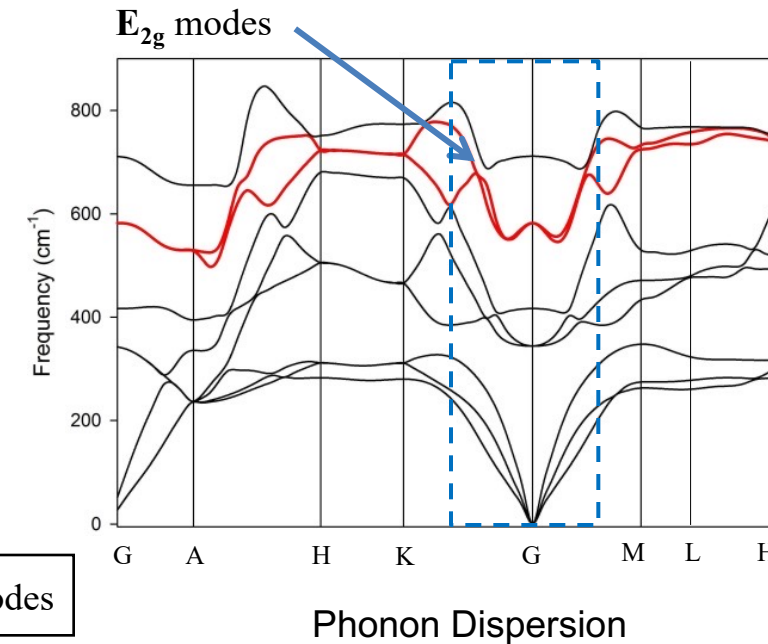
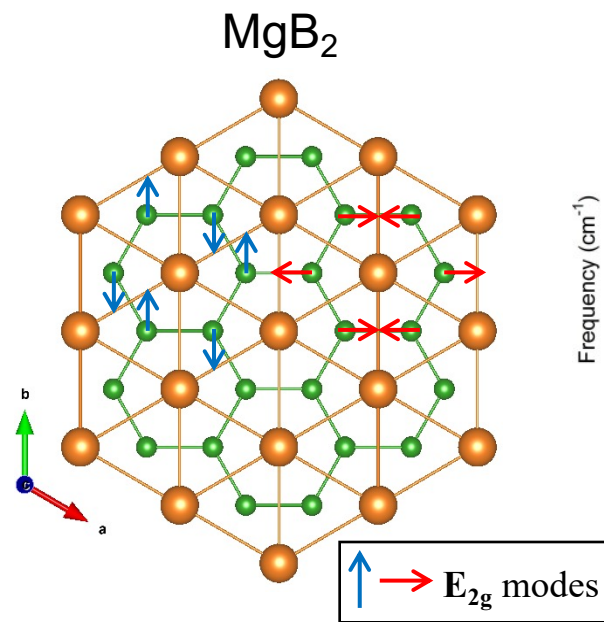
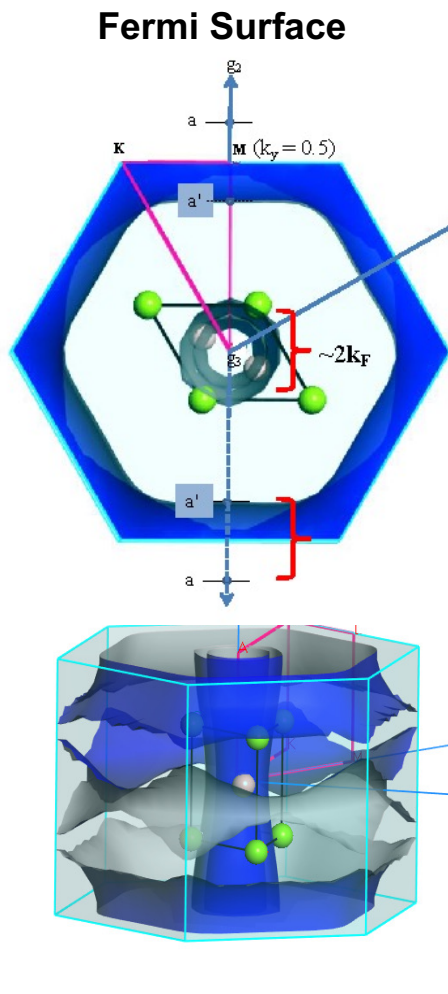
Superconductor T_c ~ 40K
AlB₂-type structure
Group symmetry P6/mmm



Alarco *et al.*, Phys. Chem. Chem. Phys., **16**, 24443-24456, 2014
Alarco *et al.*, Phys. Chem. Chem. Phys., **16**, 25386-25392, 2014
Alarco *et al.*, Phys. Chem. Chem. Phys., **17**, 25090-25099, 2015

Modelling and Simulation

Density Functional Theory – Materials Studio V8.0



- Phonon Dispersion – convergence indicates structural stability
- High computational demand for low values of x
- *Ab initio* models without post-computational corrections

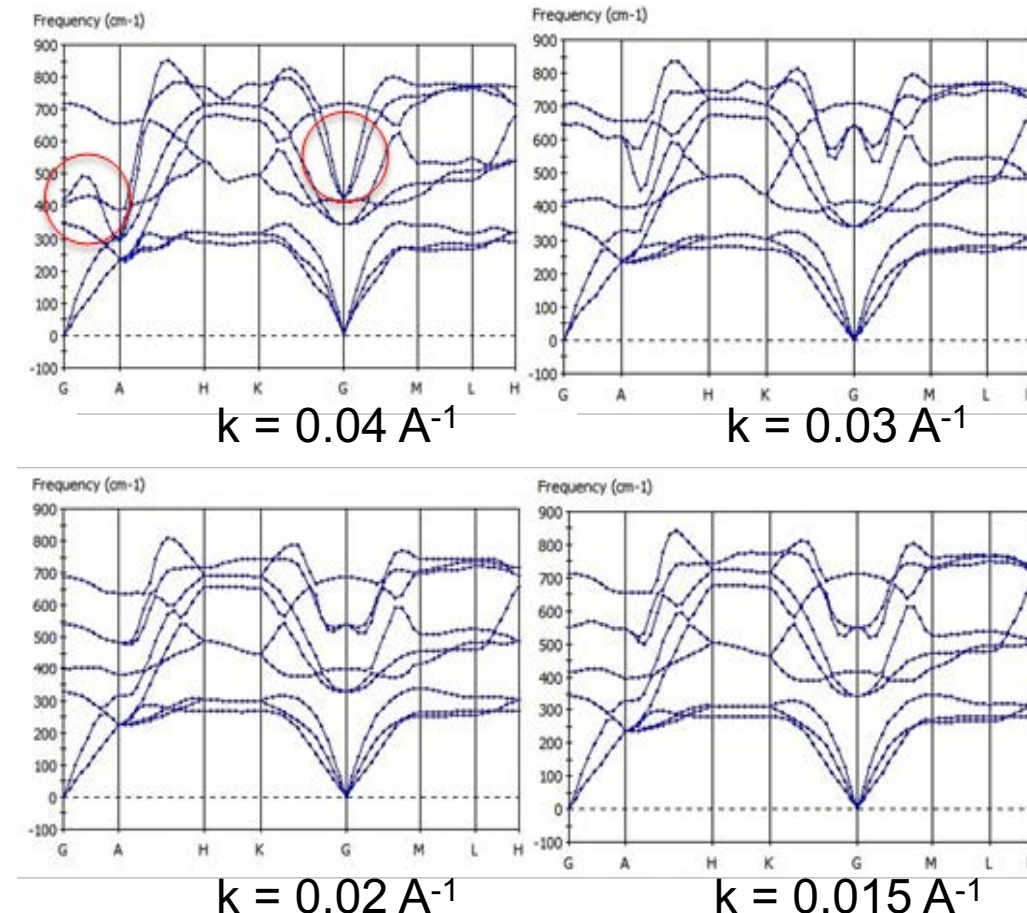
Alarco *et al.*, Phys. Chem. Chem. Phys., **16**, 24443-24456, 2014
Alarco *et al.*, Phys. Chem. Chem. Phys., **16**, 25386-25392, 2014
Alarco *et al.*, Phys. Chem. Chem. Phys., **17**, 25090-25099, 2015

Density Functional Theory

Phonon Dispersions – MgB₂

Key Factors:

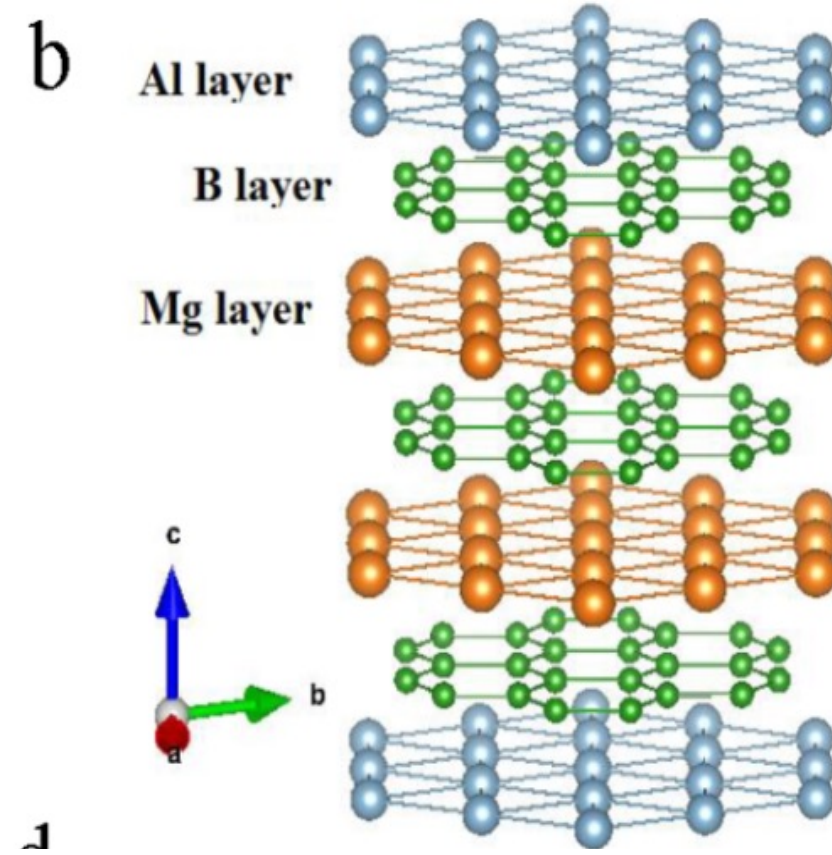
- Optimise cell parameters
- Use dense k-grid mesh
(optimise for lowest k-value)
- Avoid negative phonon frequencies
- Fractional occupancies for metal substitutions are limited
- Mean relative error ±5%



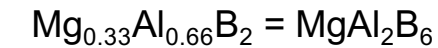
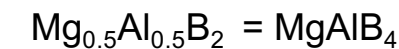
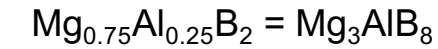
Alarco *et al.*, Phys. Chem. Chem. Phys., **16**, 24443-24456, 2014

CRICOS No.00213J

Substituted Metal Borides



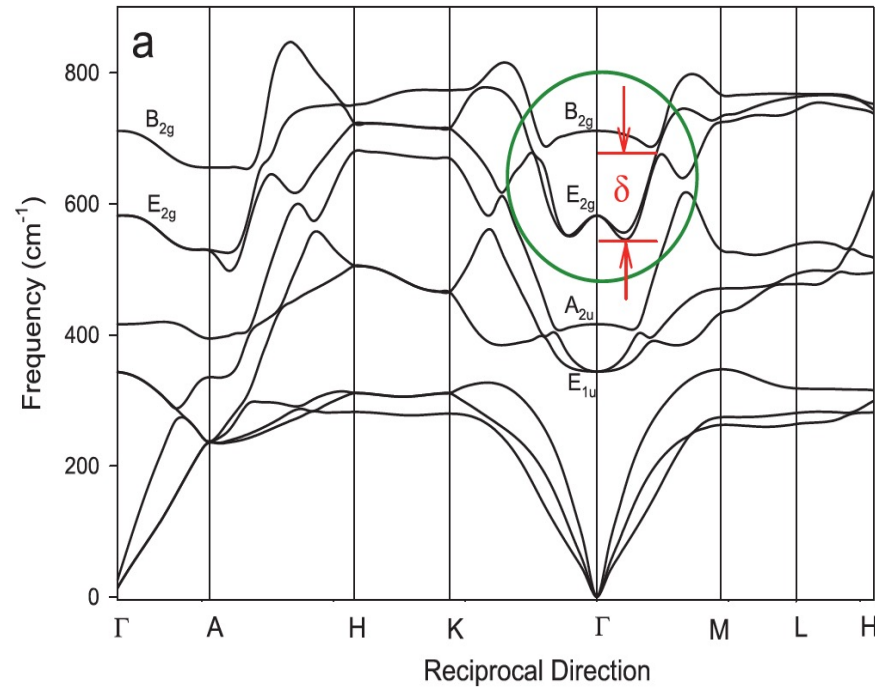
Superlattices



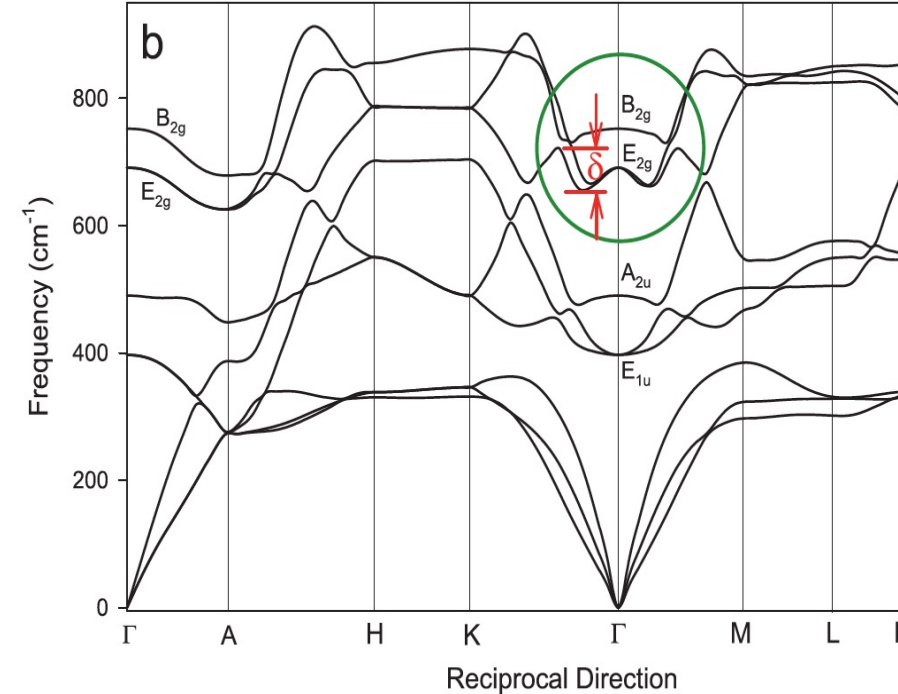
Observed by HREM
Xiang *et al.*, Phys. Rev. B, 2002
Zandbergen *et al.*, Physica C, 2002
Li *et al.*, Phys. Rev. B, 2002

Alarco *et al.*, Phys. Chem. Chem. Phys., **16**, 24443-24456, 2014
Alarco *et al.*, Phys. Chem. Chem. Phys., **16**, 25386-25392, 2014
Alarco *et al.*, Phys. Chem. Chem. Phys., **17**, 25090-25099, 2015

Superconducting T_c – MgB_2 with pressure



$P = 0 \text{ GPa}$



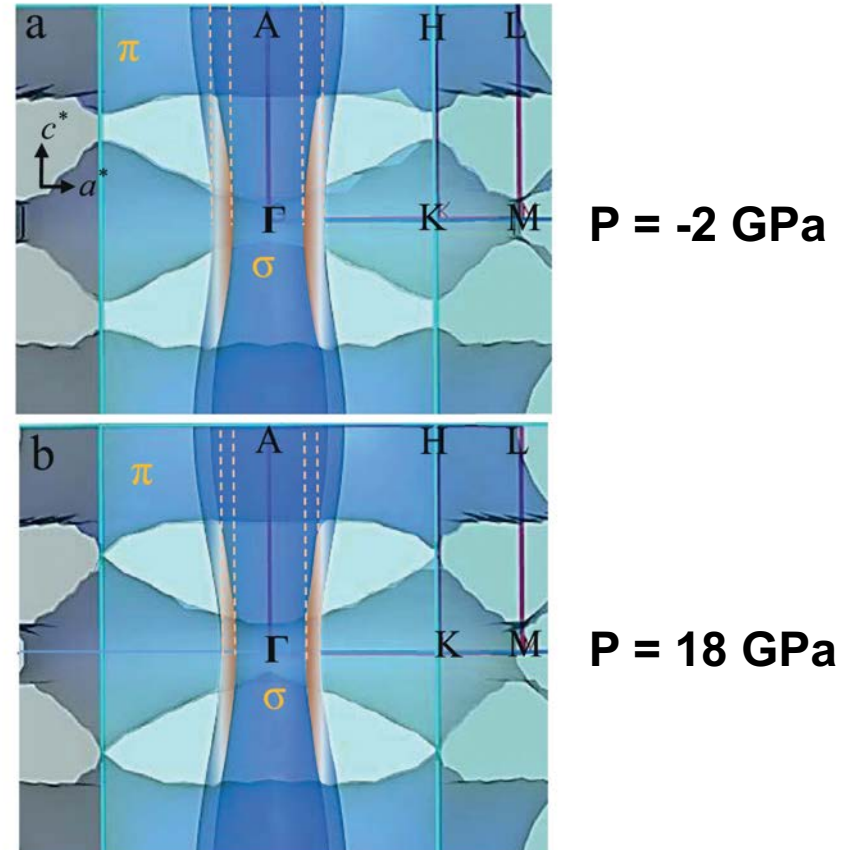
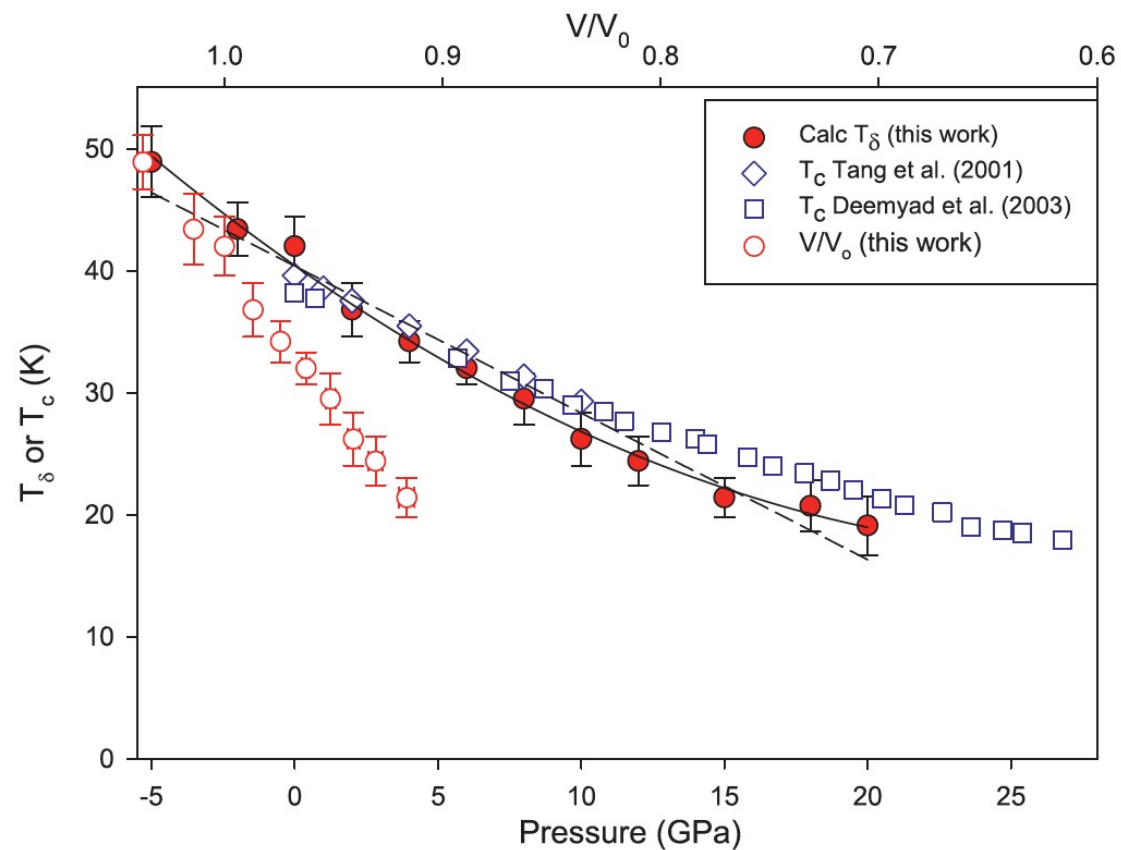
$P = 15 \text{ GPa}$

Alarco *et al.*, Physica C., 536, 11-17, 2017

CRICOS No.00213J

Superconducting T_c – MgB_2 with pressure

Theory and Experiment



Alarco *et al.*, Physica C., 536, 11-17, 2017

Superconducting T_c – AIB₂-type Structures

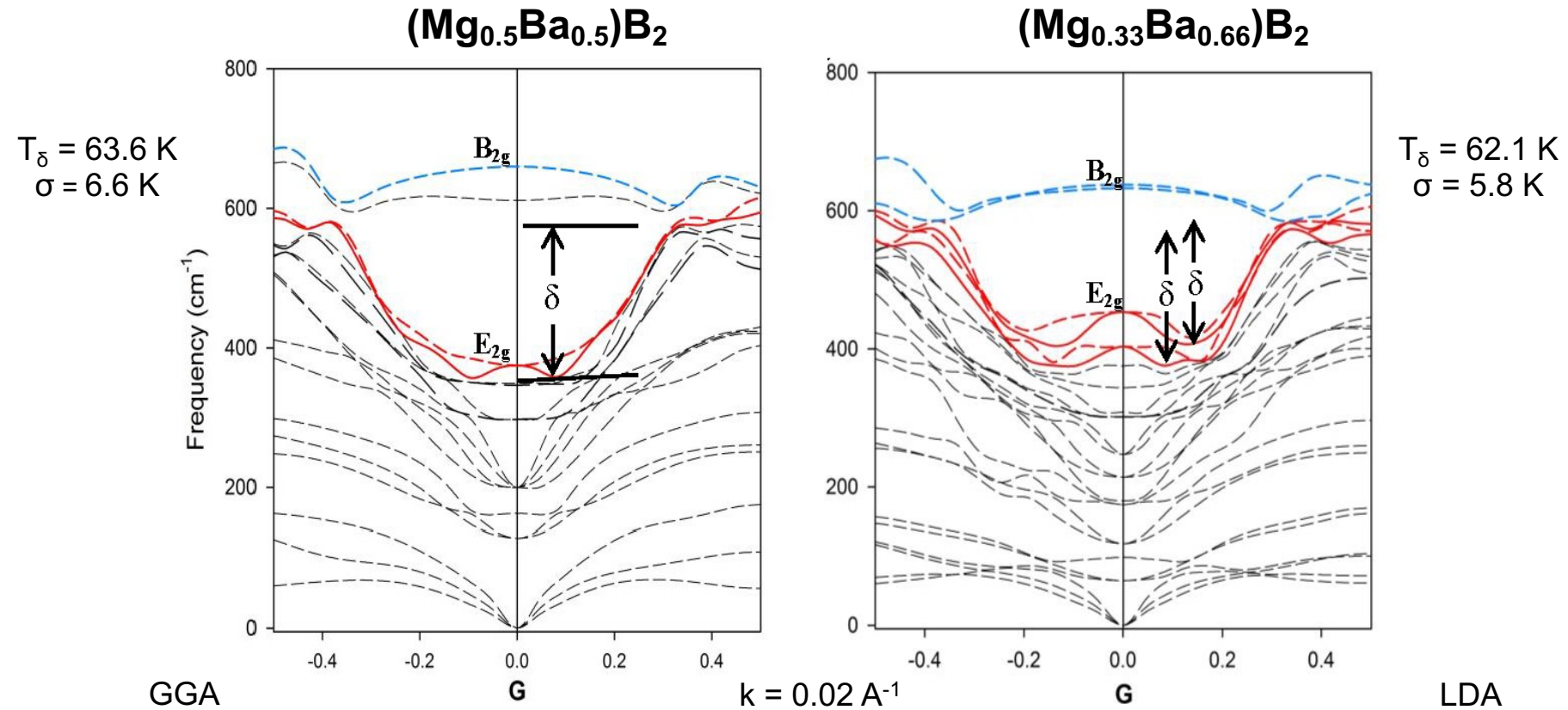
Theory and Experiment

Compound	Predicted T_c This work (K)	Experimental T_c By Others (K)
MgB ₂	42.0 (3.0)	39.2 – 40.2
(Mg _{0.8} Al _{0.2})B ₂	31.3 (3.4)	25 (2) – 33.0 (0.1)
(Mg _{0.67} Al _{0.33})B ₂	16.2 (3.3)	13.5 (0.1)
(Mg _{0.5} Al _{0.5})B ₂	4.6 (2.5)	4.0 – 13.5
(Mg _{0.86} Sc _{0.14})B ₂	31.5 (4.4)	23.0 (2.5)**
(Mg _{0.75} Sc _{0.25})B ₂	11.4 (1.0)	~8.2 (5.0)**
AIB ₂	0.0	0.0
BaSi ₂	9.3 (0.5)	8.9
Ca(Al _{0.5} Si _{0.5}) ₂	7.5 (0.5)	7.8
(Mg _{0.67} Ba _{0.33})B ₂	64.4 (2.2)	n.d.
(Mg _{0.5} Ba _{0.5})B ₂	63.6 (6.6)	n.d.
(Mg _{0.33} Ba _{0.67})B ₂	62.1 (5.8)	n.d.
BaB ₂ (~16GPa)	79.1 (10.2)	n.d.

**peak values from derivative of surface resistance

New Materials: $(\text{Mg}_{1-x}\text{Ba}_x)\text{B}_2$

DFT Predicted T_c

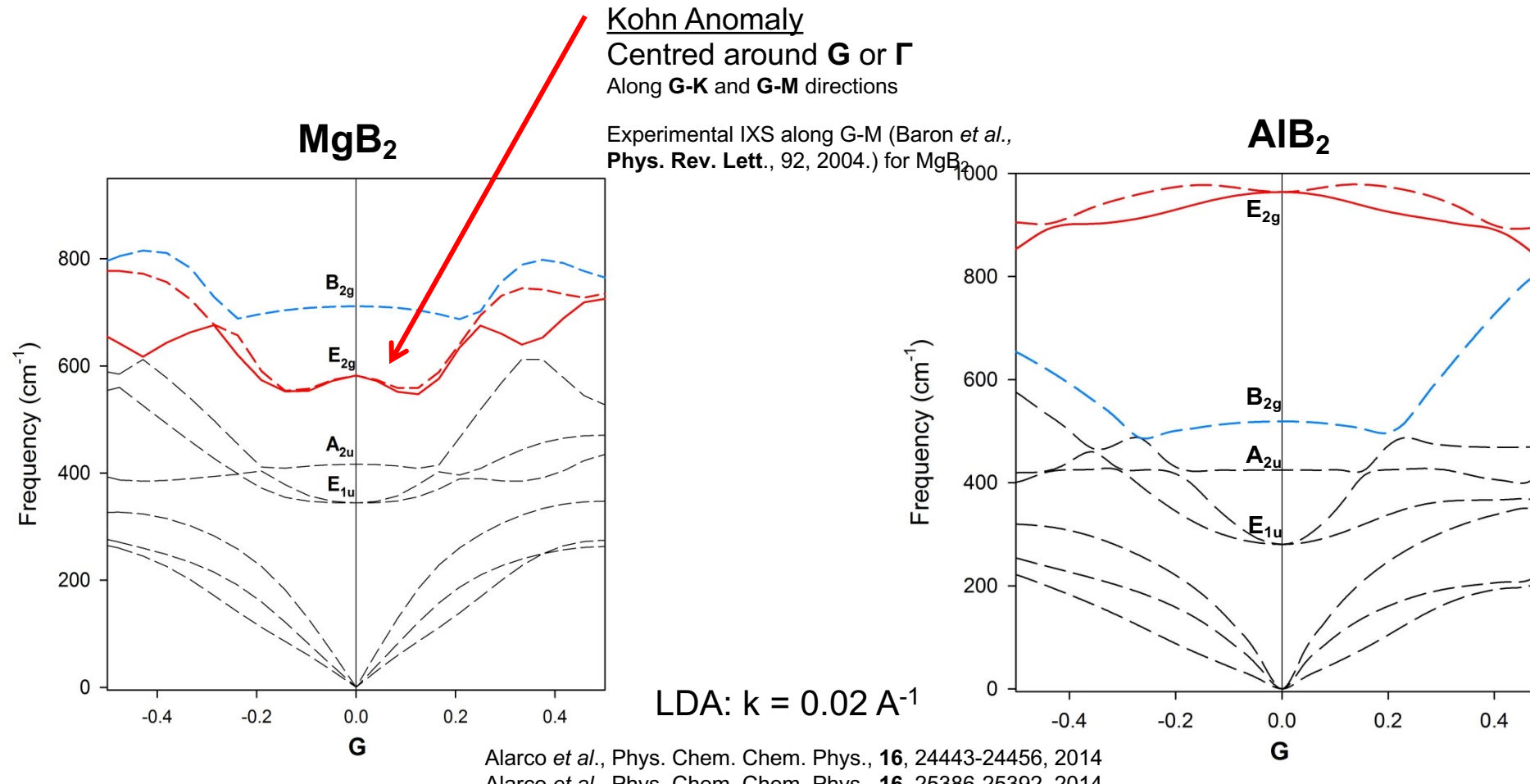


Alarco *et al.*, Phys. Chem. Chem. Phys., **17**, 25090-25099, 2015

CRICOS No.00213J

Density Functional Theory

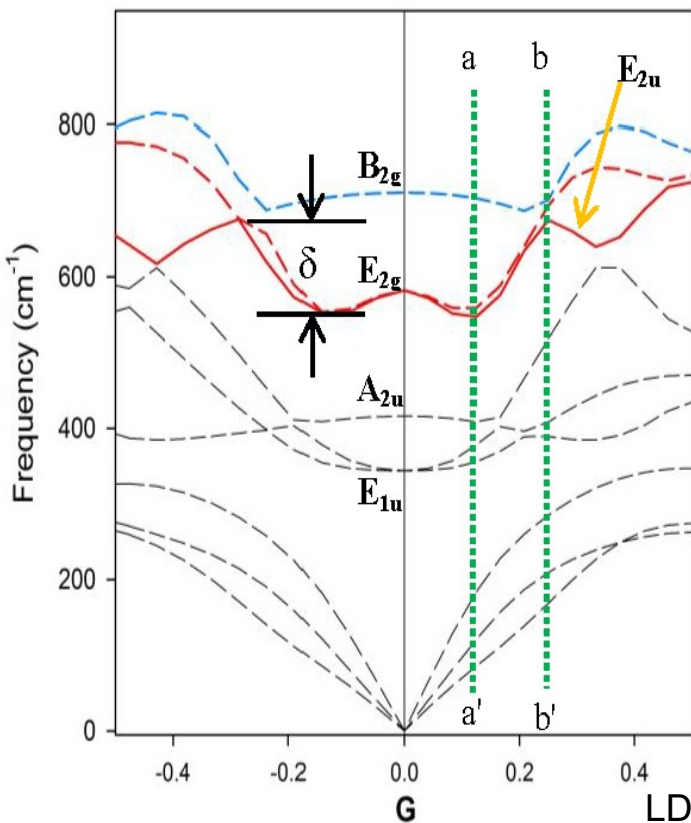
Phonon Dispersions – $Mg_{1-x}Al_xB_2$



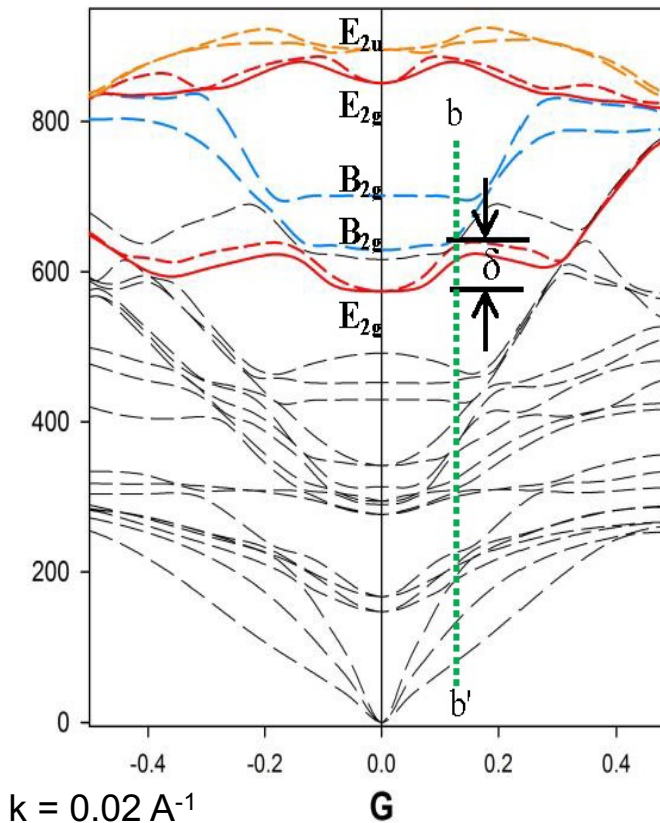
Density Functional Theory

Phonon Dispersions – $Mg_{1-x}Al_xB_2$

MgB_2



$(Mg_{0.66}Al_{0.33})B_2$



LDA: $k = 0.02 \text{ \AA}^{-1}$

$$\delta = (nN/Z) \times (k_B T_\delta / 2)$$

Alarco *et al.*, Phys. Chem. Chem. Phys., **17**, 25090-25099, 2015

CRICOS No.00213J

Superconducting T_c – $Mg_{1-x}Al_xB_2$

Theory and Experiment

$$\delta = (nN/Z)x(k_B T_\delta / 2)$$

$$\delta = (nN/Z)x(k_B T_\delta / 2)$$

δ = height of phonon anomaly (cm^{-1})

n = degrees of freedom per atom

N = number of atoms per unit cell

Z = number of formula units per cell

k_B = Boltzman's constant

T_δ = thermal energy of phonon

Solve for T_δ

T_c vs x for Mg_{1-x}Al_xB₂

